THE CRYSTAL STRUCTURE OF CAESIUM PERMANGANATE BY X-RAY DIFFRACTION.

by

L. R. NASSIMBENI, B.Sc. (Hons.), (Rhodes).

A thesis submitted in fulfilment of the requirements for the Degree of Master of Science of Rhodes University.

Department of Chemistry,
Rhodes University,
Grahamstown.

December, 1963.

A C K N O W L E D G E M E N T S

The author wishes to thank in particular Professor E. G. Prout, M.Sc., Ph.D., (S.A.), of Rhodes University, under whose careful guidance this research was conducted and for his valuable criticism and encouragement in all aspects of the work.

The author is also indebted to:

Dr. D. Feil of the University of Cape Town and to Mr. G.S. Woods for their great help and interest in the project;

Messrs. I. Ward and G. Ranftelshofer for their assistance in the technical aspects of the research.

C O N T E N T S

1. INTRODUCTION

1.1 OUTLINE OF A CRYSTAL STRUCTURE ANALYSIS.

The regular geometrical form of a crystal is due to the regular arrangement of the atoms, ions or molecules of which it is built. The regularity is that of a three dimensional pattern in which a certain unit of the structure, known as the "unit cell" is repeated in space. In practice a crystal structure analysis starts with the determination of the size and shape of the unit cell and an examination of its symmetry properties. An analysis of these factors leads to the determination of the space group. When the latter cannot be established unequivocally, use is made of special methods such as pyro-electricity, piezo-electricity, optical properties of the crystal and distribution of the intensities of X-ray reflections to assist in the determination. Having found the space group and the dimensions of the unit cell an attempt can be made to describe the contents of the unit cell in terms of the number, nature and positions of the atoms.

The preliminary work is carried out by taking single crystal rotation, Laue and Weissenberg photographs. Laue photographs give an indication of the system and class to which the crystal belongs, while rotation photographs are used to determine the approximate size of the unit cell. Weissenberg photographs allow a more accurate measurement of the cell parameters to be made and are also used for

- indexing the -

indexing the reflections unambiguously.

The second stage of the analysis consists in obtaining accurate values of integrated intensities of the many reflections. These measured intensities must be corrected to allow for several physical and geometrical factors. After the appropriate corrections have been applied one obtains a set of structure amplitudes i.e. F_{hkl} values. The electron density within the unit cell can be computed with the aid of a Fourier series, where the F_{hkl}'s are the coefficients of the series. However the Fourier transformation requires a knowledge of the phases as well as the magnitudes of the amplitudes. Since no method has been found for observing these experimentally it appears that the problem cannot be solved because of the missing phases. This constitutes the "phase problem of X-ray crystallography" which can be solved, within certain limitations, by use of the Patterson function.

Having found a structure which gives a reasonable agreement between observed and calculated intensities it is usual to refine it, i.e. to vary the location of the atoms in the structure slightly so that the agreement between experiment and theory is the best possible. Finally the accuracy of the crystal structure may be assessed by calculating the residual $R = \Sigma \| F_{obs} | - | F_{calc} \| / \Sigma | F_{obs} |$, which is taken as a "reliability index". The residual should decrease with refinement and reach a steady low value. For relatively simple structures the value of R should be less than .25 and with heavy atoms present the value should be lower still.

1.2 THE DETERMINATION OF THE UNIT CELL AND SPACE GROUP.

In order to determine the crystal identity periods and the space group symmetry elements, it is appropriate to discuss the various types of crystal photographs employed in an analysis, namely the Laue, rotating-crystal, and particularly the Weissenberg methods. The interpretation of these photographs is best carried out using the concept of the reciprocal lattice, which is discussed below.

1.2 (a) The reciprocal lattice [1,2].

To construct a lattice reciprocal to a given space lattice, one takes each interplanar spacing d_{hkl}, and plots in reciprocal space, a vector σ_{hkl} parallel to it and in length proportional to the spacing reciprocal,

$$\sigma_{hkl} = c \frac{1}{d_{hkl}} \qquad \ldots\ldots\ldots \qquad 1.01$$

where c is a proportionality constant. For most discussions c is either equal to λ, the wavelength of the radiation used, or to unity. The lattice consists of the array of points, one at the end of each such vector. This array can be represented by the collection

$$K\sigma_{hkl} = K \; c \; \frac{1}{d_{hkl}} \qquad \ldots\ldots\ldots \qquad 1.02$$

It can be shown that such an array of points forms a lattice. The Bragg equation has a precise geometrical equivalent in terms of the reciprocal lattice. This is illustrated in Fig. 1.01.

P is the reciprocal lattice point for the set of planes

XY which we suppose are in reflecting position. $XP = \lambda/d$

The X-ray beam QX is reflected by the plane at an angle θ, the reflected beam making an angle 2θ with the primary beam.

If Y lies in the plane QXR then $\hat{QXY} = \theta$.

At P construct a line perpendicular to XP to meet the incident beam at Q. R will also lie on this line.

Since $QR \parallel XY$ $\quad \hat{PQX} = \theta$

Since $\hat{QPX}$ is a right angle $\quad PX/QX = \sin\theta$

$$QX = \frac{PX}{\sin\theta} = \frac{\lambda}{d \sin\theta} = 2 \quad \text{(Bragg's Law)} \qquad 1.03$$

For every possible position of P $\hat{QPX}$ is a right angle, hence the locus of P is a cirle with QX (=2) as diameter.

The positions occupied by all the points P when the planes they symbolise are in reflecting positions are obtained by rotating the circle QPX about the diameter QX thus giving a sphere. This is known as the "limiting sphere" or "sphere of reflection".

If the point O, the centre of the sphere, is joined to P, then

$$\hat{OQP} = \hat{OPQ} = \theta$$

and $\therefore$ $\hat{XOP} = 2\theta$

OP is therefore parallel to XR and also represents the direction of the reflected ray. We may thus regard the crystal as rotating at O and the reciprocal lattice of the same crystal rotates about the point where the beam emerges from the sphere.

Cylindrical Coordinates. A practical way of specifying the location of a reciprocal lattice point is by specifying its cylindrical coordinates with respect to the rotation axis. Thus the position vector σ is resolved into components parallel with and perpendicular to the rotation axis. These two coordinates are designated by ζ (zeta) and ξ (xi) and lie in a plane containing the rotation axis and the original vector σ. This plane makes an angle ϕ with the plane containing the X-ray beam. The three quantities ϕ, ξ and ζ completely fix the point P - they are its cylindrical coordinates (Fig. 1.02). Note that for every photographically recorded spot the Bragg glancing angle θ can be calculated if desired, from measurements made on the film (Fig. 1.03). The angles 2θ, γ and χ are related by the spherical trigonometric relation

$$\cos 2\theta = \cos\gamma \cos\chi ;$$

in the cylindrical camera the angles γ and χ are given by

$$\gamma = \frac{x}{r} \text{ radians}, \qquad \tan\chi = \frac{y}{r}$$

whence $\cos 2\theta = \cos\frac{x}{r} \cos(\tan^{-1}\frac{y}{r})$ 1.04

Hence θ.

For the zero layer line $y = 0$ hence $\chi = 0$

and $\gamma = 2\theta$ ... 1.05

1.2 (b) Single crystal photographs and their interpretation.

When taking a single crystal photograph, a suitable crystal is set up on a goniometer head with a zone axis parallel to the axis

- of rotation -

Fig 1.01

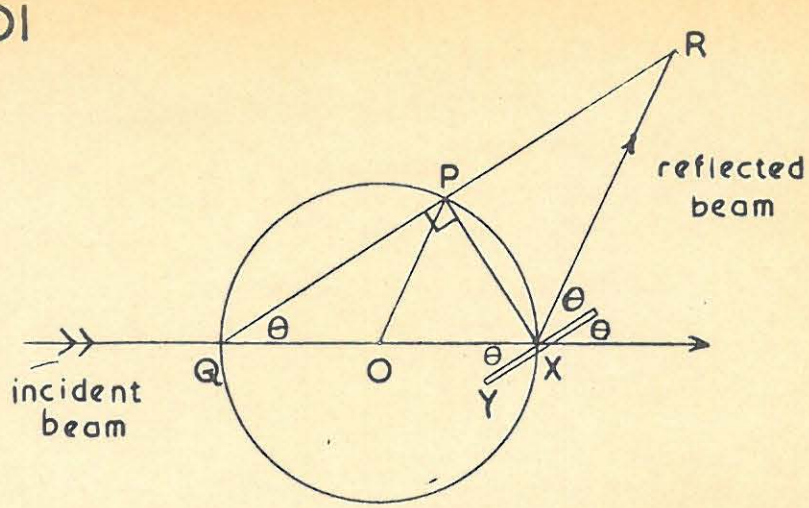

Fig 1.02

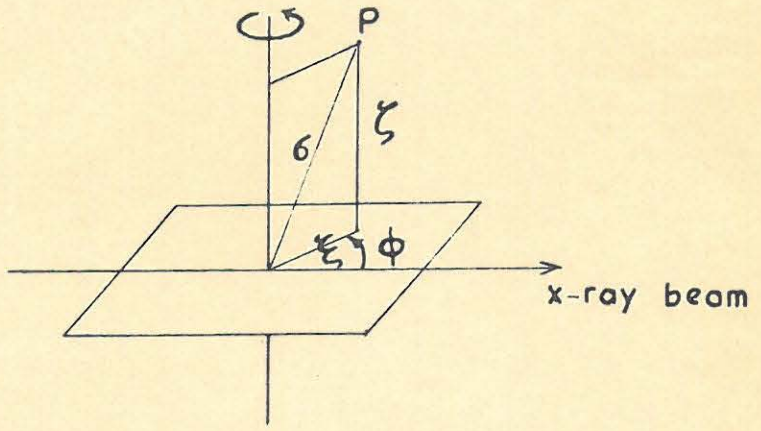

Fig 1.03

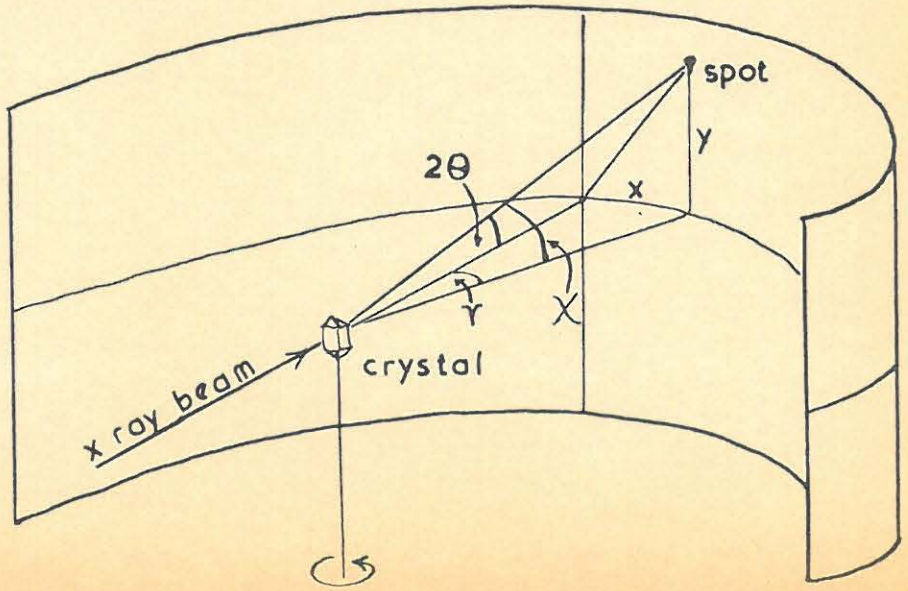

of rotation, which is perpendicular to the X-ray beam. The crystal is irradiated by a narrow beam of monochromatic X-rays and the reflections are recorded on a cylindrical film surrounding the crystal, the cylinder axis coinciding with the crystal axis of rotation.

The X-ray photographs obtained by a single crystal rotated about a principal axis show the diffraction spots arranged on a series of parallel straight lines. The interpretation of such photographs is best carried out in terms of the reciprocal lattice. The crystal may be envisaged as a collection of reciprocal lattice points. When the crystal rotates about one of its axes, the reciprocal lattice accompanies it and the reciprocal lattice points within range will pass through the sphere of reflection as shown in Fig. 1.04.

When a reciprocal lattice point cuts the sphere, a diffracted beam flashes out from the crystal to the point cutting the sphere. It can be seen that the beams will be emitted in the pattern of co-axial cones as shown in the Fig. 1.05. The diffracted beams strike a photographic film enclosed in a cylindrical camera whose vertical axis is parallel and concentric with that of the crystal. When the film is developed it shows the well known "layer lines" of spots.

Rotation photographs afford a quick and fairly accurate method of obtaining the parameters of the unit cell of the crystal. Let us suppose that the crystal is rotated about the Z axis. Along this axis there are identical diffracting units spaced a distance

of "c" apart. This row of diffracting units perpendicular to an X-ray beam produces cones of diffracted rays at angles given by $n\lambda = c \sin \nu$ (Fig. 1.06),

where λ = X-ray wavelength

c = distance between diffracting unit

ν = is the complement to the semi-vertical angle of the cone of reflection

n is a whole number.

For the zero layer line n = 0. For the 1st, 2nd, 3rd layer lines n = 1, 2, 3 etc.

To obtain the length c, the distance y is measured from the film If the camera radius is r the $y/r = \tan \nu$

$$\text{hence} \quad c = \frac{n\lambda}{\sin \nu} = \frac{n\lambda}{\sin \tan^{-1} y/r} \qquad \ldots\ldots\ldots \quad 1.06$$

By rotating the crystal about all three of its principal axes the parameters of the unit cell a, b, c can be obtained with reasonable accuracy

The indexing of single-crystal rotation photographs.

We want to find the coordinates ξ and ζ of a reciprocal lattice point which correspond to a particular spot on the film.

If the coordinates of a spot on a cylindrical film are x (along the equator) and y (along the meridian) then the distance ζ of a reciprocal lattice point from the equatorial plane is given by $\sin \nu = \sin \tan^{-1} y/r$ 1.07A

The distance ξ of the point P from the axis of rotation of the

Fig 1.04

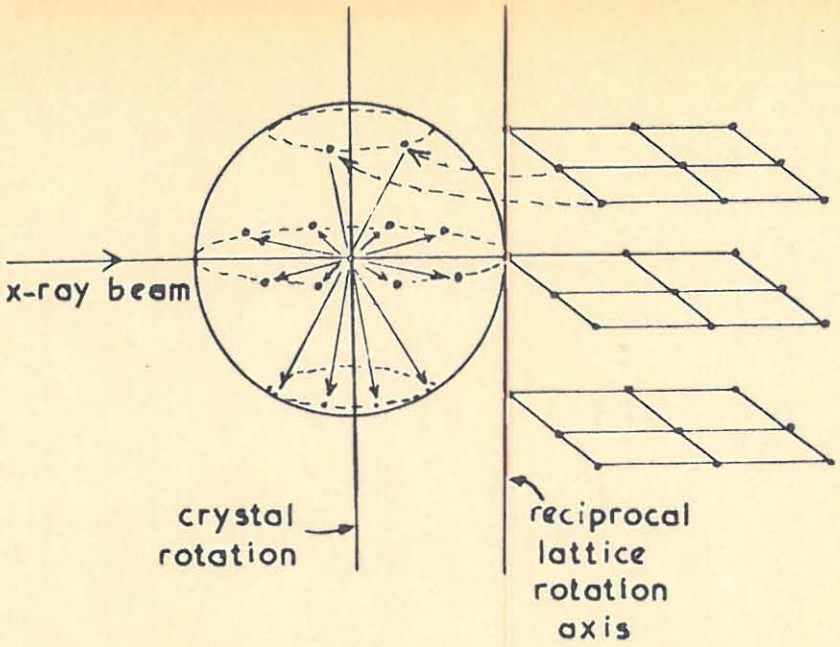

Fig 1.05

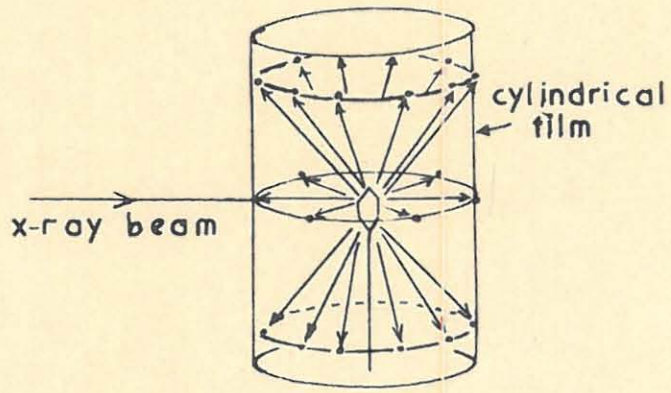

Fig 1.06

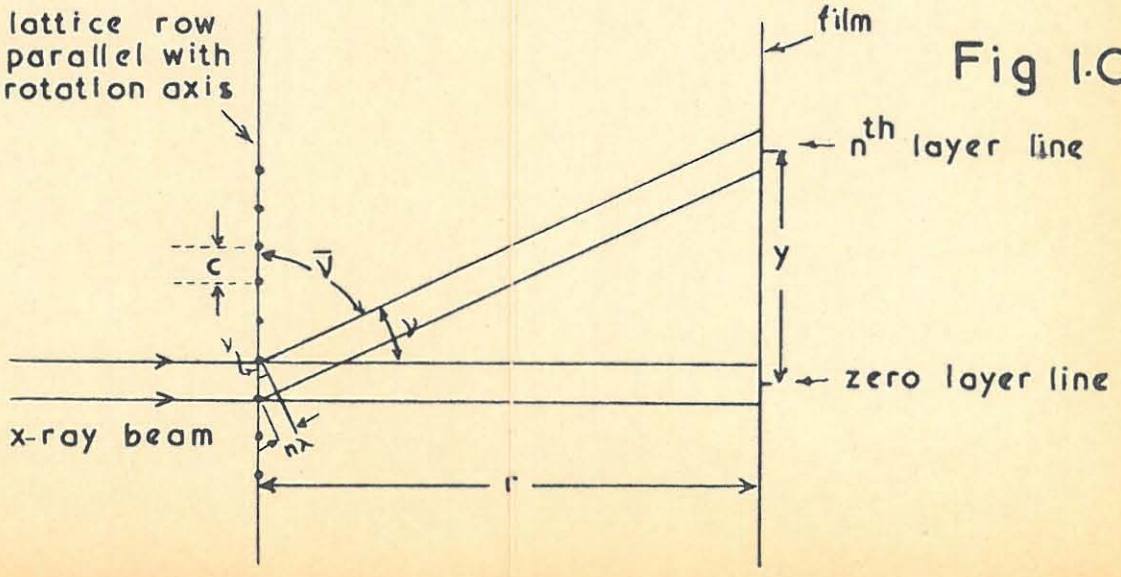

reciprocal lattice may be obtained by solving the triangle PUV in Fig. 1.07B.

UV = 1 (radius of the sphere)

UP = $\cos \nu$

ψ is the x/r radians

Then by the cosine rule

$$\xi^2 = 1 + \cos^2 \nu - 2\cos \nu \cos \psi$$

$$\therefore \quad \xi = \sqrt{[1 + \cos^2(\tan^{-1} y/r) - 2\cos(\tan^{-1} y/r) \cos x/r]} \quad \ldots\ldots \text{1.07B}$$

Indexing of the reflections may now be carried out in two ways,

(i) the film coordinates xy of each reflection can be measured and appropriately transformed to the corresponding reciprocal lattice coordinates using the formulae 1.07A, 1.07B, but the calculations are tedious, and so it is not often used;

(ii) the film coordinates are read directly from a Bernal chart. Bernal[3] worked out ξ and ζ values for all positions on a cylindrical film and drew up a chart which has lines joining points of equal ξ and ζ values. Transparent charts of this type are available for cylindrical cameras of various radii.

Indexing is then carried out as follows:-

The parameters a, b and c of the unit cell are determined from layer-line measurements from the corresponding rotation photographs. Suppose a crystal is rotated about the c axis; then the points on the zero layer of the reciprocal lattice

have indices $hk0$, the ones on the first layer have indices hkl and in general the points on the n^{th} layer have indices hkn. Thus one index of every spot is determined by its layer. It now remains to determine the two other indices h and k. This is best done graphically. The reciprocal lattice net of the zero layer of the reciprocal lattice is drawn and using the ξ value of a reflection as radius, an arc is drawn on the reciprocal lattice using the point 000 as origin. (Fig. 1.08A). The indices of the reflection are then determined by where the arc passes through an intersection in the reciprocal lattice net.

In the case of crystals belonging to orthogonal systems the reciprocal lattice net for the equatorial layer is simply repeated above and below for layers of higher order. Thus the same reciprocal lattice net can be used to index all the spots on the photograph. In the case of the monoclinic and triclinic systems however, the situation is less simple. Let us suppose that a monoclinic crystal is rotated about its c axis (Fig. 1.08B). Then the zero level of the reciprocal lattice is a rectangular array of points and indexing may be carried out as before. The other levels are also rectangular networks but they do not lie directly above and below the zero level, being displaced in the direction of a^* by distances which are multiples of $c^* \cos\beta^*$. This must be taken into account when indexing the upper layers

Fig 1.07

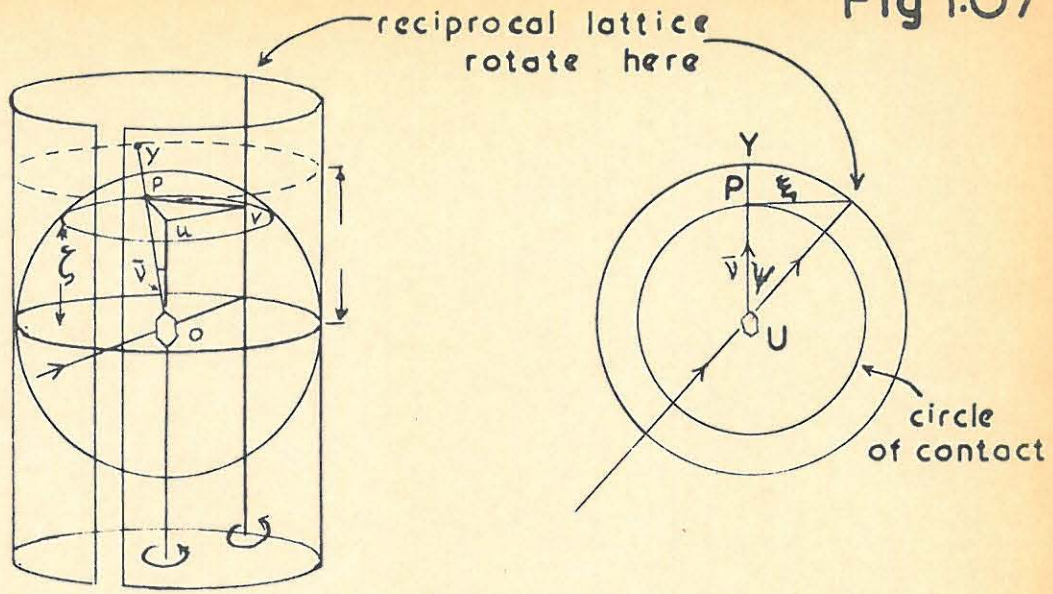

Sphere of reflection surrounded by cylindrical film of unit radius

Fig 1.08

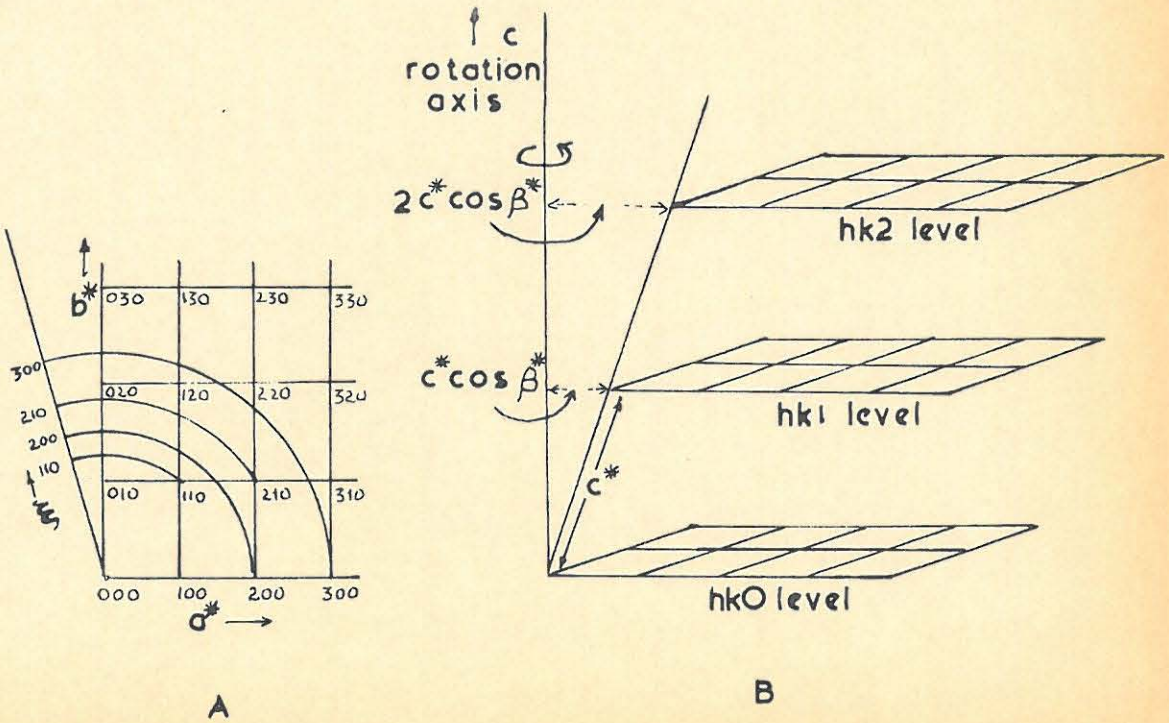

of the reciprocal lattice.

When indexing a particular reflection it often happens that the arc described with radius = ξ goes through two or more points on the reciprocal lattice net. It then becomes impossible to decide what indices to assign to a spot. This is particularly prevalent with reflections at high angles. One method of separating these "indeterminate" reflections is to take photographs while the crystal is rotated through a limited angular range. A set of several photographs is required to cover all reflections; on each photograph only certain spots appear, because only certain sets of crystal planes pass through their reflecting positions in the course of the oscillation of the crystal through the selected angular range. Thus it is usually possible to decide that because a particular spot appears on one photograph and not on others it must have been produced by a particular crystal plane. This method is laborious however, and it is better to use one of the moving-film goniometer methods, which offer a quicker and unambiguous way of assigning in indices.

1.2 (c) Moving film methods.

A reflection is associated with a particular point of the reciprocal lattice of the crystal. This point is identified by the coordinates ξ, ζ and ϕ. The plane surface of a photographic film is, however, two dimensional, and can thus only record two coordinates. It follows that one cannot, in general,

- unequivocally -

unequivocally index the reflections by rotation and oscillation photographs. We have shown that when a rotating crystal is irradiated with X-rays it gives rise to coaxial cones of diffracted rays. These cones of diffracted rays give rise to layer lines in rotation photographs, and when indexing one particular layer line of spots we are predetermining one of the indices hkl. For example, if a crystal is rotated about the c axis and the zero layer is indexed, then all the spots will have indices of the type hk0. h and k are unknown and they cannot, in general, be fixed unequivocally. This may be shown by considering Fig. 1.09. The figure shows the reflection of a beam of X-rays by two different prism faces hk0 and h′k′0.

In Fig. A the crystal is placed in an arbitary zero position where neither plane reflects.

The crystal is then turned through an angle ω_{hk0} at which setting the plane hk0 reflects the X-ray beam according to Bragg's law

$$n\lambda = 2d_{(hk0)} \sin\theta_{(hk0)}.$$

The angle θ_{hk0} depends only on the spacing of d_{hk0} of the system of planes. The angle of rotation ω_{hk0} depends on the original angle ϕ_{hk0} the plane makes with the X-ray beam before rotation starts. Now if the planes h′k′0 and hk0 should have almost the same spacing d, then their glancing angle θ would be almost identical and they would give rise to practically identical spots on a fixed film and resolution thus becomes impossible.

- A reflection -

A reflection may thus be regarded as having two coordinates: Θ , which is a function of d

ω , which is a function of d and ϕ.

If during the rotation of the crystal the film can be moved in any direction other than that of the plane of the angle Θ, then the angle ω can be measured by the corresponding film movement.

Several mechanisms have been used for this purpose, the most important being the Weissenberg method.

The Weissenberg Method.

The Weissenberg goniometer consists of a goniometer head mounted on a spindle which is coaxial with a cylindrical camera. The camera travels parallel to its axis during the rotation of the crystal. The rotation of the crystal and the translation of the camera are synchronised by a combination of worm and wheel gears. When the crystal is oscillated about a zone axis cones of diffracted rays are produced. In the Weissenberg method a single cone is selected and allowed to fall on the film, the others are absorbed by metal screens.

Instrumental constants:- Weissenberg photographs of the same crystal may differ in scale in two dimensions. One of these scales (along x) depends on only the diameter of the camera. The other (along z) depends on the coupling of film translation to crystal rotation. (Fig. 1.10).

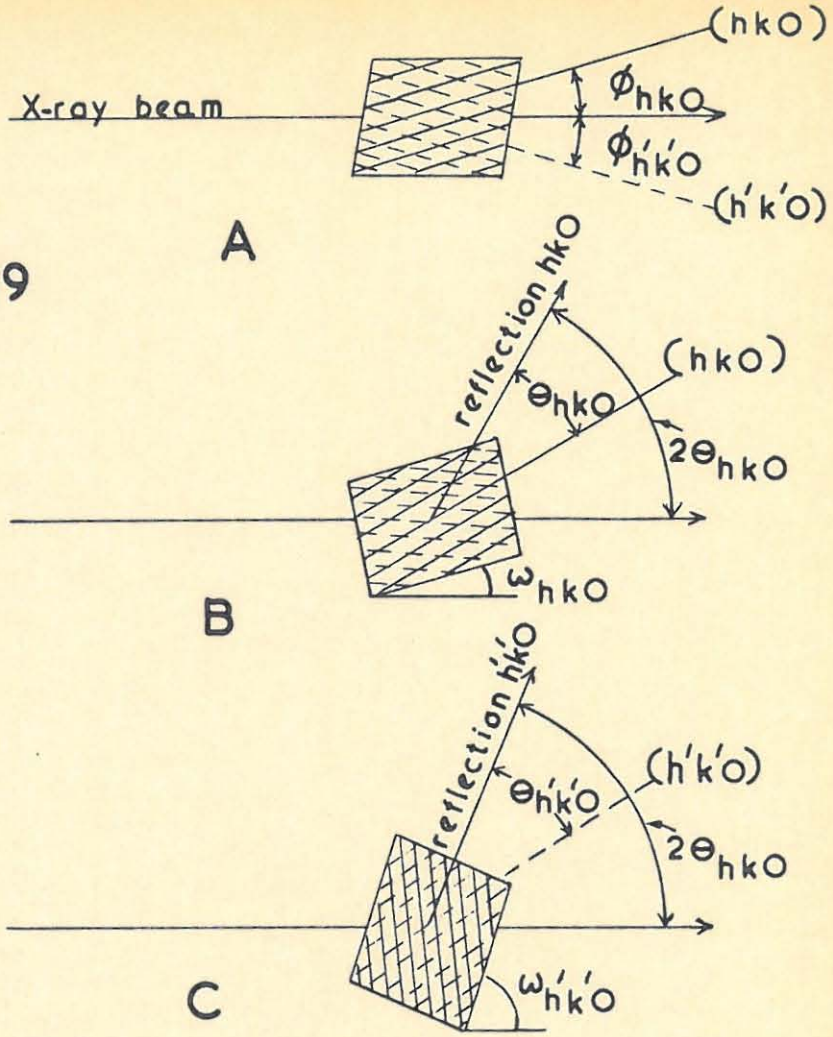

Fig 1.09

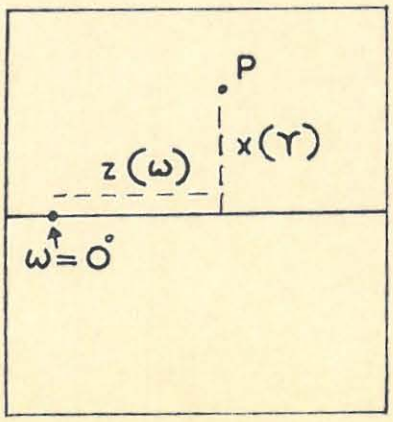

Fig 1.10

A Weissenberg instrument thus has two instrumental constants C_1 and C_2 corresponding to these two scales.

From the figure the distance $x \propto$ the reflection angle γ, $\gamma = C_1 x$, C_1 may be evaluated from the relation

$$\frac{\gamma}{x} = \frac{360}{2\pi r} \qquad r = \text{radius of camera}$$

$$C_1 = \frac{(360^\circ)}{(2\pi r)} \text{ degrees/mm} \qquad \ldots\ldots\ldots \qquad 1.08$$

Since a mm scale is most convenient for measuring x it is convenient to have C_1 equal to some simple whole number for the purpose of rapid conversion of x to γ. On most modern instruments $C_1 = 2$, which gives a camera diameter of 57.296 mm. Fig. 1.10 also shows that as the crystal rotates through an angle ω the film moves through a distance z,

$$\text{Hence} \qquad \frac{\omega}{z} = C_2 \text{ degrees/mm} \qquad \ldots\ldots\ldots \qquad 1.09$$

It is convenient to have C_2 also equal to 2 and photographs having $C_1 = C_2$ are said to have undistorted scale, whereas if they have $C_1 \neq C_2$ they have distorted scale.

The interpretation of Weissenberg photographs.

The normal beam Weissenberg method is first discussed with particular reference to the interpretation of the zero layer of the reciprocal lattice. This method is characterised by having the axis of crystal rotation normal to the direct X-ray beam.

There are certain striking features of Weissenberg photographs of which use is made in the interpretation. The

photographs show that some of the spots appear in straight lines running diagonally across the photograph and others are on a family of curves. The reason for the diagonal lines of spots can be understood from Fig. 1.11. In this figure the line OQ represents a continuous series of potential reflecting points P. This line passes through the origin of the reciprocal lattice and as the crystal rotates the line rotates about the point O until any point P cuts the sphere of reflection, when a reflected beam flashes out. The question is, how does the reflection position P move across the film as the abscissa ω varies? This may be answered directly from the figure.

Bisect $\angle \gamma$

hen $\frac{\gamma}{2} + \hat{SOT} = 90^\circ$

$\omega + \hat{SOT} = 90^\circ$

$\therefore \quad \frac{\gamma}{2} = \omega$

$\therefore \quad \frac{\gamma}{\omega} = 2$ 1.10

since γ and ω are Weissenberg film coordinates the above equation may be plotted directly on the film. Fig. 1.12. The plot shows that if the line OQ is rotated it produces a series of reflections OL on the film. This line passes off the positive side of the film at $\omega = 90^\circ$, and at the same time reappears on the negative side. This occurs because reflection angles up to 180° appear on the upper part of the film, while those between 180° and 360° appear on the lower half of the film. The cycle is then repeated by the negative half of OQ',

starting at $\omega = 180^{o}$. The latter discussion applied only to "central" rows, but the laws of reflections for any lattice row may be derived with the aid of Fig. 1.13. For simplicity the derivation is only applied to the zero layer of the reciprocal lattice. The figure shows line GG representing the reciprocal lattice row at a distance d from the rotation axis. The lattice row, in general, intersects the sphere of reflection on two points P′ and P′′, developing two reflections having $\angle$'s γ' and γ''. Assuming that the lattice row has initial direction of $\emptyset = 0$, then $O\hat{S}T = \omega$, and the two reflection $\angle$'s are,

$$\gamma' = \omega + \delta$$

$$\gamma'' = \omega - \delta$$

the $\angle$ δ may be evaluated from

$$\cos \delta = \frac{ST}{SP} = \frac{D_2}{1} \qquad \ldots\ldots\ldots \text{(i)}$$

where $D_2 = D_1 + d$

D_1 may be evaluated from

$$\cos \angle OST = \cos \omega = \frac{D_1}{1}$$

where $D_1 = \cos \omega$

and $D_2 = D_1 + d$

$= \cos \omega + d$

substituting in (i)

$$\cos \delta = \frac{\cos \omega + d}{1}$$

The reflection $\angle$'s can now be completely evaluated as

$$\gamma', \gamma'' = \omega \pm \cos^{-1} \frac{(\cos \omega + \delta)}{1} \quad \ldots \quad 1.11$$

- where the -

Fig 1.11

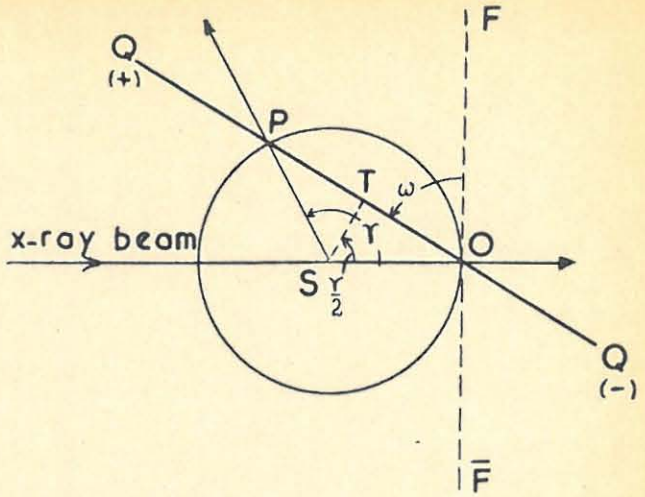

Fig 1.12

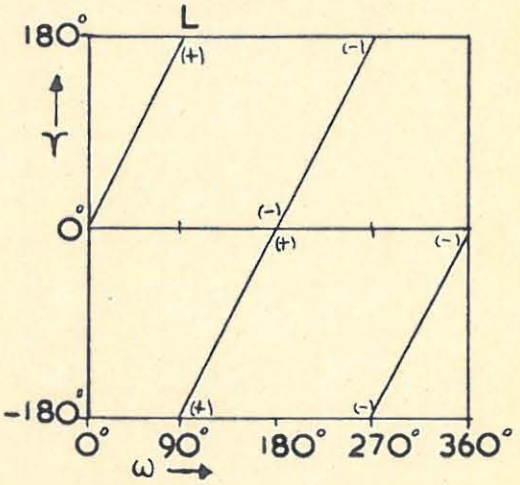

Fig 1.13

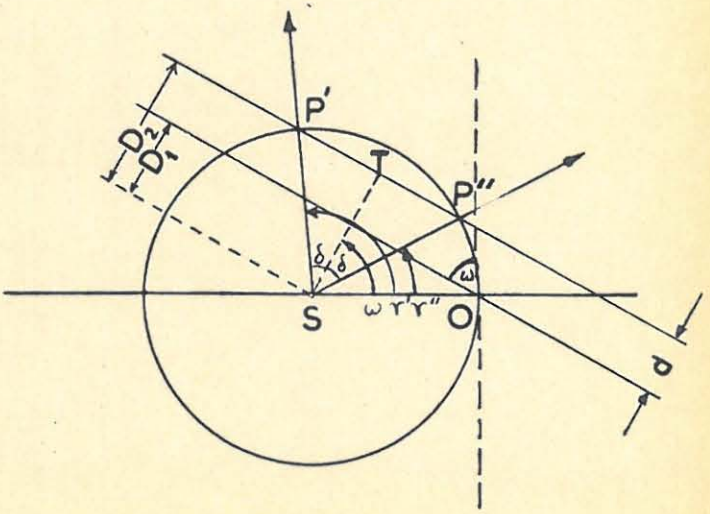

when the above equation is plotted on the Weissenberg film it gives rise to the characteristic curves as shown in Fig.1.14.

So far the discussion has been applied to the special case of a reciprocal lattice line originally located along $\phi = 0$. It can easily be extended to the more general case where $\phi = \phi_1$ (Fig. 1.15). We wish to find ξ and ϕ for the spot corresponding to the reciprocal lattice point P.

ξ is obtained from the distance x of the spot from the centre line of the film. $\gamma = 2x$ (camera diameter 57.3 mm)

$$\gamma = 2x \quad \text{(camera diameter 57.3 mm)}$$

From Fig. 1.15 $\xi = 2 \sin \frac{\gamma}{2}$

The angle ϕ_1 is given by the fact that

$$\phi_1 = \frac{\gamma}{2} - \omega$$

for the zero layer of the reciprocal lattice $\gamma = 2\theta$ (from equation 1.05) whence the above equations reduce to:

$$\xi = 2 \sin \theta \quad \ldots\ldots\ldots \quad 1.12$$

$$\phi = \theta - \omega \quad \ldots\ldots\ldots \quad 1.13$$

The whole zero layer of the reciprocal lattice can thus be plotted directly using polar coordinates ξ and ϕ.

Cartesian coordinates are more convenient however. These are given by

$$f = \xi \sin \phi, \quad e = \xi \cos \phi \quad \ldots\ldots\ldots \quad 1.14$$

Charts giving cartesian coordinates for all positions on the film have been constructed and by placing the base line of such a chart on the line of a photograph for which $\theta = 0$

the rectangular coordinates of the reciprocal point corresponding to any spot on the film can be read. This is true whatever the system of symmetry to which the crystal belongs. In general it does not matter where along the central line of the film the central line of the chart is placed. The coordinates read will of course depend on the position of one relative to the other, but when reciprocal points are plotted on squared paper the result will always be essentially the same. The only effect of moving the chart relative to the film is to rotate the reciprocal lattice of the crystal relative to the axes of the graph paper on which the plot of the reciprocal lattice points is made. In practice, however, one diagonal line of the chart is made to coincide with a prominent diagonal line on the photograph for convenience in reading the coordinates. With this setting spots will in general fall consecutively on only one set of curves of the chart. When the reciprocal net is orthogonal, spots will fall simultaneously on both sets of curves of the chart. In the interpretation of spots corresponding to an oblique reciprocal net, the coordinates are read and plotted on squared paper as before and, in addition, the choice of the unit mesh of the reciprocal net has to be made.

The relations between γ and ω have only been derived for the zero layer of the reciprocal lattice, but can easily be extended to cover any layer of the reciprocal lattice. However, the normal beam Weissenberg method is not the most convenient

for the interpretation of the higher layer lines of the reciprocal lattice. This is because to interpret normal beam non zero-layer photographs a Wooster chart is used. To each value of ζ there corresponds a separate chart, which gives the polar coordinate of each spot.

There is, however, a method of recording the higher layers of the reciprocal lattice which allows the use of the Weissenberg chart for reading the coordinates of the spots. This is the equi-inclination method, which is now described.

The equi-inclination Weissenberg method.

Firstly the geometry of the X-ray reflections of the normal beam and equi-inclination are compared. The three geometric arrangements are shown in Fig. 1.16.

Two angles are used to define each arrangement:-

the angle μ is the complement of the angle between the incident beam and the oscillation axis,

the angle ν is the complement of the semi-angle of the cone of reflected rays.

When $\mu = 0$ then we have the "normal beam" arrangement Fig. 1.16A and B.

When $\mu = -\nu = \sin^{-1} \zeta/2$ we have the equi-inclination arrangement.

The maximum practical value of the angle ν is about 40^{o}.

VV shows the axis of oscillation of the crystal. The reciprocal lattice oscillates about X. In the equi-inclination method the

- incident X-rays -

Fig 1.14

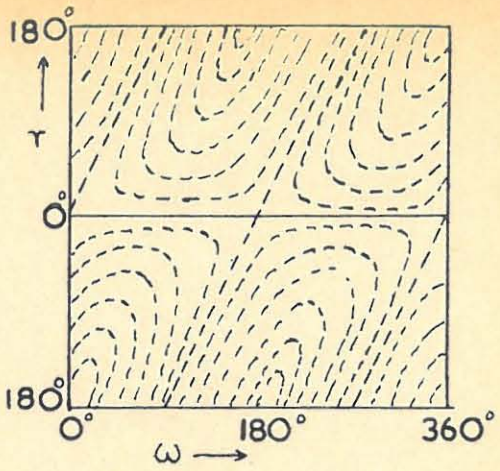

Fig 1.15

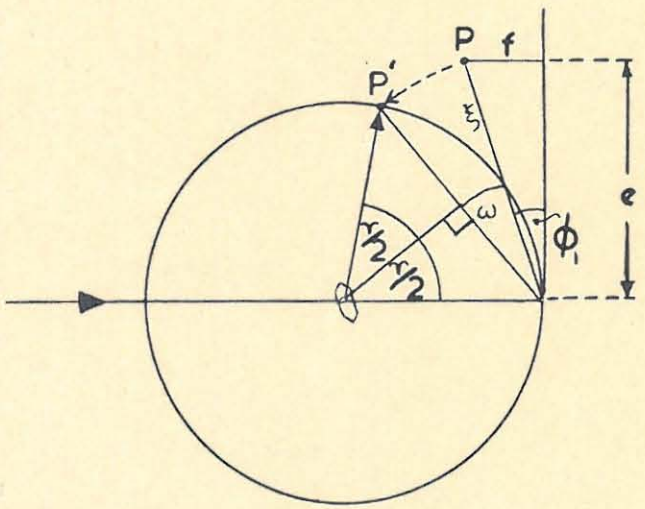

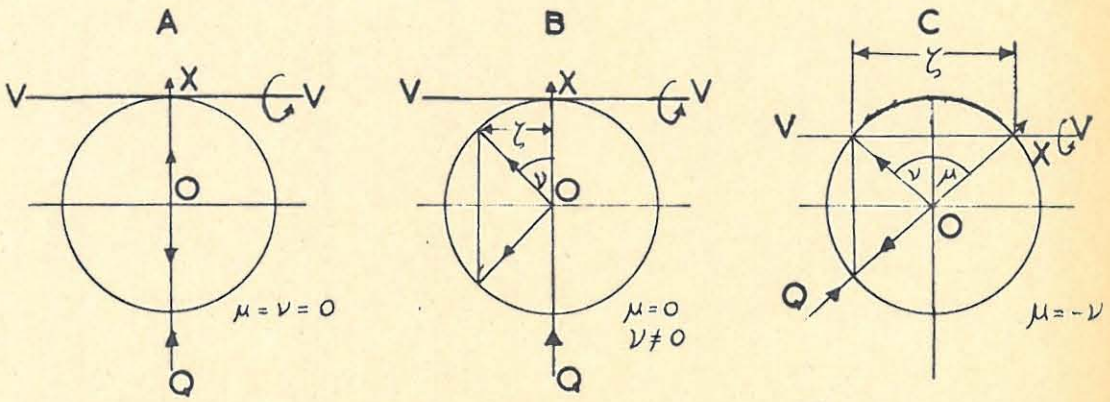

Normal beam zero layer

Normal beam non-zero layer

Equi inclination non-zero layer

Fig 1.16

incident X-rays form one of the generators of the cone of diffracted rays.

In Fig. 1.17 P is the foot of the perpendicular from X on the reciprocal lattice plane. If there is a lattice point at P, the reflecting circle, which has PR as its diameter, will stand in almost the same relation to the reciprocal lattice points as the equatorial reflecting circles stood to the points in Fig. 13A The only difference is that the radius of the circle PR is $\sqrt{1 - \zeta^2/4}$ instead of unity, and consequently, if the coordinates are read off on the equatorial Weissenberg chart the values must all be multiplied by the factor $\sqrt{1 - \zeta^2/4}$ to bring them to the correct value. Thus equi-inclination photographs have the advantage that the same Weissenberg chart can be used as for normal beam equatorial photographs.

1.2 (d) The Laue photograph.

The chief feature of the Laue X-ray goniometer is that no part of it moves during the taking of the photograph. Usually a flat film is employed. In the transmission photograph the incident beam strikes the crystal and then falls normally on the photographic film. In the back reflection photograph the X-rays pass through an aperture in the film before reaching the crystal and the beams which are reflected backwards are then recorded on the film. It is sometimes convenient to use a cylindrical camera in taking a Laue photograph as this allows the greatest range of angles of reflections to be recorded on the film.

White radiation, which consists of a range of wavelengths, is used. White radiation is best obtained from an X-ray tube with a tungsten target. When a copper target is used the characteristic K wavelengths are removed with an iron filter.

The reflection of X-rays occurs according to Bragg's equation $n\lambda = 2d \sin \theta$. For a given set of planes d is a constant and since the crystal is stationary, θ is fixed by the setting of the specimen. The wavelenth λ is variable because white radiation is used. Thus the set of planes "selects" the X-rays of appropriate wavelenth from the incident non-monochromatic beam, and causes a reflection to occur.

The indexing of the reflections is carried out with the aid of the gnomonic projection. The procedure is laborious however, and although in the past Laue photographs were used extensively, they are now used almost exclusively for showing the diffraction symmetry or "Laue symmetry" of a crystal. The information obtained from the Laue symmetry is meagre. It allows the distinction to be made between the different crystal systems, and in the more symmetrical systems it also helps to distinguish between different classes within a system.

1.2 (e) The Space Group.

A study of the external forms of crystals reveals that most of them possess geometrical symmetry, namely the occurrence of one or more of the following symmetry elements:- axes of rotation, centre of symmetry, reflection planes and axes of inversion.

Crystals may be classified into seven main "systems" each characterised by the possession of a certain minimum of symmetry elements and referable to certain characteristic axes, e.g. the tetragonal system has a single four-fold axis and is referable to three orthogonal axes, two of them equal.

The systems may be further divided into classes by the addition of the remaining number of symmetry elements. The geometry of any crystal is then classified by the possession of a group of symmetry elements known as a point group. There are 32 point groups which include all the known types of crystal symmetry. The crystal system may be determined by optical goniometry or by taking Laue photographs and analysing the Laue symmetry of the crystal, e.g. if a crystal has Laue symmetry mmm it belongs to the orthorhombic system. The above methods may also give an indication of the class to which the crystal belongs.

The space group requires the additional knowledge of the internal symmetry operators, that is symmetry operators involving translation as well as rotation and reflection: namely screw axes and glide planes. The space group cannot be deduced from the external form of the crystal. It may however be determined by examining systematic absences in the X-ray reflections.

Procedure in deducing the space group.

The list of reflections is first examined to find the lattice

type, whether it is simple (P), or compound. Systematic absences throughout the whole range of reflections indicate a compound lattice, the type of absences showing whether the cell is body centred (I), side centred (A, B, C) or face centred (F).

Systematic absences throughout a zone of reflections indicate a glide plane normal to the zone axis, while systematic absences of reflections from a single principal plane indicate a screw axis normal to the plane.

The Laue group is determined, thus also confirming the system. We may now write the diffraction symbol of the crystal. This includes the Laue symbol, followed by the lattice type followed by detectable glide planes and screw axes, e.g. mmm P $2_1 2_1 2_1$ means that the Laue symmetry is mmm, thus placing the crystal in the orthorhombic system, that the unit cell is primitive and that it has three two-fold screw axes parallel with the three edges of the unit cell.

The diffraction symbol may correspond to one particular space group, which is thus unequivocally identified. However, there may be several space groups corresponding to a given diffraction symbol. The identification of the space group may then be aided by several methods:-

(i) knowledge of the crystal class which may be obtained sometimes from the morphology of the crystal;

(ii) study of pyroelectric and piezoelectric effects. These phenomena are shown by crystals without a centre of symmetry. Pyroelectricity shows itself as

the separation of electric charge which occurs on heating or cooling the crystal. This may be tested very simply by suspending a crystal on a silk thread into a vacuum flask containing liquid air. If the crystal is pyroelectric it will be attracted to the walls.

Piezoelectricity is the charge which builds up in a crystal when mechanical pressure is exerted on it. It is more difficult to detect, but is still used as a test.

(iii) The statistical distribution of the X-ray intensities with the angle Θ can be used to find whether the crystal has a centre of symmetry and can, in some cases, identify the crystal class.

Wilson showed that for a given unit cell the average value of F^2 is a constant whatever the symmetry, but the distribution of the magnitudes around the average does depend on the symmetry. Howells, Phillips and Rogers worked out distribution curves for centrosymmetrical and non-centrosymmetrical crystals expressed as the proportion of reflections having F^2 values less than or equal to a given fraction of the average F^2. The curves are used to decide whether a crystal has a centre of symmetry or not. Fig. 1.18 shows the distribution for an

unknown crystal which is evidently non-centrosymmetric This method is, however, subject to certain limitations in that the atoms should all be in general positions and should not be too dissimilar in diffraction power.

1.3 THE MEASUREMENT OF INTENSITIES AND THEIR CORRECTION.

1.3 (a) The integrated intensity.[4]

A crystal almost invariably consists of a mosaic of small crystalline blocks which are inclined at small angles to each other. Thus the intensity of an X-ray reflection cannot be measured by simply reflecting the incident beam from the crystal face because not all the elements of the mosaic would reflect simultaneously. This difficulty can be surmounted if the crystal is turned through a small angular range, including the position for reflection, and the total amount of radiation at all angles is integrated. If a crystal reflects an amount $R(\Theta)$ per second when set at the angle Θ, and the incident radiation measured in the same way is I per sec then the integrated reflection is defined as

$$\rho = \int_{\Theta_{hkl}-\epsilon}^{\Theta_{hkl}+\epsilon} \frac{R(\Theta)\, d\Theta}{I} \qquad \ldots\ldots\ldots \qquad 1.15$$

Θ_{hkl} is the Bragg angle of reflection

ϵ varies with the particular crystal, and is usually of the order of $\frac{1}{2}^{o}$.

The intensity reaches a maximum at the Bragg angle

- then falls -

and then falls away rapidly as the Bragg angle is exceeded. This is illustrated in Fig. 1.19. The area under the curve represents the "integrated" intensity, and the height of the peak represents the "peak" intensity.

1.3 (b) The measurement of intensities.

Intensity measurements may be carried out using a photographic film or a quantum counter. With either of these two devices it is possible to measure either the peak intensity or the integrated intensity. The photographic method is more widely used. The X-ray reflections from the different crystal planes are recorded as spots of varying darkness on a photographic film. The conventional method of measuring photographic densities is to pass a beam of light through the dark spot, allow it to fall on a photocell and measure the deflection on a galvanometer connected to the photocell. This deflection is compared with that for the clear film. From the results one can compute the density of the spot. This, however, is a peak density, whereas what is required is the integrated density. Several methods to overcome this difficulty have been devised, some of the more important ones are:

(i) The Density Wedge Method - the density on the photograph is balanced with a known density on a density "wedge". Two equal beams of light (from the same source) are passed, one through the photograph and the other through the density "wedge". One adjusts the position of the latter until the two

Fig 1.17

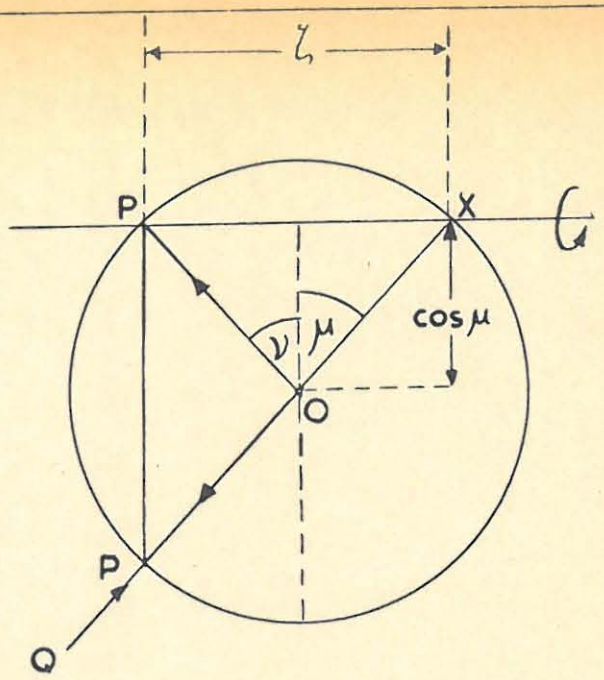

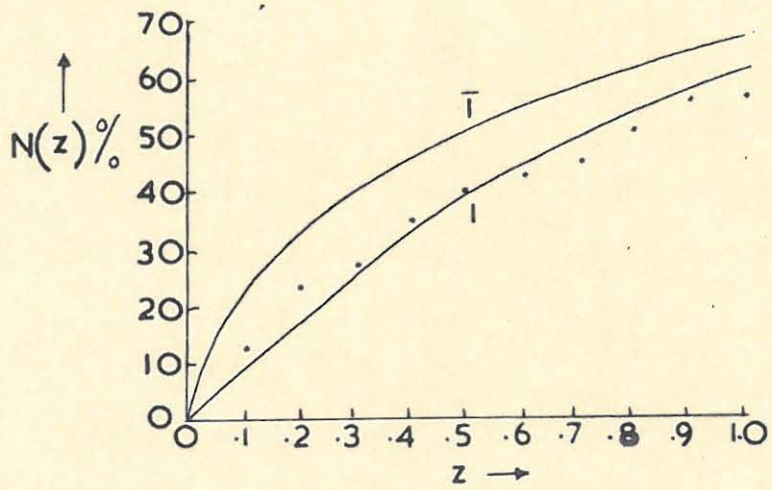

Fig 1.18

Fig 1.19

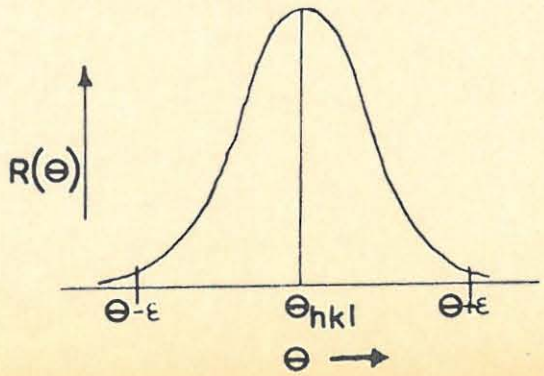

densities are equal.

(ii) Photometry based on scattering. Bretano[5] devised a method of photometry which depends on the amount of light scattered by the film. The amount of light scattered by silver particles is proportional to the number of particles which is in turn proportional to the X-ray intensity. This only holds up to the region where more than one quantum is received by the same grain. In this favourable region the light scattered by a given area of film is proportional to the integrated intensity.

(iii) The "Dawton Positive Print Method".[6] This method depends on the possibility, well known in ordinary photography, of making a perfect image of an object. By controlling the entire photographic procedure, the resulting photographic image should be such that each point on it should reflect the same as the corresponding point on the original object. In X-ray photography this result can be attained by preparing a positive print of a suitably developed X-ray negative under carefully controlled conditions of exposure and development. By matching the negative and positive processes the positive print consists of a collection of transparent spots on a black background. The total transmission of each spot is proportional to the integrated X-ray intensity which reaches the spot on the original film.

(iv) Scanning methods. Robertson and Dawton[7] devised a completely different method for measuring the integrated intensities of spots on a photograph. Their method works on the principle of a rapid scan of the X-ray reflection, similar to the scanning used in television. The spot on the X-ray film is scanned by a small spot of light which is passed into a photocell followed by valve amplification. The output from the valve is proportional to the optical transmission of the film. This output is fed into a non-linear electrical circuit which, in effect, transforms the light received by the photocell to the density and hence to the X-ray intensity of the spot.

1.3 (c) The correction of intensities.

The intensity of an X-ray reflection is controlled by several factors which fall into two main categories:-

(i) the geometrical factors: Lorentz, polarization and multiplicity;

(ii) the physical factors: extinction, absorption and thermal vibration.

Each of these will be mentioned in turn.

The Lorentz factor, L, expresses the relative time any crystal plane spends within the narrow angular range over which reflection occurs. In terms of the reciprocal lattice concept, each "point" of the reciprocal lattice has a finite size and as it rotates through the sphere of reflection each point spends a

finite time passing through the surface of this sphere. This factor varies with the type of photograph. For the equatorial reflections on a normal rotation photograph it is $\frac{1}{\sin 2\theta}$. Polarisation, which occurs on reflection, causes a diminution of the intensities of X-rays with increasing $\angle$ of reflection. The intensity of any reflection is reduced by this effect to the fraction $\left(\frac{1 + \cos^2 2\theta}{2}\right)$. The multiplicity factor only arises in the methods of recording X-rays which cannot separate certain reflections $h_1k_1l_1$, $h_2k_2l_2$ ..... $h_mk_ml_m$, resulting in the reflection having total energy

$$E_{Total} = E_{h_1k_1l_1} + E_{h_2k_2l_2} \ldots\ldots = \sum_j E_{h_jk_jl_j}$$

When the energies are symmetrically equivalent we have

$$E_{Total} = mE_{hkl}$$ m is the multiplicity factor.

In the Weissenberg method, however, only one plane of the crystal reflects to a particular position on the photograph, therefore $m = 1$.

Most actual crystals are imperfect. A crystal behaves as if it consisted of a number of blocks of the order of 10^{-5} cm in diameter, and hence in structure determination it is usually safe to assume that the intensity of a reflection is proportional to the square of the structure amplitude. If the crystal is not ideally imperfect but consists of rather large lattice blocks, the intensities of the reflections are proportional to a power of F between 1 and 2; this is "primary extinction". "Secondary extinction" affects only the strongest reflections

- and is due -

and is due to the fact that the top layer of a crystal reflects away an appreciable portion of the primary beam. The strongest reflections are thus experimentally less strong than they should be in comparison with the weaker reflections. Extinction is very difficult to allow for experimentally because it depends on the physical perfection of the crystal. Primary extinction is rare, while secondary extinction can be kept low by using small crystals.

Absorption occurs in small crystals to a large extent, and it is important that it should not be ignored. It has the effects of diminishing the intensities at small $\angle$'s much more than those of the "back reflections". Corrections have been calculated for cylindrical and spherical specimens and it is advantageous to have regularly shaped crystals in order to apply the absorption correction accurately.

Finally a comment on the effect of the thermal vibrations of the atoms on X-ray reflections. They have the effect of lowering the intensity of the diffracted beam particularly for the more closely spaced planes, where the atomic displacement may be comparable with the plane spacing. The effect increases with the $\angle$ of reflection and with rising temperature.

The corrections applied to an imperfect crystal may now be gathered together and if relative intensities are calculated, then the following equation holds for a normal beam rotation photograph (equatorial layer)

- Intensity -

$$\text{Intensity} \propto F^2 \, m \, \frac{(1 + \text{Cos}^2 2\theta)}{(\sin 2\theta)} \, TA \qquad \ldots\ldots \quad 1.16$$

F = structure amplitude
T = temperature factor
A = absorption factor

For any particular crystal all these factors are tabulated in the International Tables and Intensities can easily be converted to their respective structure factors.

1.4 FOURIER SYNTHESIS.

1.4 (a) The structure factor.

It can be shown that the wave scattered by a crystal can be characterised by a complex quantity whose magnitude is the amplitude of the scattered wave and whose direction in the complex plane is determined by the phase of the scattered wave. Since this quantity depends on the arrangement of matter in the crystal, it is called the "structure factor". The composition of the structure factor is shown in Fig. 1.20.

F is the resultant of the waves having amplitudes f_1, f_2 ... and phases ϕ_1, ϕ_2 ... and may be written as

$$F_{hkl} = f_1 e^{i\phi_1} + f_2 e^{i\phi_2} + \ldots f_j e^{i\phi_j}$$

$$= \sum_j f_j e^{i\phi_j} \qquad \ldots\ldots\ldots \quad 1.17$$

the summation is taken over the J atoms of the unit cell.

ϕ_j can be expressed as a function of the fractional coordinates x_j, y_j, z_j.

- therefore -

$$\therefore \quad F_{hkl} = \sum f_j e^{i2\pi(hx_j + ky_j + lz_j)} \quad \ldots\ldots\ldots \quad 1.18$$

For the purpose of computation it is convenient to express the structure factor in terms of its real and imaginary components. From Fig. 1.20 :

$$F_{hkl} = |F_{hkl}| \cos \phi + i |F_{hkl}| \sin \phi \quad \ldots\ldots\ldots \quad 1.19$$

$$\therefore \quad F_{hkl} = \left(\sum_j f_j \cos \phi_j \right) + i \left(\sum_j f_j \sin \phi_j \right)$$

$$\ldots\ldots\ldots \quad 1.20$$

1.20 can be rewritten as an explicit function of the atom coordinates,

$$F_{hkl} = \left(\sum_j f_j \cos 2\pi(hx_j + ky_j + lz_j) \right) + i \left(\sum_j f_j \sin 2\pi(hx_j + ky_j + lz_j) \right) \quad \ldots\ldots\ldots \quad 1.21$$

As an abbreviation it is convenient to write (Fig.1.21)

$$A = \cos \phi$$

$$B = \sin \phi \quad \ldots\ldots\ldots \quad 1.22$$

Hence 1.20 can be written as

$$F_{hkl} = \left(\sum_j f_j A_j \right) + i \left(\sum_j f_j B_j \right) \quad \ldots\ldots\ldots \quad 1.23$$

It follows that

$$A = \cos 2\pi(hx + ky + lz)$$

$$B = \sin 2\pi(hx + ky + lz) \quad \ldots\ldots\ldots \quad 1.24$$

<u>The phase of the structure factor</u>.

Fig 1.20 shows that the phase of the structure

factor can be computed from

$$\tan \phi_{hkl} = \frac{\sum_j f_j B_j}{\sum_j f_j A_j} \qquad \ldots\ldots\ldots \quad 1.25$$

$$\cos \phi = \frac{\sum_j f_j A_j}{F_{hkl}} \qquad \ldots\ldots\ldots \quad 1.26$$

$$\sin \phi = \frac{\sum_j f_j B_j}{F_{hkl}} \qquad \ldots\ldots\ldots \quad 1.27$$

When B = 0 the phase $\angle\ \phi$ degenerates to 0 or π.
This amounts to giving a sign to the structure factor
namely: when $\phi_{hkl} = 0$, F_{hkl} is +

when $\phi_{hkl} = \pi$, F_{hkl} is -

The sign formation is required when a structure is to be elucidated by Fourier methods.

1.4 (c) Fourier Summation.

In order to follow the relationship between the structure factors and the electron density in the unit cell, we use Fourier's theorem. This was first recognised as applicable to crystal structure analysis by W. H. Bragg[9].

Any continuous periodic function f(x) can be represented as an infinite series of cosine and sine terms.

$$f(x) = a_0 + a_1 \cos x + a_2 \cos 2x + \ldots\ldots\ldots$$
$$+ b_1 \sin x + b_2 \sin 2x + \ldots\ldots\ldots$$

- which may -

which may be written $f(x) = a_o + \sum_{-\infty}^{+\infty} (a_n \cos nx + b_n \sin nx)$ 1.28

This function repeats itself every $x = 2\pi$

The idea may be extended to three dimensions.

A continuous three dimensional function $f(x, y, z)$ which repeats itself every $x = 2\pi$, $y = 2\pi$, $z = 2\pi$ can be written as

$$f(x, y, z) = a_{ooo} + \sum_{p=\infty}^{\infty} \sum_{q=\infty}^{\infty} \sum_{r=\infty}^{\infty} [a_{pqr} \cos(px + qy + rz) + b_{pqr} \sin(px + qy + rz)] \quad ..... \quad 1.29$$

it being understood that the term for $p = q = r = 0$ be omitted from the bracketed terms.

This equation is adaptable to the case of a continuously variable electron density $\rho(x, y, z)$ which repeats every a, b, c along the axes of x, y, z.

∴ the series becomes

$$\rho(x, y, z) = a_{ooo} + \sum_{-\infty}^{+\infty} \sum_{-\infty}^{+\infty} \sum_{-\infty}^{+\infty} [a_{pqr} \cos 2\pi(px + qy + rz) + b_{pqr} \sin 2\pi(px + qy + rz)] \ldots \quad 1.30$$

where x, y, z are the practical coordinates of atoms in the unit cell.

It can be shown [10] that the relation between the coefficients a_{pqr}, b_{pqr} and the structure factors is simple and gives rise to the following expression for the observed electron density $\rho(x, y, z)$ at any point

- in the -

in the unit cell.

$$\rho(x, y, z) = \frac{1}{V}\left\{F(000) + \sum_{-\infty}^{+\infty}\sum_{-\infty}^{+\infty}\sum_{-\infty}^{+\infty} |F(hkl)\ obs|\ x \right.$$
$$\left. \cos\left[2\pi(hx + ky + lz) - \phi(hkl)\right]\right\} \quad \ldots\ldots \quad 1.31$$

where, V = volume of the unit cell,

$F(000)$ = number of e's in the unit cell,

$\phi(hkl)$ = phase $\measuredangle$ of the reflection hkl.

Ideally the summation of the electron density equation should be carried out for an infinite number of terms but in practice only those $F(hkl)_{obs}$ values which are available from intensity measurements can be used. If only a few $F(hkl)_{obs}$ values are used there will be a termination-of-series error in the computed values of the electron density map, and the resulting atomic peaks in the map will be poorly resolved. The labour of computing the electron density, at regular small intervals (say 1/60th of cell edges) throughout the unit cell is very great and will take several hundred hours if only a desk calculator is used. For this reason computer methods are widely employed nowadays.

In practice the electron density is computed at intervals of 1/60th or 1/120th of the unit cell edge . One usually computes a two dimensional electron density projection of the crystal when working with relatively simple structures. The unit cell projection is divided up into 60 (or 120) intervals along the edges and the calculated electron density is plotted

on the correct point of the drawn network. Contours may then be drawn at suitable intervals, and the result is an electron density map, the atoms being indicated by a series of peaks on the map.

The magnitudes of the F's can be determined from the measured intensities, but there is no experimental means of observing the phases ϕ_{hkl}. Thus the data for computing a Fourier synthesis are insufficient and it appears that crystal structures are indeterminate due to the unknown phases. This constitutes the "phase problem" of X-ray crystallography which can be solved, within certain limits, by application of the Patterson function.

1.5 THE PATTERSON AVERAGING FUNCTION.[11]

1.5 (a) Theory.

Patterson derived a function in the form of a Fourier series depending on the $|F_{hkl}|^2$'s alone, which are available directly from intensity measurements. This kind of function can be derived by forming products of each F_{hkl} with its complex conjugate. These products can be devised from products in the electron-density function.

The Fourier representation of the electron density at a fractional coordinate x of a one dimensional structure of period a is

$$\rho(x) = \frac{1}{a} \sum_{h=-\infty}^{+\infty} F_h \, e^{-i2\pi hx} \qquad \ldots\ldots\ldots \quad 1.32$$

The electron density at another point $x + u$ is

$$\rho(x + u) = \frac{1}{a} \sum_{h=-\infty}^{+\infty} F_h \, e^{-i\, 2\pi h(x + u)} \qquad \ldots\ldots\ldots \quad 1.33$$

The product of these is

$$\rho(x)\rho(x + u) = \left(\frac{1}{a} \sum_{h-\infty}^{+\infty} F_h \, e^{-i2\pi hx} \right) \left(\frac{1}{a} \sum_{h=-\infty}^{+\infty} F_h \, e^{-2\pi h(x + u)} \right)$$

$$\ldots\ldots\ldots \quad 1.34$$

It can be shown that the <u>average</u> electron density product for points separated by the chosen interval u is

$$A(u) = \frac{1}{a} \sum_{h=-\infty}^{+\infty} \frac{1}{a} (F_h F_{-h}) \, e^{i2\pi hu} \qquad \ldots\ldots\ldots \quad 1.35$$

F_{-h} is the complex conjugate of F_h.

Expressing F as the sum of its real and imaginary parts

$$F_h = A + iB$$

$$F_{-h} = A - iB$$

then $$F_h F_{-h} = A^2 + B^2 = |F_h|^2 \qquad \ldots\ldots\ldots \quad 1.36$$

Thus the Fourier series can be written as

$$A(u) = \frac{1}{a^2} \sum_{h-\infty}^{+\infty} F_h{}^2 \, e^{i2\pi hu} \qquad \ldots\ldots\ldots \quad 1.37$$

This means that the average electron density product at a selected fractional separation u can be found from a

Fourier series having $|F_h|^2/a^2$ as coefficients.

The function may also be derived in two- and three-dimensional form, e.g. for a two dimensional form the Patterson function will be

$$A(u,v) = \frac{1}{S^2} \sum_{h=-\infty}^{+\infty} \sum_{k=-\infty}^{+\infty} |F_{hko}|^2 e^{i2\pi(hu + ky)} \quad \ldots\ldots\ldots \quad 1.38$$

where S = area of the unit cell projection.

1.5 (b) <u>The interpretation of the Patterson map</u>.

The Patterson map is plotted in the same way as a Fourier map, but the ensuing peaks are interpreted differently. Patterson showed that a Fourier synthesis employing values of F^2 yields peaks at vector distances from the origin which are equal to the vector distances between pairs of atoms in the cell. The relation between peaks in the Patterson synthesis and the corresponding atoms is conveniently discussed for the two dimensional Patterson which is the most practical form of the function. Consider the projection ab of the unit cell of a crystal having atoms ABC as shown in Fig. 1.22. The resulting Patterson function will give rise to peaks A′, B′ and C′ as shown in Fig. 1.22 such that OA′ = AB, OB′ = BC and OC′ = AC. The height of each peak is proportional to the product of the scattering powers of the two atoms concerned. The Patterson function always has a large peak at the origin which signifies the electron density product of each atomic peak with itself.

The usefulness of the Patterson synthesis is subject to certain limitations which are inherent in all vector diagrams. In the case where a structure contains several atoms whose atomic distances do not vary by very much, some of the vectors will be very close together and the individual peaks will not be resolved. Further, the number of peaks in a vector map rises rapidly with the number of atoms in the cell. If there are N atoms in the cell, then there will be $N(N-1)$ peaks in the vector map.

One way to overcome the difficulty of interpreting the Patterson synthesis is to have a crystal which contains a small number of heavy atoms per unit cell. The Patterson peaks due to these atoms then stand out against a background of overlapping smaller peaks, thus giving the coordinates of the heavy atoms. This allows a large number of the phases to be calculated and the remaining atoms can be subsequently located by direct Fourier methods.

1.5 (c) <u>The minimum function</u>.[12]

The Patterson synthesis is essentially the vector set of the electron density, so that it is possible to analyse Patterson syntheses by vector-set methods. This implies finding suitable functions which will automatically find images in a Patterson synthesis. Such a function is called an image-seeking function. The desired characteristics of such a function can be seen from Fig. 1.23. This figure shows the points of a vector set

- assembled -

Fig 1.20

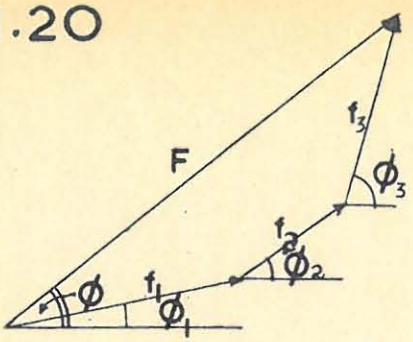

Fig 1.21

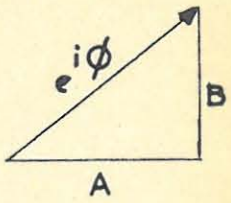

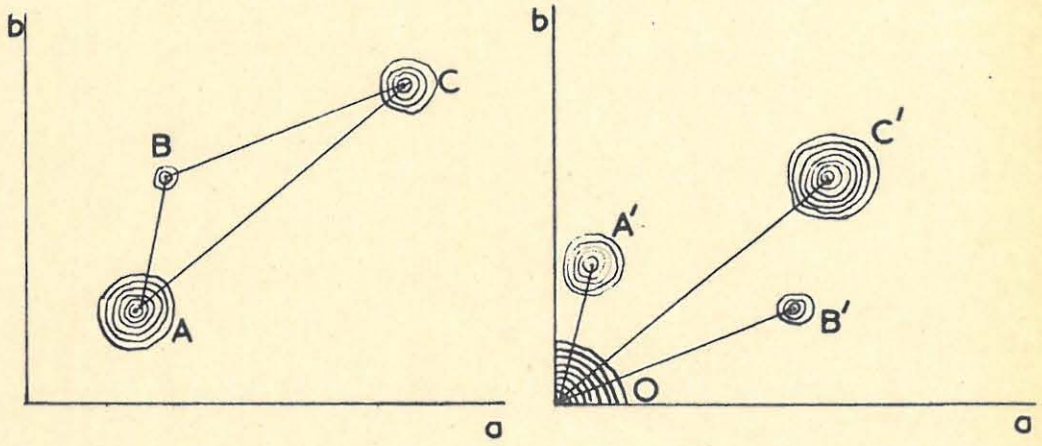

Fig 1.22

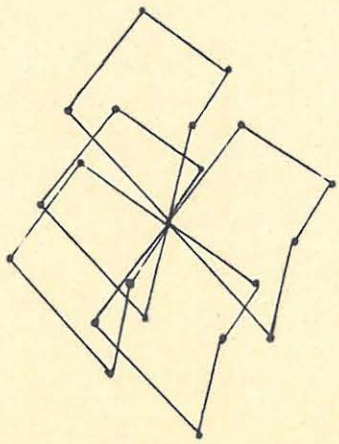

Fig 1.23

assembled into a set of n n-gons (n = 5 in this case).

Let us suppose that the solution is known, i.e. that one knows the relative positions of the vertices of one polygon. The relative position can be defined by the origin plus (n-1) other points, namely 000, $u_1v_1w_1$, $u_2v_2w_2$, $u_3v_3w_3$, $u_4v_4w_4$ in this case. The polygon is now moved to another location of the cell by a translation having components xyz. The new location of the coordinates of the vertices are

$$\left.\begin{array}{rcl} 000 & + & xyz \\ u_1v_1w_1 & + & xyz \\ \vdots & & \\ u_4v_4w_4 & + & xyz \end{array}\right\} \qquad \text{(i)}$$

Then a desirable image-seeking function would be one which would have a value of zero when the translation xyz does not cause the original polygon to coincide with one of its images, but which would have a high value when the translation does cause such a coincidence. Such a function is the minimum function, which is defined as the minimum value of the several Patterson values which occur at the vertices of the polygon used to search for images of itself.

If the original polygon has p vertices at 000, $u_1v_1w_1$ ..... u_{p-1}, v_{p-1}, w_{p-1}, then on translating the polygon through xyz, its vertices have p sets of coordinates similar to those listed in (i). The minimum function may be then designated by

$$- Mp\ (xyz) = -$$

$$Mp(xyz) = M\,[P(000 + xyz),$$
$$K_1\ P(u_1v_1w_1 + xyz),$$
$$\vdots$$
$$K_{p-1}\ P(u_{p-1}, v_{p-1}, w_{p-1} + xyz)] \quad \ldots\ldots\ldots \quad 1.39$$

The K's are constants which normalise the values of the Patterson function at the vertices of the polygon to the same value.

A simple application of the minimum function is to images composed of centrosymmetrical interactions. The relation between the electron density and M_2 is demonstrated by Fig. 1.24.

Fig. 1.24A shows a simple centrosymmetrical fundamental set while 1.24B shows its Patterson projection.

Note that all centrosymmetrical interactions, aa and bb have single weight while the others are multiple.

If a line from the origin to aa is established as a line whose images are to be found, then the minimum values at the ends of the line when in image position have the form

$$^{a}M_2\,(xyz) = 2\rho_a\rho(xyz) \quad \ldots\ldots\ldots \quad 1.40$$

The only exception occurs for images containing the origin for which the coefficients 2 in 1.40 does not appear due to the unit nature of point aa.

If we want to seek for images of bb we obtain the vector set shown in 1.24C and the minimum function may be

- written as -

written as

$$ {}^{b}M_2\,(xyz) = {}^{2}\rho_b\,\rho(xyz) \qquad \ldots\ldots\ldots \quad 1.41 $$

Buerger has shown that due to overlaps of "squared atoms" 1.40 and 1.41 should be written as inequalities, which may in turn be combined to give a more powerful inequality.

$$ \frac{1}{2\rho_a}\,{}^{a}M_2\,(xyz) \geqslant \rho\,(xyz) \qquad \ldots\ldots\ldots \quad 1.42 $$

$$ \frac{1}{2\rho_b}\,{}^{b}M_2\,(xyz) \geqslant \rho\,(xyz) \qquad \ldots\ldots\ldots \quad 1.43 $$

$$ M\left[\frac{1}{2\rho_a}\,{}^{a}M_2\,(xyz);\ \frac{1}{2\rho_b}\,{}^{b}M_2\,(xyz)\right] \geqslant \rho\,(xyz) \qquad \ldots\ldots \quad 1.44 $$

1.44 may be represented by Fig. 1.24D. This shows that the combination of two minimum functions seeking line images is equivalent to a minimum function seeking quadrilateral images. Thus we may write from 1.42, 1.43, 1.44

$$ M\left[\frac{1}{2\rho_a}\,{}^{a}M_2\,(xyz);\ \frac{1}{2\rho_b}\,{}^{b}M_2\,(xyz)\right] = {}^{ab}M_4\,(xyz) \qquad \ldots\ldots\ldots \quad 1.45 $$

and 1.44 shows

$$ {}^{ab}M_4\,(xyz) \geqslant \rho\,(xyz) \qquad \ldots\ldots\ldots \quad 1.46 $$

The practical application of the minimum function.

Suppose that a two dimensional Patterson synthesis is to be decomposed by means of the minimum function. If the centrosymmetrical image point has coordinates u, v then the minimum value of the function ${}^{uv}M_2(xy) = M\,[P(xy);\ P(u + x,\ v + y)]$ can be determined from examining the numerical values of the Patterson function at all pairs of point xy and x + u,

y + v and noting the minimum value for each such pair.

In order to have the origin of x and y in the resulting map coincide with an inversion centre, Fig. 1.24A and B shows that this minimum value should be recorded on the map of the minimum function at $\frac{1}{2}(u + x)$, $\frac{1}{2}(v + y)$ instead of at xy. This new map contains a set of definite values of the minimum function $uv_{M2(xy)}$. This analytical method has the disadvantage, however, of being discontinuous.

A continuous procedure for finding M_2 requires a contoured Patterson map. Two Patterson syntheses are prepared and they are contoured in colour. The tracings are superimposed, and the minimum function can be contoured by tracing on a third sheet the contours from the two underlying Patterson maps which show the minimum values. This now gives the minimum function M_2. Maps of the minimum function of higher rank may also be derived. In practice this is done by tracing two M_2 maps based on two different centrosymmetrical image points and combining these to form an M_4 map. This procedure may be extended when necessary. The firal result is a rough electron density map which gives the approximately correct position of the atoms, which may be recognised by the relative heights of the peaks.

1.5 (d) <u>The Patterson Box</u>.

An optical transformation from crystal structure to the Patterson projection can be carried out with the aid of a Patterson Box. This was shown by Robertson[13], Hägg[14], Bragg[15]

- and Vand[16] -.

and Vand[16]. The theory of Robertson's method is shown in Fig. 1.25. AA′, BB′, CC′ are planes at right angles to the paper. A diagram of the crystal structure, is placed in the plane AA′ with atoms in positions marked 1, 2 etc. A duplicate diagram on a smaller scale is placed in the plane BB′. The scale is such that the rays 11′, 22′ etc converge at O on CC. For simplicity let BB′ be halfway between AA′ and CC′, then the map on BB′ is on half scale of that on AA′.

The ray from any atom in AA′ to the same atom in BB′ arrives at O in CC′, which is the Patterson origin.

The ray from any atom (say 1) in AA′ to a different atom in BB′ (say 2′) arrives at a point in CC′ (point 12′) whose distance from O is equal to the interatomic distance 1, 2′ in the crystal structure. Thus the plane CC′ shows the location of the Patterson peaks corresponding to the atom locations in AA′.

The construction is equally valid in two dimensions, and the points in CC′ will constitute a vector map of the points in AA′.

Hägg pointed out that if the atoms in AA′, BB′ are represented by holes punched in cardboard, the pattern produced at CC′ will represent the Patterson peaks, and the total intensity in a Patterson Peak can be correctly reproduced by making the holes in AA′ and BB′ proportional to numbers of electrons in the corresponding atoms. The Patterson Box thus affords a rapid method of solving a simple crystal structure by trial and error methods. Essentially one makes a series of cards of possible structures and compares the resulting Patterson projections with the calculated Patterson projection, the correct structure giving the required Patterson pattern.

Fig 1.24

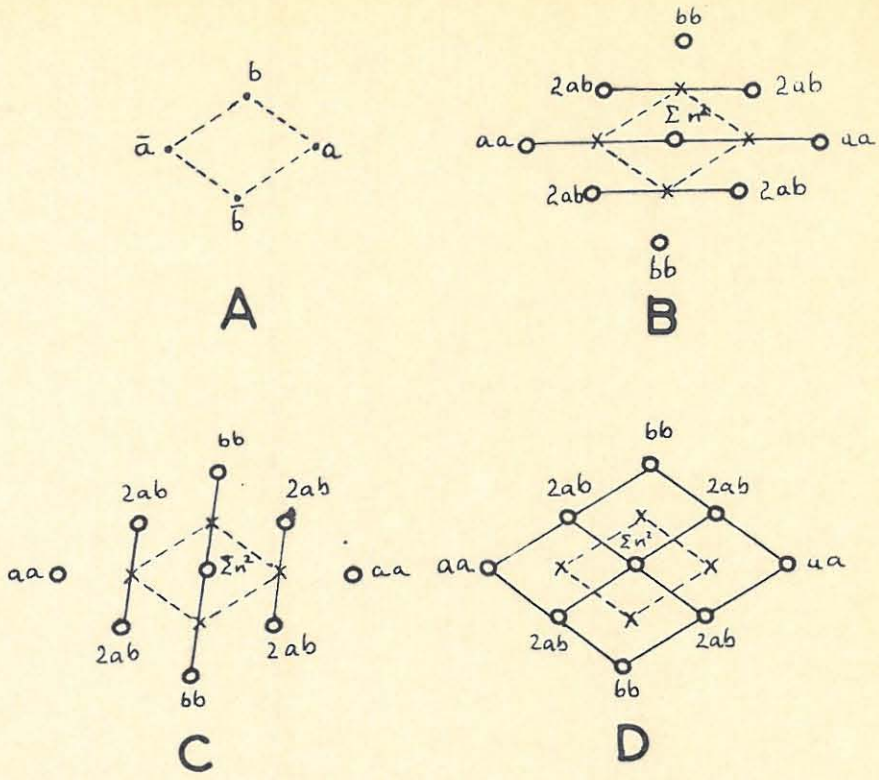

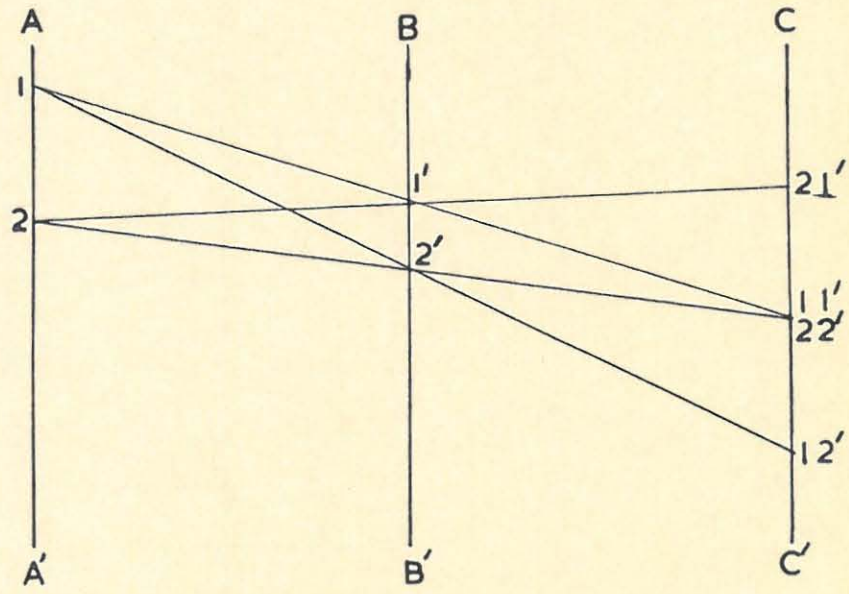

Fig 1.25

2. PREVIOUS WORK ON $CsMnO_4$.

W. Muthmann[17] prepared $CsMnO_4$ crystals from the solution obtained by treating an aqueous solution of $Ba(MnO_4)_2$ with an aqueous solution of Cs_2SO_4, and filtering off the precipitated $BaSO_4$. He found by optical methods that the dark violet, orthorhombic, bi-pyramidal crystals have the axial ratio a:b:c = 0.8623:1:0.6853, and gave 3.5974 for the specific gravity and 70.042 for the molecular weight. W. Muthmann also found that the salt was sparingly soluble in cold water and freely soluble in hot water.

R. J. Meyer and H. Best[18] prepared $CsMnO_4$ from the liquid obtained by treating an aqueous solution of $AgMnO_4$ with an aqueous solution of CsCl and filtering off the precipitated AgCl.

E. Moles and M. Crespi[19] obtained the salt from a solution of 3.2 g of $KMnO_4$ and 4 g $CsNO_3$ in 50 ml of water at 60°C and cooled to 0°C. They gave 3.5 g for the specific gravity.

I.I. Saslawsky[20] gave 3.55 for the specific gravity and calculated the contraction which occurs in forming the salt from its elements.

3. OBJECT OF RESEARCH.

The object of the research was to find the crystal structure of $CsMnO_4$ by X-ray diffraction methods.

4. APPARATUS.

4.1 THE X-RAY GENERATORS AND ACCESSORIES.

Two generators were used in the project:

(a) A Philips PW 1009, employing a sealed X-ray tube, and operated at a voltage of 40 Kv and a tube current of 20 mA. A copper target was used.

(b) A Hilger and Watts Microfocus Generator, which has an X-ray tube which is continuously evacuated by an oil diffusion pump backed by a rotary oil pump. The generator was operated at 50 Kv and 3 mA, and a demountable copper target was used.

The Laue camera and the rotation and Weissenberg goniometers used were made by Unicam. The integrating Weissenberg was made by Stoe (Heidelberg).

The goniometer heads on the instruments are interchangeable and the rotation goniometer has an optical goniometer.

The films used were Kodak "Industrex D" for the determination of intensities and Kodak "Kodirex" for other purposes. The Kodirex films were developed in D 19 b developer for 5 minutes at 20°C, immersed for 5 seconds in a stop bath of 3% acetic acid, and fixed for 5 minutes with agitation in Kodak X-ray fixer. This was followed by a 10 minute suspension in the fixer. The films were then washed in running water for 30 minutes and subsequently dried in a fume cupboard in order to avoid dust.

- 4.2 The -

4.2 THE PHOTOMETER.

The Steinheil Densitometer used by Woods[21] was used to measure the intensities of the diffraction spots.

The instrument is shown in Fig. 4.1. The light source consisted of a Philips cold lamp rated at 50 watts which was cooled by a stream of compressed air. 8 volts was supplied across the lamp from a bus battery which was in turn charged by a battery-charger while in use. The voltage was kept constant by means of a variable resistance in the circuit.

The light transmission was measured by a photo-emissive search head connected to an electronic photometer, both manufactured by the Photovolt Corporation of New York. The photocell was covered by a head having an adjustable aperture enabling the measurement of spots of different size. While not in use, the search head, consisting of the photo-cell and lead-wires, was kept in a desiccator over silica gel. This was done so as to avoid the break down of electrical insulation which occurs due to atmospheric moisture. The whole system was very stable and gave reproducible results in the measurement of intensities.

Fig 4.1

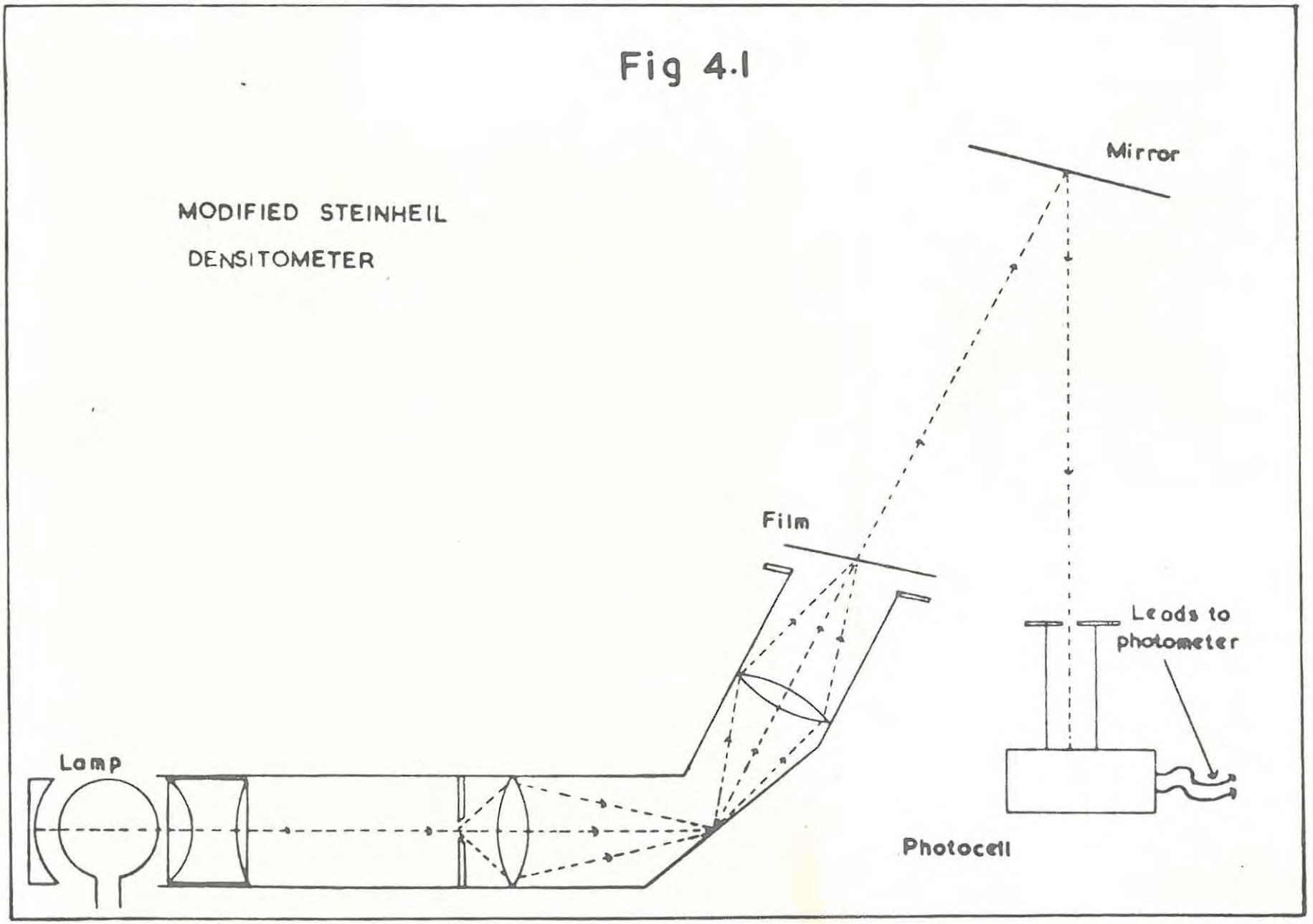
MODIFIED STEINHEIL
DENSITOMETER
Mirror
Film
Leads to
photometer
Lamp
Photocell

5. EXPERIMENTAL.

5.1 PREPARATION OF $CsMnO_4$ CRYSTALS.

Small impure crystals of caesium permanganate were obtained by adding an aqueous solution containing 5 g of $CsNO_3$ to an aqueous solution containing 4 g of $KMnO_4$, both solutions being at 60°C. The reagents were of AnalaR quality. The solution thus obtained cooled to 0°C and the crystals obtained were purified by recrystallising four times from distilled water. A great deal of difficulty was encountered in growing suitable crystals. The methods employed are listed below:

(i) Cooling a saturated solution from 90°C to room temperature in a bolt-head flask (a) slowly, (b) fast (using an ice bath). Rough uneven crystals were obtained.

(ii) Cooling a saturated solution from 70°C to room temperature in a thermos flask. The crystals obtained were too small to use.

(iii) Pouring a saturated solution at 60°C on a perspex surface. Very rough crystals were obtained.

(iv) Heating a saturated solution to 80°C, cooling to room temperature, evaporating to 2/3 the original volume under an Infra-Red lamp and filtering through a cintered glass [No.4 porosity] filter. The filtrate, now comparatively free of nuclei was further evaporated to half the original volume under an Infra-Red lamp and allowed to cool to room temperature. It was then allowed to stand for 2-4 days, looking at it every few hours, until large enough crystals were formed. Suitable crystals were obtained.

(v) a refinement to the above method was carried out by using dust-free water and working in a dust-free laboratory. This method yielded more and better crystals than the above.

5.2 SELECTION OF MATERIAL SUITABLE FOR CRYSTAL STRUCTURE ANALYSIS.

5.2 (a) Choice of crystal size.

From consideration of elementary absorption theory it can be shown that:

$$I = I_o e^{-\mu t} \qquad \ldots\ldots\ldots \quad 5.1$$

where I = intensity of X-ray beam,

I_o = initial intensity of X-ray beam,

μ = linear absorption coefficient,

t = thickness of Xal traversed by X-ray beam,

and further that the optimum crystal size is of the order of $\mu/2$. Unfortunately it sometimes happens that the optimum thickness thus calculated is exceedingly small, due to a high μ, and a compromise has to be reached, taking into account the shape and size of the crystals available. Crystal size and shape are of importance because, as will become evident in the discussion later on, it is difficult to correct diffraction intensities for the absorption of the crystal. Usually crystals of approximately .1 - .2 mm in cross sectional diameter are appropriate for intensity determination, but the size should be checked by taking a preliminary zero-layer Weissenberg photograph. If the reflections near the centre line of the photograph show less intense centres this indicates that absorption is still high and a smaller crystal should be used.

5.2 (b) Defective crystals.

There are two ways in which a crystal may be seriously

defective: it may be twinned or it may be excessively imperfect.

Twinning - The basic difficulty with twins is that, in effect, one examines the interpenetrating reciprocal lattices of the individuals of the twin under the impression that one is dealing with the reciprocal lattice of a single crystal. This implies that one misjudges the point group symmetry, space group symmetry, the $|F_{hkl}|$'s and possibly the unit cell of the crystal too. Twinning may be suspected when studying characteristic extinctions. In general twinning has the effect of annulling extinctions, so that a crystal which appears to belong to a space group with few or no extinctions should be regarded with suspicion.

Crystal imperfection - What is regarded as a single crystal sometimes behaves as an aggregate of smaller crystals in sub-parallel orientation. This imperfection is due to growth, and the photographs from such crystals are characteristic. Each reflection consists of a main reflection accompanied by some satellite reflections. The photographs are quite unsuitable for intensity determination.

In the case of the particular compound being studied in this project, it was found that thin plate-like crystals of $CsMnO_4$ on long exposure to the atmosphere, curved considerably and gave Laue photographs showing streaky and ill defined reflections, presumably due to internal strain in the crystal. Laue photographs were subsequently used as a test before any photographs for intensity determination were taken.

5.3 OPTICAL GONIOMETRIC STUDY.

A goniometric study was carried out using a R. Fuess (Berlin) single circle optical goniometer. The readings obtained are only accurate to within 10 minutes of a degree because the crystals were very small and the reflections obtained were not always good. The readings obtained were:

the angle between (210) and $(2\bar{1}0)$ = $81^{\circ}50'$

$$\tan 40^{\circ}55\tfrac{1}{2}' = \frac{a}{b} = 1.734$$

the angle between (001) and (101) = $38^{\circ}16^{8}$

$$\tan 38^{\circ}16' = \frac{c}{a} = 0.789$$

the angle between (001) and (011) = $53^{\circ}52'$

$$\tan 53^{\circ}52^{8} = \frac{c}{b} = 1.370$$

the angle between (001) and (211) = $64^{\circ}24'$

$$a : b : c = 1.734 : 1 : 1.370$$

Muthmann quoted the values a : b :c = 0.8623 : 1 : 0.6853. These were evidently obtained using incorrect indices, because if the following indices are used with the experimental readings:

the angle between (110) and $(1\bar{1}0)$ = $81^{\circ}50'$

$$\tan 40^{\circ}55\tfrac{1}{2}' = 0.867$$

the angle between (001) and (012) = $53^{\circ}52'$

$$\tan 53^{\circ}52' = \frac{c}{b/2} = 1.370$$

$$a : b : c = 0.867 : 1 : 0.685 \quad \frac{c}{b} = .685$$

These compare closely to Muthmann's values.

A stereographic projection, and an accurate drawing of the crystal are shown on the next page. The radius of the stereogram is $2\frac{1}{2}$ inches.

Stereographic Projection of

CAESIUM PERMANGANATE

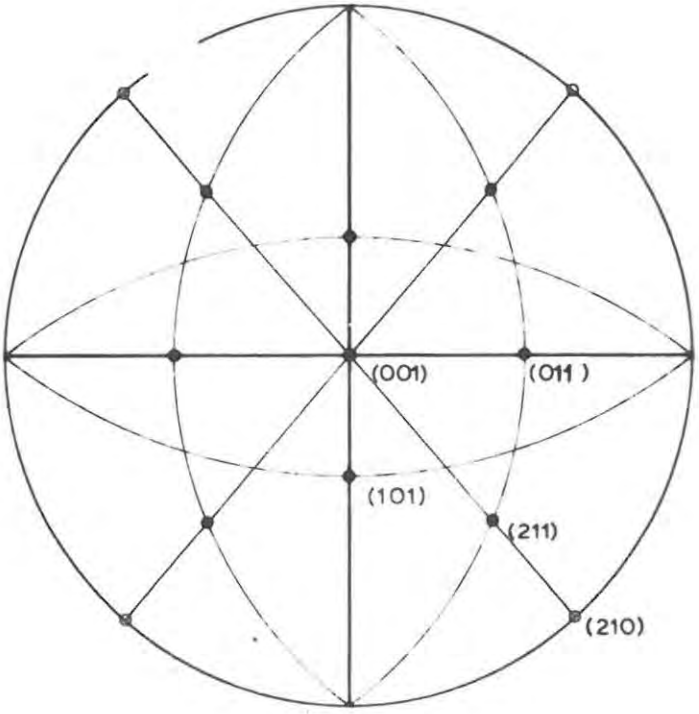

a	b	c
1·734	1	1·370

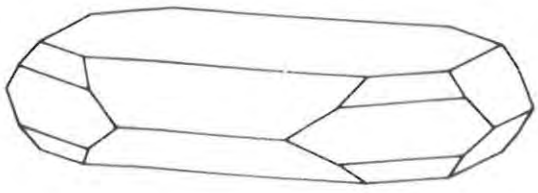

5.4 ACCURATE SETTING OF CRYSTALS.

When crystals had suitable faces, they were accurately set by means of the optical goniometer. However, when the faces of the crystals were imperfect and gave diffuse optical reflections or when the faces were too few, then the crystals were set by preliminary X-ray photographs. Several methods were used.

5.4 (a) Small angle oscillation photographs[23].

The crystal was set approximately parallel to the axis of rotation by optical methods, and a small angle ($10 - 15^{\circ}$) oscillation photograph was taken with one of the arcs of the goniometer head set parallel to the beam for the mean position of the crystal. The equatorial reflections are found to be on a curve, the shape of which shows how the crystal is mis-set. This is best appreciated in terms of the reciprocal lattice (Fig.5.1). In Fig. 5.1A. the c axis of the crystal is displaced from the rotation axis in the plane normal to the beam. The zero layer of the reciprocal lattice is tilted in the same way and its plane cuts the sphere of reflection as shown by the dots.

In Fig. 5.1B. the c axis of the crystal is tilted in the plane of the incident X-ray beam.

On the flattened out film the spots form on curves as shown in Fig. 5.1. When the displacement of the c axis has components in both directions, an intermediate curve is obtained (Fig. 5.1C). The angle α of the equatorial line gives the correction to be supplied to the corresponding arc.

This method is slow and not always satisfactory because

- sometimes -

sometimes very few spots occur on the photograph and it is very difficult to determine the shape of the curve and measure the angle α.

5.4 (b) Laue photographs.

A simple and quick method of setting a crystal is by using Laue photographs. This method can only be used for crystals of high symmetry. The crystal was set approximately by optical methods with one of the principal axes parallel to one of the goniometer arcs. A Laue photograph was then taken with one of the arcs parallel to the incident beam. The photograph then revealed directly the displacement of the component of the rotation axis perpendicular to the incident beam α_1 Fig. 5.2A.

The crystal was rotated through 90° and another Laue photograph taken, thus revealing the displacement α_2 of the rotation axis parallel with the other arc on the goniometer head, Fig. 5.2B.

This method has the advantage of being quick, but is not accurate to more than $\frac{1}{2}^{\circ}$, which is insufficient for taking good rotation and Weissenberg photographs.

5.4 (c) A third[24] method for setting crystals is to take three rotation photographs at slightly different angle settings, and hence work out the correct orientation by a simple graphical procedure. The shape of the zero layer line on the film was as shown in Fig. 5.3. The angle α for any setting was obtained from measurements of l and ϵ from the photograph, but it was found that the distance 2ϵ was difficult to judge on the film due to the

Fig 5.1

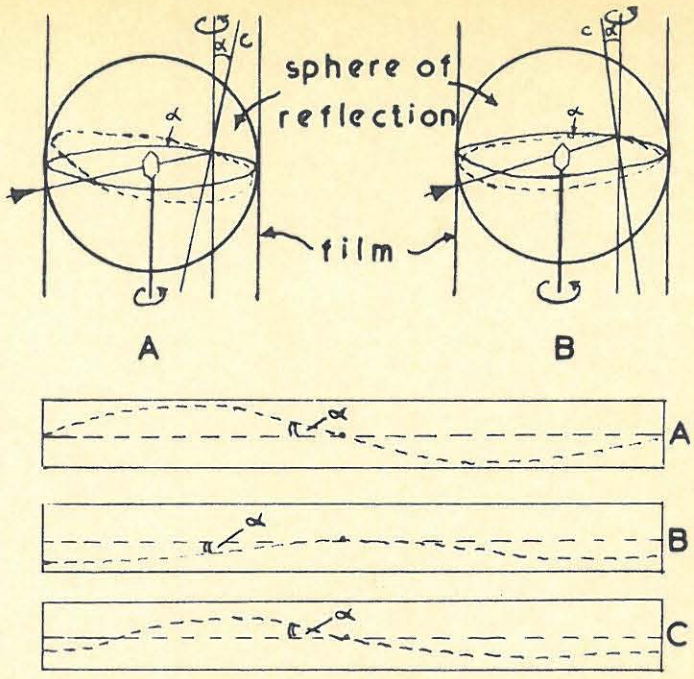

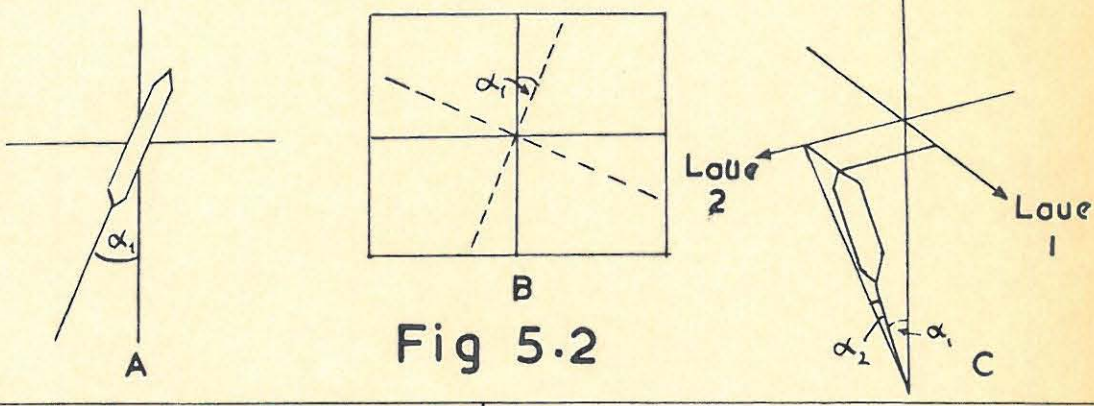

Fig 5.2

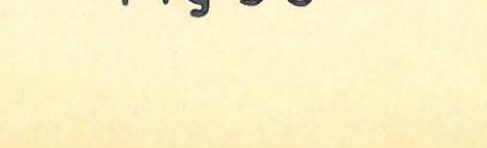

Fig 5.3

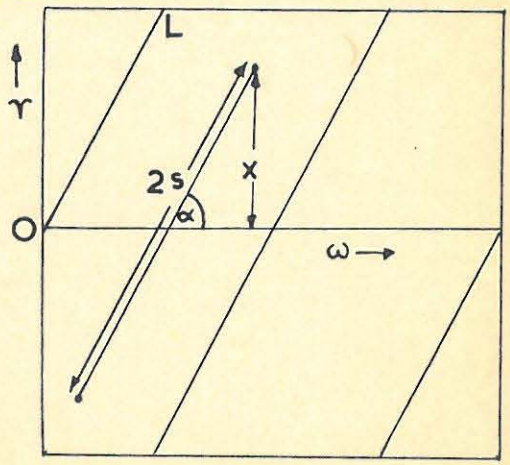

Fig 6.1

varying sizes of the spots, and the method proved to be generally unsatisfactory.

5.4 (d) The method finally used[25] consisted of taking a Laue photograph of a crystal on a cylindrical camera and having one of the arcs of the goniometer head parallel to the incident beam. A second photograph is superimposed on the first by turning the crystal through 180°. From this composite photograph it is possible to determine both arc errors and the direction of each can be deduced if one of the components of the photograph is given a longer exposure than the other. Hendershot[26] has shown that an angular error i_1 in the arc perpendicular to the beam,

$$\delta_{\perp} = R \sin 2\theta \sin i_1 \quad \ldots\ldots\ (i)$$

and for an angular error i_2 in the arc parallel to the beam,

$$\delta_{\parallel} = R(1 - \cos 2\theta) \sin i_2 \quad \ldots\ldots\ (ii)$$

$\delta_{\perp}$ $\delta_{\parallel}$ are distances of displaced points from the ideal position of the zero layer line at Bragg angle θ. R = radius of the camera.

Equations (i) and (ii) show that at $\theta = 45^{\circ}$, the value of $\delta_{\parallel}$ is half its maximum and that if $\delta_{\perp}$ is at its maximum. At $\theta = 90^{\circ}$, the value of $\delta_{\parallel}$ is a maximum and that of $\delta_{\perp}$ is zero. The displacement at $\theta = 45^{\circ}$ on one side of the film, is due to the sum, and on the other side to the difference of the errors in the two arcs. $(\delta_1 + \delta_2)$ and $(\delta_1 - \delta_2)$ can be measured at $\theta = 45^{\circ}$ on the film, and $\delta_{\perp}$ and $\delta_{\parallel}$ are obtained. For a camera of radius 2.865 cm, $2\delta_{\perp}$ and $2\delta_{\parallel}$ in mm are equal to the errors in degrees (i_1 and i_2 respectively) in the two arcs.

- The direction -

The direction of the erros for each arc can be found from comparing the curve of the zero line with the heavier exposure with the specimen curves given in the article.

The method proved to be very reliable, and was used frequently in the project.

5.5 LAUE PHOTOGRAPHS, ROTATION PHOTOGRAPHS, WEISSENBERG PHOTOGRAPHS.

5.5 (a) Laue photographs.

In order to establish the Laue class and the orthogonality of the crystal, six Laue photographs were taken as follows. The crystal was accurately set up with the a axis vertical, and perpendicular to the X-ray beam. A Laue photograph was taken with the incident beam parallel to the b axis. The crystal was then turned through 90° and a second Laue photograph was taken with the incident beam parallel to the c axis. Both photographs exhibited mm symmetry which proved that $a \perp b \perp c$. This result was checked by taking two other sets of photographs with the crystal set so that the b and c axes respectively were perpendicular to the X-ray beam.

Three specimen Laue photographs taken with the incident beam parallel to the a, b and c axes respectively are shown in Fig. 5.4. They all exhibit mm symmetry.

The Laue photographs were taken with the camera at a distance of 5.00 cm from the crystal. Kodak Industrex "D" film was used. The details of the Laue photographs are as follows:

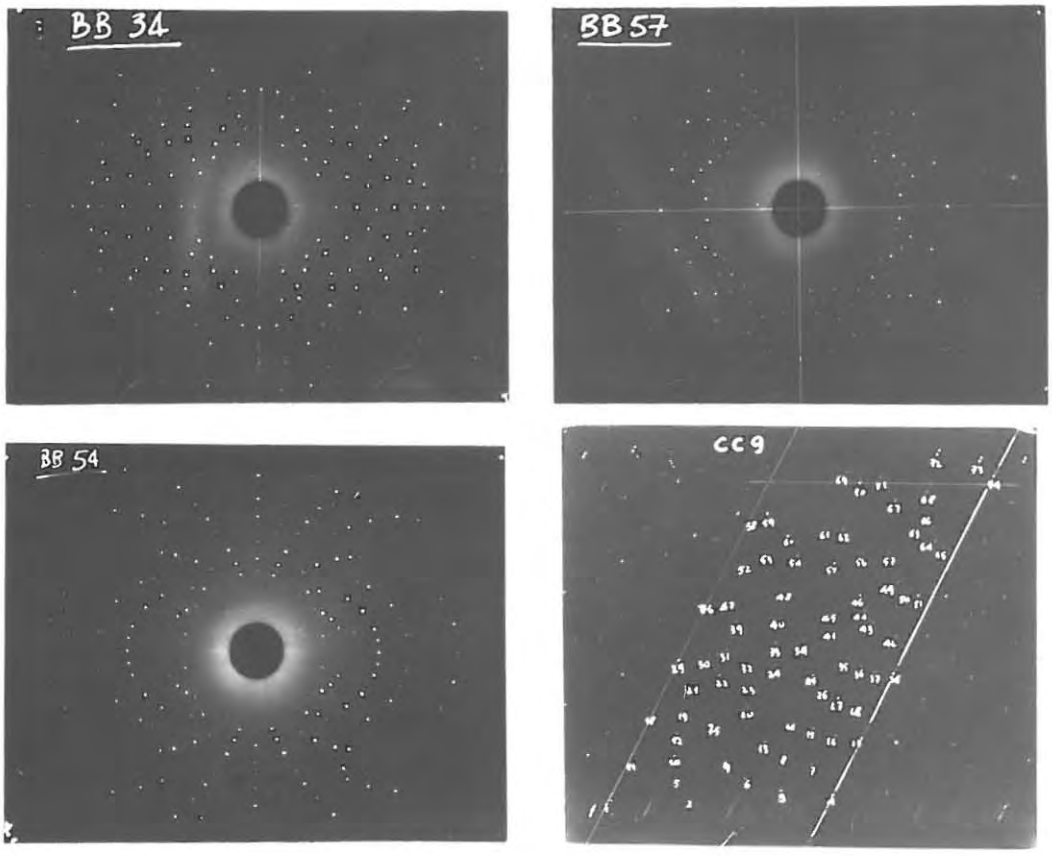

Fig 5·4

Photograph BB 34 - X-ray beam parallel to "a" axis - exposure 4 hours.

Photograph BB 57 - X-ray beam parallel to "b" axis - exposure 4 hours.

Photograph BB 54 - X-ray beam parallel to "c" axis - exposure 4 hours.

5.5 (b) Rotation photographs.

Rotation photographs of the crystal rotating about the three orthogonal axes were taken using two cameras of radii 3.00 cm and 5.73 cm respectively. The photographs taken on the smaller camera were used for the indexing of the reflections, while those taken on the larger camera were used for determining the magnitude of the unit cell parameters from layer line measurements.

Fig. 5.5 shows rotation photographs with the crystal rotating about the three orthogonal axes. Kodak Industrex "D" film was used. The details of the rotation photographs are as follows:

BB 47 rotation about "a" axis - exposure 8 hrs. Camera radius 3.00 cm.

BB 30 rotation about "b" axis - exposure 4 hrs. Camera radius 3.00 cm.

BB 43 rotation about "c" axis - exposure 8 hrs. Camera radius 3.00 cm.

BB 31 rotation about "b" axis - exposure 16 hrs. Camera radius 5.73 cm.

5.5 (c) Weissenberg photographs.

Zero layer normal beam and equi-inclination higher layer Weissenberg photographs were taken with the crystal oscillating

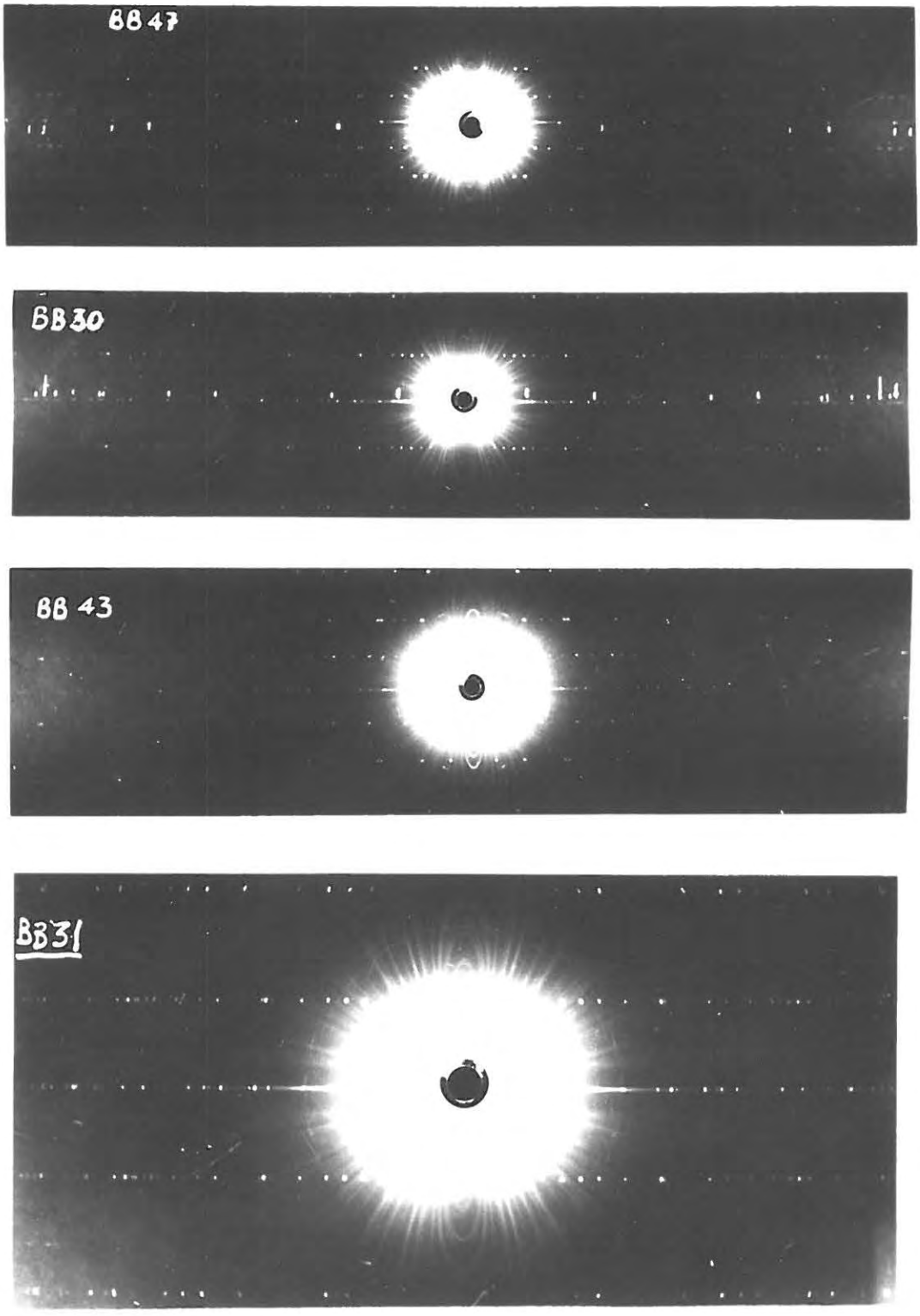

Fig 5.5

about the three orthogonal axes. Fig. 5.4 shows photograph cc 9 a zero layer Weissenberg photograph with the crystal oscillating about the b axis.

Kodak "Kodirex" film was used, the exposure being 10 hours on a camera of diameter 5.73 cm. Some of the spots are numbered to facilitate indexing.

5.6 THE DAWTON POSITIVE PRINT TECHNIQUE.[6, 27.]

The intensities of the X-ray reflections were measured using the Dawton positive print method. The theory of this method was outlined in the introduction (page 26). Buerger has shown that to make a positive print it is necessary that the photographic density D of the positive should be a linear function of the logarithm of the relative exposures of the negative (log E). This is the same as saying that the transmission T of the positive be a linear function of the relative exposure E of the negative.

The reciprocity law is obeyed by films exposed to X-rays hence, if the time factor is constant, the exposure is proportional to the intensity and thus the transmission of the spots on the positive will be proportional to the intensity on the negative. This is only true up to a limiting value of the density. Arising from this it can be shown[28] that if γ is the slope of the straight central part of the curve D vs log E, a condition for perfect reproduction can be shown to require that $\gamma_P \gamma_N = 2$. P and N refer to positive and negative. In choosing the correct materials and procedures required to obtain suitable positive prints, we must consider (i) the choice of X-ray

film to be used as negative and the determination of its γ curve, (ii) the development technique in order to develop the negative to a suitable γ-value, (iii) the choice of a film to be used as positive, (iv) the printing times for the positive so as to obtain a linear relationship between the transmission of the positive and the exposure of the negative. These factors are now discussed in turn.

(i) Two type of film were used as negative throughout the project: Industrex "D" and Kodirex. These films have relative speeds of 27 and 55 respectively and it was decided to use Industrex "D" because being the slower film it has finer grain and is less prone to background fogging. Industrex "D" film is normally developed for 5 minutes at 20°C in Kodak D 19b developer. From these conditions we obtain a γ value of 3 and consequently the positive film would have to be developed to a γ of 0.3

(ii) Kodak Commercial Ortho Sheet film was chosen for the positive print. It was decided to develop this to a value of $\gamma = 0.5$ and hence the γ of the Industrex "D" had to be lowered to a value of 2 in order to satisfy the condition $\gamma N \gamma P = 1$.
To obtain a lower contrast for the Industrex "D", shorter development times in D 19b were tried, but to no avail. The desired effect was obtained by using Kodak D 76 developer, to which 2 cc 1% KI and 20 cc 2.5% KBr had been added per 4 litres of developer[29]. The final experimental procedure was as follows: the film was presoaked in water for 2 minutes and developed for 3 minutes with constant agitation at 20°C. The film was then dipped into a stop bath of 3% CH_3COOH and fixed in Kodak X-ray

- X-ray fixer -

fixer solution for 10 minutes. It was finally washed for 30 minutes in running water and dried in a dust-free room. The γ value of the film thus processed was close to 2.

The Density vs log Exposure curve, whose slope gives the value of γ was obtained as follows: A lead sheet was fitted in front of a flat plate camera, and a small circular hole was cut into it. The camera was clamped 230 cm from the X-ray window and was aligned with the aid of a Geiger-Muller counter so that the X-ray beam fell on the hole in the lead. A series of exposures were taken with the generator running at 27 Kv and 1.6 mA and the camera in the mentioned position. The exposures gave a suitable range of densities (Table 5.1), which were measured with the instrument described on page 47.

The D vs log E curve drawn from these data is shown in Fig. 5.6.

(iii) Kodak Commercial Ortho Sheet film had the desired characteristics for use as the positive. The film was developed by constant swabbing with cotton wool affixed to a hoe-shaped glass rod for 8 1/4 minutes at 20^{o}C in D 76 developer, after presoaking the film for 2 minutes in water. The γ of the film thus developed was 0.5. The film was fixed by constant agitation for 10 minutes in Kodak Acid Fixing Salt with Hardener, and it was then washed for 30 minutes in running water.

The D 76 developer was found to deteriorate very rapidly so in order to prevent this and obtain reproducible results, the developer was made up in two parts. One solution, containing

borax only, was made up separately from another solution which contained "Metol", sodium sulphite and hydroquinone. These two components were allowed to equilibrate in a thermostat for two hours before use, they were mixed just prior to use, and the developing itself was carried out in a thermostat.

(iv) A printing box was especially constructed to ensure accurate exposures in printing the positives. The box is made to accommodate a frame of 7 ins x 5 ins and is 7 feet in length. The printing frame has a piece of opal glass (which allows 21% transmission of light) which diffuses the printing light and thus prevents shadows from dust particles from appearing on the print. The frame is also spring loaded to ensure a good contact between the negative and the print. The light source was a small 5 c.p. bulb which was fed by a constant voltage stabiliser, and was placed 6 feet from the film. The voltage across the filament was 5 volts. With this set up it was found than an exposure of 24 seconds gave a good linear relationship between the exposure of the negative and transmission of the positive up to a density of 2 on the negative (see Fig. 5.7). The data for this graph are found in Table 5.2, along with the transmissions for printing times of 22 and 25 seconds. Linearity was also found for these printing times, but it was found that the point of departure from linearity was at a density less than 2. Hence the choice of printing time was 24 seconds, this value giving the widest range of linearity between transmission of the positive and exposure of the negative.

Exposure Time of Negative.	Relative Exposure (E)	Log E	D
23 secs.	1.022	0.01	0.050
45 "	2	0.30	0.145
1.5 min.	4	0.60	0.240
3 "	8	0.90	0.360
5 "	13.3	1.13	0.545
6 "	16	1.20	0.595
8 "	21.3	1.33	0.770
12 "	32	1.51	0.985
17 "	45.3	1.66	1.125
24 "	64	1.81	1.325
33 "	88	1.95	1.595
48 "	128	2.11	1.930
75 "	200	2.30	2.205
96 "	256	2.41	2.330
192 "	512	2.71	2.750

TABLE 5.1.

Exposure Time of Negative.	Trans. of Pos. for 22 Sec. Printing.	Trans. of Pos. for 24 Sec. Printing.	Trans. of Pos. for 25 Sec. Printing.
23 secs.	0	0	0
45 "	2.25	1.75	2.0
1.5 min.	5.25	5.0	3.75
3 "	8.25	8.75	5.25
5 "	17.25	15.5	15.0
6 "	17.75	18.0	16.5
8 "	26.75	24.5	23.5
12 "	42.25	44.0	41.5
17 "	54.25	59.0	53.5
24 "	66.25	71.0	66.5
33 "	98.75	103.5	104.0
48 "	131.25	148.5	141.5
75 "	133.25	156.0	171.5
96 "	155.25	161.0	171.5
192 "	167.25	181.0	176.5

TABLE 5.2.

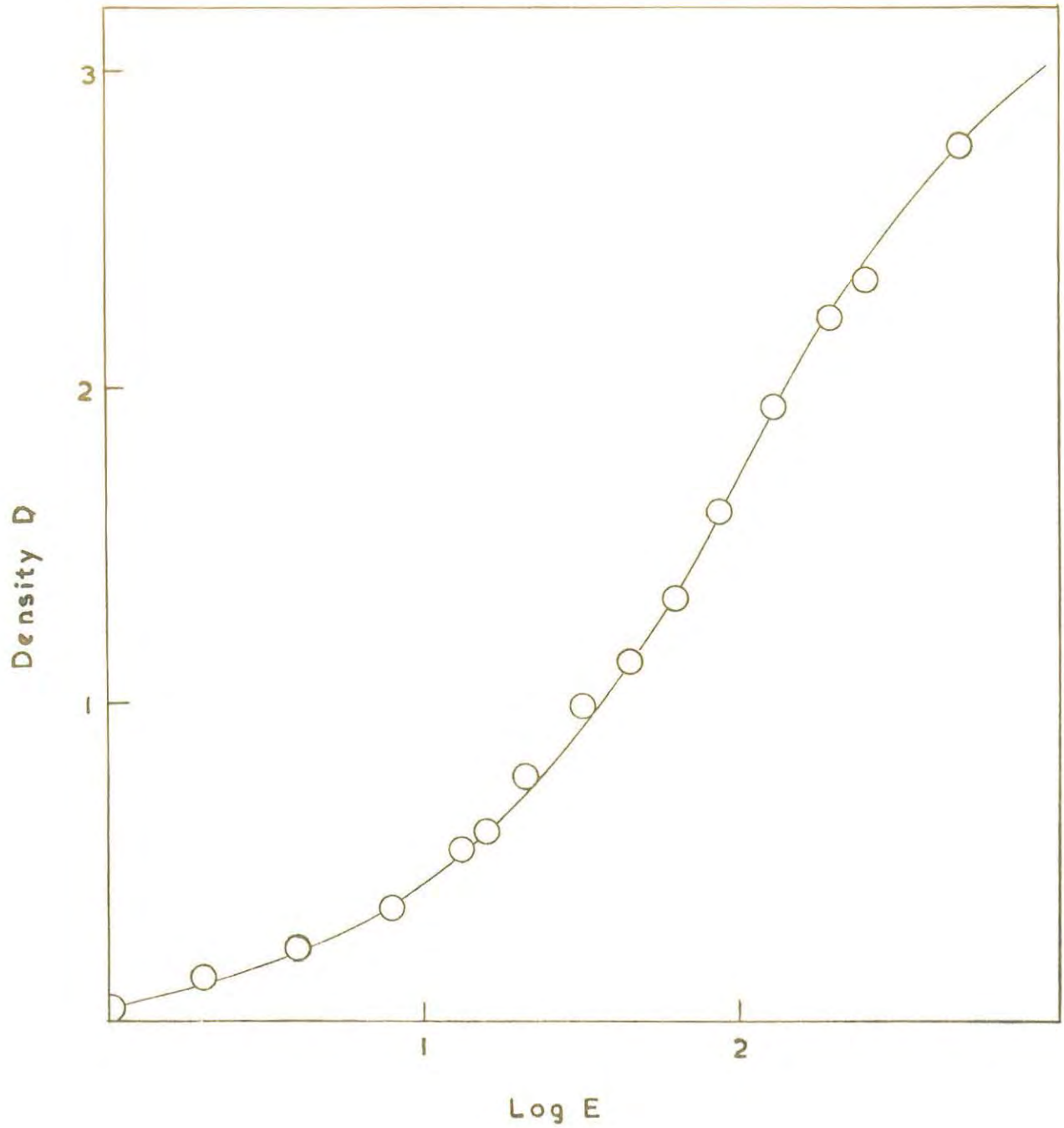

Fig 5.6

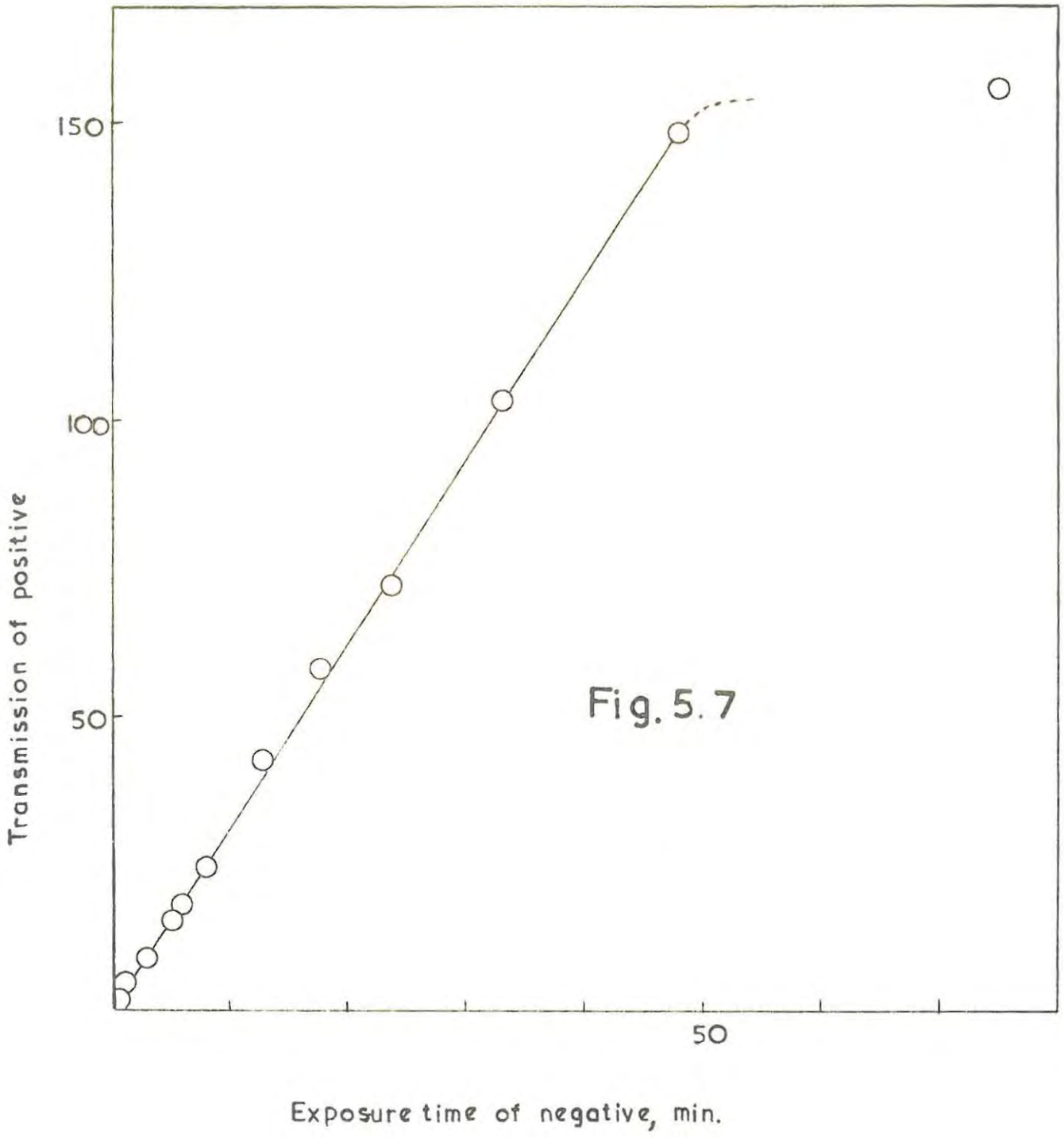
150
100
50
Transmission of positive
50
Exposure time of negative, min.

Fig. 5.7

The exposure time of the negative was such that the darkest spots had a density of 2 or less, and by following the above procedure, it was found possible to measure the integrated intensities of all the spots on the negative.[30]

5.7 THE MEASUREMENT OF INTENSITIES.

For the γ curve of Industrex "D" film, the densities were measured by adjusting the photometer to read densities directly. The aperture covering the photoemissive cell in the search head was opened so that its size was less than that of the spot to be measured, and the position of the spot was adjusted until its image fell on the aperture.

To measure intensities of the reflections on the positive print, the photometer was made to measure on the transmission scale. The following procedure was adopted: firstly the instrument was adjusted so that it read zero deflection with the aperture closed. The aperture was then opened so as to allow all the light from the spot to fall on the photocell and the deflction on the photometer was noted. Keeping the aperture exactly the same size the transmission of the background immediately next to the spot was then measured. The transmission of the spot was then obtained by subtracting the first reading from the background reading. The voltage across the lamp was kept at a constant 8 volts. For reflections having low Θ angles, the $K\alpha_1$ and $K\alpha_2$ diffraction spots were superimposed and thus did not give rise to any difficulties. At high Θ angles, however, the two spots were resolved and their transmission was measured separately and added.

To measure the intensities of the reflections on the films from

- the integrating -

the integrating Weissenberg, the aperture on the search head was kept constant in order to measure only the intensity of the plateaux of the integrated reflections. The procedure adopted was as follows: The density of the background near a spot was adjusted to read zero on the density scale by altering the voltage across the lamp. The plateau of the spot was now moved over the aperture and its density was read directly on the density scale. The background of the film was found to have a fairly uniform low density, so that only small alterations of the voltage were required to set the instrument to zero for each spot.

6. ANALYSIS OF RESULTS.

6.1 THE MEASUREMENT OF PARAMETERS FROM ROTATION PHOTOGRAPHS.

The parameters of the unit cell were first measured from rotation photographs taken with a semicircular camera of radius 5.73 cm. The distance between spots on the first layer lines on either side of the equatorial reflections was measured with a travelling microscope for each rotation photograph. The distance between layer lines of higher order was not measured because using a camera of such high radius resulted in these higher layers which were somewhat distorted, and not well defined when viewed under the microscope. The parameters were calculated using the formular 1.06.

The following readings were taken:

Photograph number.	BB 52	BB 31	BB 44
y cm	1.776	3.180	2.283(5)
$\bar{\nu}$	$81^{o}11'$	$74^{o}29'$	$78^{o}44'$
parameter in Å	a=10.07	b=5.765	c=7.893

6.2 THE ACCURATE MEASUREMENT OF PARAMETERS FROM WEISSENBERG PHOTOGRAPHS.

The attainment of accurate values for the cell parameters depends on (i) the utilization of d's in the sensitive region, (ii) the

elimination of systematic errors in the recording of reflection angles. These two factors are discussed in turn.

6.2 (i) The utilization of d's in the sensitive region[31].

The determination of parameters is made by measuring inter-planar spacings, d, of appropriate planes. Very accurate results can be obtained if measurements are made from reflections at high Bragg angles, because these angles are very sensitive to small changes in cell dimension. This can be seen by differentiating the Bragg equation,

$$d = (\lambda \operatorname{cosec} \theta)/2 \qquad \ldots\ldots\ldots \quad 6.1$$

$$\delta d = -\lambda \operatorname{cosec} \theta \cot \theta \, \delta\theta/2$$

$$= -d \cot \theta \, \delta\theta \qquad \ldots\ldots\ldots \quad 6.2$$

since $\cot \theta$ tends to 0 as θ tends to 90° an error of $\delta\theta$ in θ will result in a relatively much smaller error δd in d. In practice any reflections having $\theta > 60^{\circ}$ are used in the determination.

6.2(ii) The elimination of systematic errors.

The chief systematic errors are due to the eccentricity of the specimen with respect to the axis of the film cylinder, the lack of knowledge of the exact film radius and the absorption of the specimen.

The film shrinkage was determined as follows:-

The film was laid flat under a template and four small marks were made on it with a sharp needle which passed through small holes in the template. The distance between the marks was measured under the

- travelling -

travelling microscope and the film was then developed, fixed and washed. When dry, the distance between the fiducial marks was remeasured. No film shrinkage was detected with Industrex D film.

Refinement was first attempted by determining the Bragg angle of reflection for spots on the equatorial layer of rotation photographs and plotting d vs $\sin^2\theta$ [32]. This method did not give good plots because of the uncertainty of distinguishing particular spots on the rotation photograph and because the indices of some of these spots were indeterminate. The extrapolation against $\sin^2\theta$ is based on the assumption that errors due to eccentricity of the specimen and the shrinkage of the film are larger than those due to absorption. It was realised that this was unlikely, since $CsMnO_4$ is highly absorbing ($\mu = 848.7$).

Buerger[33] suggests that if fairly large crystals of high absorption are used, the mechanical errors of the eccentricity of the specimen and inexact knowledge of the camera radius may be neglected, and that d may be plotted against the absorption error function $\cot\theta \cos^2\theta$. The correct value of d is then obtained by extrapolation to $\theta = 90^\circ$.

In determining the parameters of an orthorhombic crystal, only three constants a, b and c are involved. Suppose that the crystal is oscillated about its c axis, then the Bragg angles of spots lying on the zero layer line of the resulting photograph are given by

$$\sin^2\theta_{hk0} = \frac{1}{4}(h^2a^{*2} + k^2b^{*2}) \quad \ldots\ldots\ldots \quad 6.3$$

$$= \frac{\lambda^2}{4}\left(\frac{h^2}{a^2} + \frac{k^2}{b^2}\right) \quad \ldots\ldots\ldots \quad 6.4$$

In order to analyse the photograph, approximate values of a and b

- are required -

are required. These were obtained from layer line measurements of rotation photographs. Rewriting equation 6.4,

$$\sin^2\Theta_{hk0} = \left(\frac{\lambda}{2a}\right)^2\left(h^2 + \frac{a^2}{b^2}k^2\right) \qquad \ldots\ldots\ldots \quad 6.5$$

$$a = \left(\frac{\lambda}{2}\sqrt{h^2 + \frac{a^2}{b^2}k^2}\right)\operatorname{cosec}\Theta \qquad \ldots\ldots\ldots \quad 6.6$$

If h is large with respect to k, a small error in a/b will not greatly affect the derived value of a. Several values of a are thus derived from various reflections having a Bragg angle $> 60^\circ$, and the true value obtained by extrapolating against $\cot\Theta\cos^2\Theta$. If, from the first graph drawn, the value of a/b is considerably in error, the calculations may be repeated with the more accurate value, and further refinement similarly carried out if necessary. When an accurate value of a has been obtained, this can be used in turn to obtain an accurate value of b using the equation

$$b = \left(\frac{\lambda}{2}\sqrt{h^2\frac{b^2}{a^2} + k^2}\right)\operatorname{cosec}\Theta \qquad \ldots\ldots\ldots \quad 6.7$$

and similarly for c.

It was decided to use zero layer Weissenberg photographs which give large distances between spots, and no uncertainity in the indexing. The Bragg angle for a particular spot was determined as follows: The distance 2s between a pair of spots on the upper and lower half of the Weissenberg photograph was measured. These two spots lie on a line parallel to the straight line OL of Fig. 1.12. This line has a slope of 2 (Equation 1.10). The perpendicular distance x from the spot to the centre line on the photograph represents the angle $\gamma = 2\Theta$ (Equation 1.05).

- From Fig. 6.1 -

From Fig. 6.1 $x = S \sin \alpha = S \sin \tan^{-1} 2$. Θ may then be calculated from the equation

$$\frac{2\Theta}{180^{\circ}} = \frac{x}{\pi r} \qquad \ldots\ldots\ldots \quad 6.8$$

The values of d were calculated on a computing machine. Values of sin Θ were obtained to six figures from tables. The X-ray wavelengths used were $CuK\alpha_1 = 1.54051$ Å $CuK\alpha_2 = 1.54433$ Å [34]. The refinement was started using the approximate values of the parameters obtained from rotation photographs:

$$a = 10.07 \text{ Å} \qquad b = 5.765 \text{ Å} \qquad c = 7.893 \text{ Å}$$

From a zero layer Weissenberg photograph with the crystal oscillating about the b axis, the value of c was calculated, using

$\frac{c}{a} = \frac{7.893}{10.07} = 0.78381$. The results are somewhat erratic, but they suggest that $c \approx 7.9516$ Å (Fig. 6.2). The calculation was repeated with $\frac{c}{a} = \frac{7.9516}{10.07} = 0.78963$ and the results were now consistent (Fig. 6.3), giving an extrapolated value $c = 7.9470$. This final value of c was in turn used to calculate the parameter a. Using

$\frac{a}{c} = \frac{10.07}{7.9470} = 1.26714$, $a = 10.0692$. The computation did not require further refinement (Fig. 6.4).

The value of b was calculated similarly. The calculation required two stages of refinement, the final value being $b = 5.8080$, (Figs. 6.5, 6.6, 6.7).

The final values of the three parameters obtained were

$a = 10.0692$ Å $\qquad b = 5.8080$ Å $\qquad c = 7.9470$ Å.

The axial ratio $a : b : c = 1.7337 : 1 : 1.3683$ compares well with the axial ratio obtained from the optical goniometric study

$a : b : c = 1.734 : 1 : 1.370$.

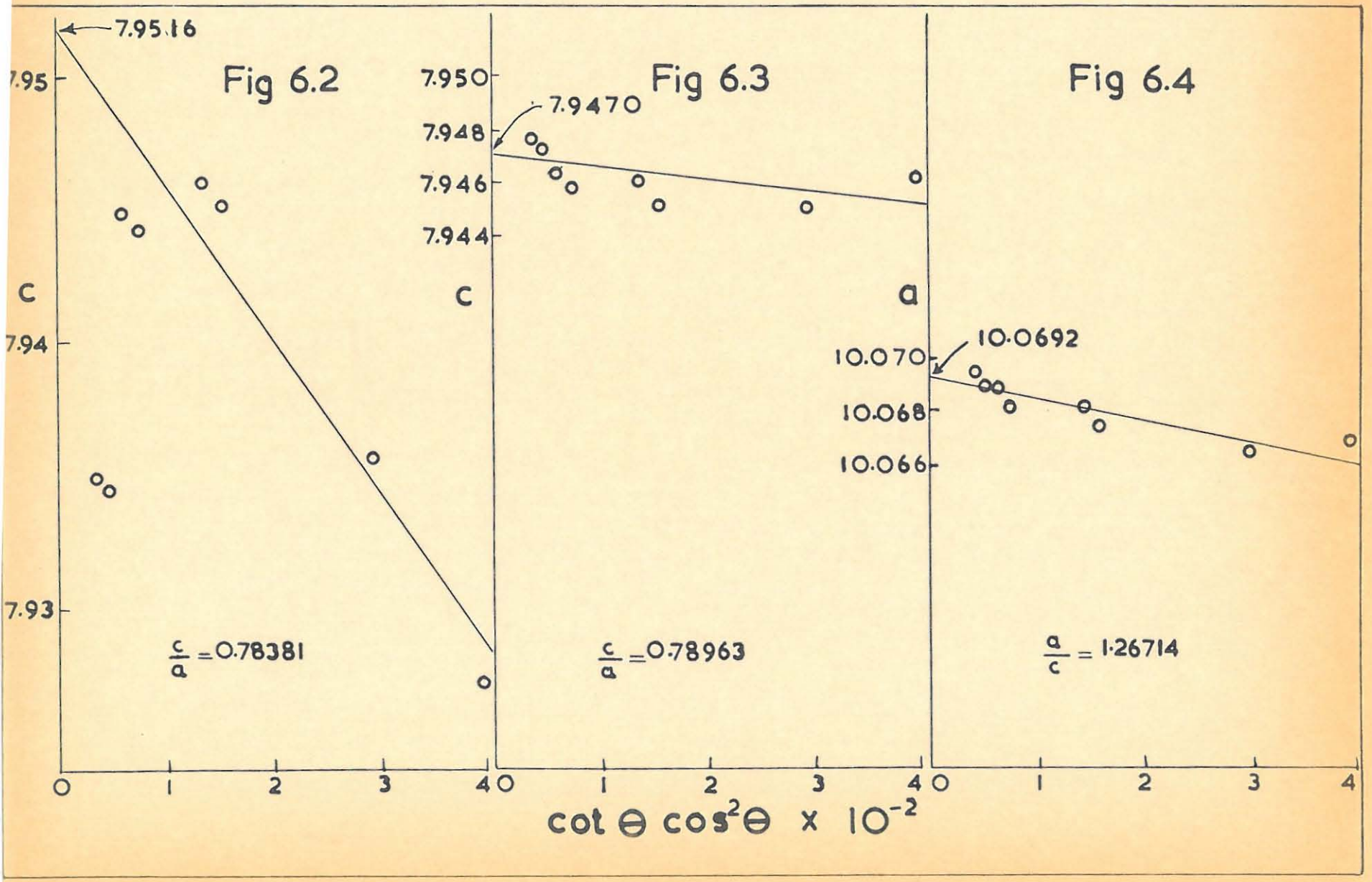
Fig 6.2
7.9516
7.95
7.94
7.93
c
$\frac{c}{a}$ = 0.78381
Fig 6.3
7.950
7.948
7.946
7.944
7.9470
c
$\frac{c}{a}$ = 0.78963
Fig 6.4
10.070
10.068
10.066
10.0692
a
$\frac{a}{c}$ = 1.26714
0 1 2 3 4
0 1 2 3 4
0 1 2 3 4
cot θ cos²θ x 10⁻²

Fig 6·5

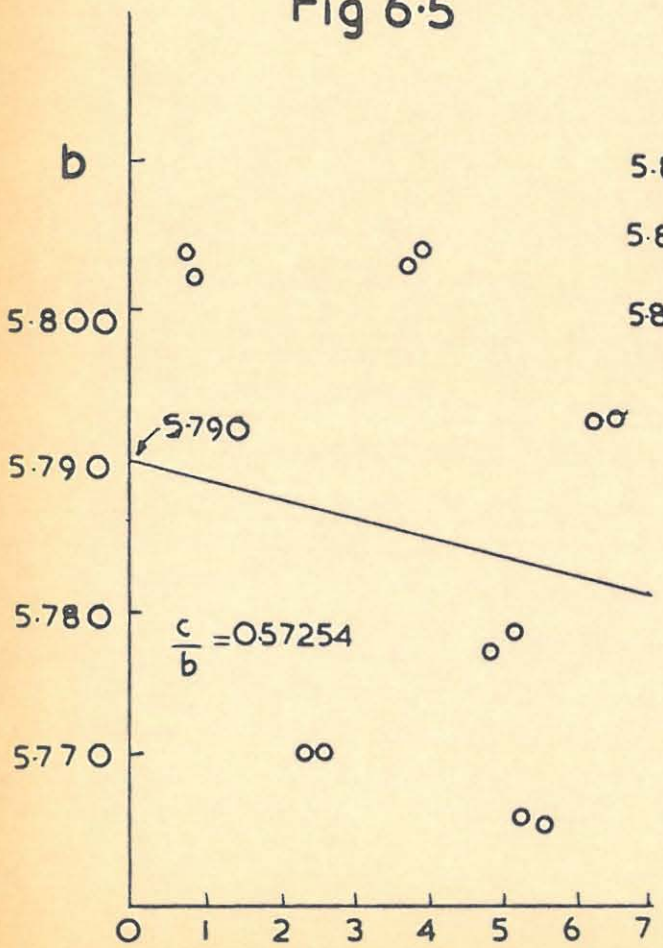

Fig 6.6

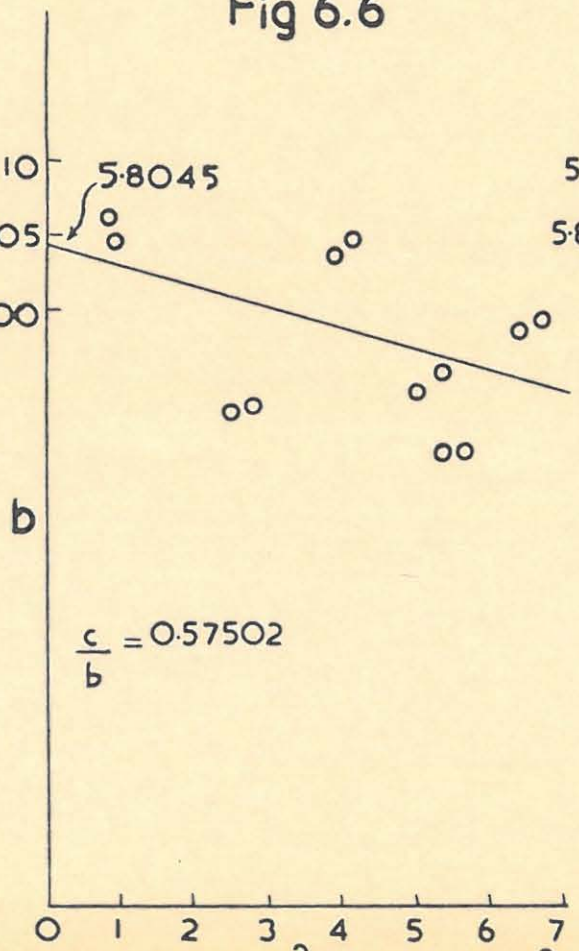

Fig 6.7

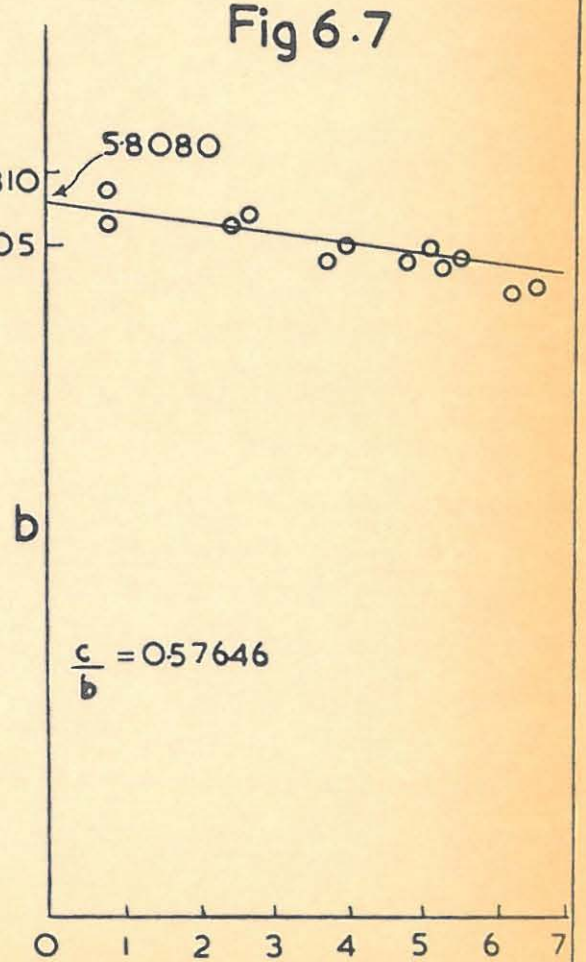

$\cot\theta \cos^2\theta \times 10^{-2}$

6.3 THE NUMBER OF MOLECULES PER UNIT CELL.

Knowing the size of the cell parameters, it is possible to calculate the volume of the unit cell. In the orthorhombic system the principal three axes are mutually perpendicular, and thus the volume may be calculated by multiplying the lengths of the three parameters.

$$\text{Volume of the unit cell} = 10.0692 \times 5.8080 \times 7.9470 \text{ Å}^3$$
$$= 464.7558 \text{ Å}^3$$
$$= 464.7558 \times 10^{-24} \text{cm}^3$$

Multiplying this volume by the density (3.597 gm/cc) we obtain the weight of the unit cell in grams.

$$W = 464.7558 \times 10^{-24} \times 3.597$$
$$= 1671.7266 \times 10^{-24} \text{g}$$

This weight is converted to a.m.u. by dividing by the theoretical weight of 1 atom = 1.6604×10^{-24}gm. (O = 16.0000).

$$\therefore W = \frac{1671.7266 \times 10^{-24}}{1.6604 \times 10^{-24}} \text{ a.m.u.}$$
$$= 1006.8216 \text{ a.m.u.}$$

If there are n molecules/unit cell, then

$$n \times \text{Molecular weight} = \text{weight of unit cell}$$

The molecular weight of

$$CsMnO_4 = 251.85$$
$$\therefore n = \frac{1006.8216}{251.85}$$
$$= 3.9977$$
$$= 4 \text{ molecules/unit cell.}$$

6.4 THE EXAMINATION OF SYSTEMATIC ABSENCES AND THE DETERMINATION OF THE SPACE GROUP[35].

Zero and upper layer Weissenberg photographs were taken with the crystal oscillating about all three principal axes. The photographs were indexed and an examination of the indices was carried out.

The upper layer photographs showed that there were no restrictions for h + k + l, thus the crystal has a primitive lattice P. The reflections from the zero layer photographs showed the following conditions for the indices:

Reflection.	Condition.
0kl	k + l = 2n
h0l	no conditions
hk0	h = 2n
h00	h = 2n
0k0	k = 2n
00l	l = 2n

The diffraction symbol is thus m m m P n a - which corresponds to two possible space groups, depending on the choice of axes. If the axes are taken as abc the space group is P n m a, while if they are taken as acb, the space group is P n a 2_1. Both these space groups, however, give rise to the plane group pgg when projected down the b and c axes respectively. The space group P n m a was chosen by analogy with the structure of $KMnO_4$ [36]. Since there are four molecules per unit cell the atoms were placed in the following special positions:

x, 1/4, z; $\bar{x}$, 3/4, $\bar{z}$; 1/2-x, 3/4, 1/2+z; 1/2+x, 1/4, 1/2-z.

The space group P n m a thus has the special positions 1/4 and 3/4 along the b axis. These were later confirmed by Fourier methods, thus proving that P n m a is the correct space group.

The above space group shows that the crystal must have a centre of symmetry. To confirm this the following qualitative test for pyro-electricity was carried out: crystals were placed on a metal plate and dipped in liquid air and allowed to cool. The plate was then tilted to a vertical position and the crystals fell off, showing that $CsMnO_4$ crystals are not pyro-electric and thus have a centre of symmetry.

6.5 THE MEASUREMENT AND CORRECTION OF INTENSITIES.

The intensities of the X-ray reflections were measured as described earlier on page 61. The intensities of the reflections obtained from zero layer Weissenberg photographs with the crystal oscillating about the b axis were measured using the positive print technique. The positive prints were obtained from two different negatives and the intensities obtained from the two separate positive prints were normalised by equalising the intensities of the strongest reflection 200. The agreement between the intensities of reflections having the same Miller indices was satisfactory. The intensities of the reflections obtained from zero layer Weissenberg photographs with the crystal oscillating about the c axis were measured directly from the negative obtained using the integrating Weissenberg camera. Only one film was used, and the agreement between intensities of reflections having the same Miller indices was very good.

The reflections were indexed and the interplanar distance d_{hkl} was calculated from the formula,[37]

$$d_{hkl} = \frac{abc}{\sqrt{(h^2b^2c^2 + k^2c^2a^2 + l^2a^2b^2)}} \quad \ldots\ldots\ldots \quad 6.9$$

Using Bragg's equation $\lambda = 2d \sin\theta$ the Bragg angle for each reflection was subsequently calculated.

The Lorentz and Polarisation corrections.

As the Lorentz factor L and the polarisation factor p always occur together, it is in practice convenient to be able to correct

- them simultaneously. -

them simultaneously. The Lp function appropriate to zero layer reflections for Weissenberg photographs is $1 + \cos^2 2\theta / \sin 2\theta$ [38]. This is tabulated in the International Tables for X-ray crystallography[39].

From equation 1.16 we see that

$$\rho \propto Lp|F|^2 \qquad \ldots\ldots \qquad 6.10$$

thus the measured relative intensities are divided by Lp to obtain the true relative intensities.

The Absorption correction.

It was shown earlier that the optimum size of a crystal to be used in X-ray investigations is given by

$$t = \frac{2}{\mu} \qquad \ldots \text{(Section 5.2)}$$

where t is the thickness of the crystal in cm. μ is the linear absorption coefficient. The latter quantity may be calculated from the mass absorption coefficients, μ_m [40], of the constituent elements using

$$\mu = \rho \sum_p p \mu_m$$

where the summation is over all the constituent elements. ρ is the density of the compound and p is the proportion of each element in the compound. For caesium permanganate used in conjunction with CuK_α radiation of wavelength 1.5418 Å

$$\rho = 3.597 \text{ g/cc}$$
$$\mu_m \text{ (Cs)} = 322 \text{ cm}^2 \text{ g}^{-1}$$
$$\mu_m \text{ (Mn)} = 289 \text{ cm}^2 \text{ g}^{-1}$$
$$\mu_m \text{ (O)} = 11.7 \text{ cm}^2 \text{ g}^{-1}$$

This gives $\mu = 848.7 \text{ cm}^{-1}$ and $t = 0.00236$ cm.

Handling crystals of such minute dimensions is very impracticable, so the crystals used were as small as could be conveniently handled.

In order to obtain accurate absorption corrections, it is preferable that the crystal should have either a cylindrical or a shperical shape, as the corrections are then comparatively simple. When possible the crystals should be ground into cylindrical or a spherical shape[41] but the $CsMnO_4$ crystals were extremely brittle, so that it was impracticable to do this. For the [hOl] reflections (crystal oscillating about the b axis) the crystal eventually selected was prismatic and had a cross section of dimensions 0.280 mm x 0.069 mm. As a first approximation the crystal was treated as a cylinder having a diameter equal to the mean of these two values. The radius of the cylinder was thus taken as 0.008725 cm and hence $\mu R = 848.7 \times 0.008725 = 7.4$. For the [hkO] reflections (crystal oscillating about the c axis) the crystal selected was block shape of dimensions 0.375 mm x 0.125 mm x 0.213 mm. This was treated as a sphere having a mean radius of 0.0119 cm, whence $\mu R = 848.7 \times 0.0119 = 10$. The absorption corrections for cylindrical crystals[42] and spherical crystals[43] of varying radii are dependent on the Bragg angle of reflection and are given in the International Tables for X-ray crystallography. The intensities, corrected for this factor, can now be employed as coefficients in the Patterson summation

6.6 THE SUMMATION OF THE PATTERSON FUNCTION.

The Patterson function derived earlier (Equation 1.38) may be extended to the three dimensional form:

$$A(uvw) = \frac{1}{V^2} \sum_{h=-\infty}^{+\infty} \sum_{k=-\infty}^{+\infty} \sum_{l=-\infty}^{+\infty} |F_{hkl}|^2 \, e^{i2\pi(hu + kv + lw)} \quad \ldots \quad 6.11$$

This may be compared with the exponential form of the electron density function:

$$\rho(xyz) = \frac{1}{V} \sum_{h=-\infty}^{+\infty} \sum_{k=-\infty}^{+\infty} \sum_{l=-\infty}^{+\infty} F_{hkl} \, e^{i2\pi(hx + ky + lz)} \quad \ldots\ldots\ldots \quad 6.12$$

Note that the additional factor $\frac{1}{V}$ arises in the Patterson function. This is because it was derived by taking the average value of the electron density product over the volume V. If the function had been derived as the simple integral of the electron density product over the volume V the Patterson function would have resulted in P(uvw) instead of A(uvw). These are related by $A(uvw) = \frac{1}{V} P(uvw)$[44] 6.13

The Patterson function is thus written as

$$\rho(uvw) = \frac{1}{V} \sum_{h=-\infty}^{+\infty} \sum_{k=-\infty}^{+\infty} \sum_{l=-\infty}^{+\infty} |F_{hkl}|^2 \, e^{2\pi i(hu + kv + lw)} \quad \ldots\ldots \quad 6.14$$

The latter form has the advantage of being simpler and comparing more directly with the Fourier form (Equation 6.10). It can be shown[45] that the Patterson function as written in Equation 6.12 may be written as

$$P(uvw) = \frac{1}{V} \sum_{h=-\infty}^{+\infty} \sum_{k=-\infty}^{+\infty} \sum_{l=-\infty}^{+\infty} |F_{hkl}|^2 \cos 2\pi(hu + kv + lz) \quad \ldots\ldots \quad 6.15$$

- which is -

which is the more usual form of the Patterson summation.

For an orthorhombic crystal the three dimensional Patterson summation modifies to [46]

$$P(uvw) = \frac{8}{V} \sum_{h=0}^{\infty} \sum_{k=0}^{\infty} \sum_{l=0}^{\infty} |F_{hkl}|^2 \cos 2\pi hu \cos 2\pi kv \cos 2\pi lz \quad .. \quad 6.16$$

where u, v, w are fractional coordinates of the atoms.

Written in two dimensional form Equation 6.14 reduces to

$$P(uv) = \frac{4}{S} \sum_{h=0}^{\infty} \sum_{k=0}^{\infty} |F_{hk0}|^2 \cos 2\pi hu \cos 2\pi kv \quad ..... \quad 6.17$$

Practical methods of summing a Fourier series.

In summing up a Fourier series of the type shown in Equation 6.17 advantage can be taken of the symmetrical or antisymmetrical properties of the trigonometric function about the angles 0, $1/4.2\pi$, $1/2.2\pi$, $3/4\ 2\pi$ and 2π. By appropriate arrangement the Fourier summation can be limited to the range 0 to 1/4 of the cell edge. A Fourier function which provides the value of $\rho(x,y)$ does so for continuously variable values of the parameters x and y. In practice it is necessary to select a limited set of samples of x and y at such intervals that the value of ρ does not vary greatly between adjacent points. Contours can then be drawn at arbitrary values of the function ρ and the variation of ρ over the unit cell can then be seen at a glance. The fineness of the interval chosen between sampled values depends on the amount of detail required and on the size of the unit cell.

Lipson and Cochran[47] discuss the subdivision of the cell edges and suggest that the minimum number of intervals into which the cell edge should be divided is at least four times the highest corresponding index. For $CsMnO_4$, on the xz projection the highest indices are h = 12, l = 10, so that the cell edges should be divided at least into 48 and 40 parts respectively. It is inconvenient to adopt different values of subdivision for each crystal, so that usually one divides the cell into 60 or 120 parts. Both these subdivisions were used in the project, depending on the amount of detail required from the Fourier maps.

From trigonometrical considerations it can be shown that if

Ce = cos $2\pi hx$, when h is even x = 0 to 1/4

Co = cos 2 hx, when h is odd x = 0 to 1/4

Se = sin $2\pi hx$, when h is even x = 0 to 1/4

So = sin $2\pi hx$, when h is even x = 0 to 1/4

then for x = 0 to 1/4

$$\left.\begin{aligned} \Sigma C &= \Sigma\,(Ce + Co) \\ \Sigma S &= \Sigma(Se + So) \end{aligned}\right\} \quad \ldots\ldots\ldots \quad 6.18$$

and for x = 1/2 to 1/4

$$\left.\begin{aligned} \Sigma C &= \Sigma(Ce - Co) \\ \Sigma S &= \Sigma(Se - So) \end{aligned}\right\} \quad \ldots\ldots\ldots \quad 6.19$$

The range of x may be extended beyond x = 1/2, and similar relationships can thus be derived.

Summation of a one-dimensional series.

Suppose that we wish to sum the series

$$C = \sum_{h=0}^{H} A_h \cos 2\pi hx \qquad \ldots\ldots\ldots \qquad 6.20$$

Use is made of "strip" methods of summation. These were introduced by Beevers and Lipson[48,49,50] and Patterson and Tunnel[51] as well. The Beevers and Lipson strip method was employed in the project. Specifically it provides the values of

$$A_h \cos 2\pi hx \qquad \ldots\ldots\ldots \qquad 6.21$$

$$A_h \sin 2\pi hx \qquad \ldots\ldots\ldots \qquad 6.22$$

for all values of A and h within practicable limits. For a particular value of A, the amplitude, and h, an integer, the values of Equations 6.21 and 6.22 are printed on a strip of cardboard for the 16 successive x locations of $\frac{0}{60}, \frac{1}{60}, \frac{2}{60} \ldots\ldots \frac{15}{60}$. For example for A = 39 and h = 4 the values of Equation 6.21 for the parameter x are printed on a strip as follows:

x = 0 1 2 3 4 5 6 7 8 9 10 11 12 13 14 15

39 C	4	39	36	26	12	$\bar{4}$	$\bar{19}$	$\bar{32}$	$\bar{38}$	$\bar{38}$	$\bar{32}$	$\bar{19}$	$\bar{4}$	12	26	36	39

One starts with numerical values for Equation 6.21 for each A and h to be summed, and to perform the summation of Equation 6.20 the H + 1 strips are placed so that their successive x values lie in vertical columns and one adds the numbers in each column. The strips are arranged in blocks corresponding to Ce and Co of Equation 6.18,

- and the -

and the corresponding sums are then ΣCe and ΣCo. The final Fourier summation of Equation 6.20 for the range $x = 0$ to $\frac{15}{60}$ is obtained by $\Sigma Ce + \Sigma Co$ (Equation 6.18), and for the range $x = \frac{30}{60}$ to $\frac{15}{60}$ by $\Sigma Ce - \Sigma Co$ (Equation 6.19) Since this is a cosine synthesis it is symmetrical about $\frac{1}{2}$, so the above values cover the complete range.

Summation of a two-dimensional series.

If a two dimensional Fourier series is expressed in product form as in Equation 6.17, then we may regard the summation as successive sets of one-dimensional series. Omitting the scale factors equations similar in form to 6.17 may be written as

$$\rho\ (x,y) = \sum_{h=0}^{H}{}' \sum_{k=0}^{K}{}' F_{hk0} \cos 2\pi hx \cos 2\pi ky \quad \ldots\ldots\ldots \quad 6.23$$

The prime marks after the $\sum'$'s indicate that the intensities of axial reflections enter the series at half value because they occur on a line of symmetry.

One may sum Equation 6.23 over k first, keeping h constant.

Thus
$$\begin{aligned}\rho(x,y) = \Big\{ &\Big[\sum_k F_{0k0} \cos 2\pi ky\Big] \cos 2\pi 0x \\ &+ \Big[\sum_k F_{1k0} \cos 2\pi ky\Big] \cos 2\pi 1x \\ &+ \Big[\sum_k F_{2k0} \cos 2\pi ky\Big] \cos 2\pi 2x \\ &\quad\vdots \\ &+ \Big[\sum_k F_{Hk0} \cos 2\pi ky\Big] \cos 2\pi Hx \Big\} \quad \ldots\ldots\ldots \quad 6.23\end{aligned}$$

$$\rho(x,y) = \sum_h \left[\sum_k F_{hk0} \cos 2\pi ky\right]_{h \text{ constant}} \cos 2\pi hx$$

The process is described by saying that one sums first over k (h being constant), and then over h.

When summing the Patterson synthesis Equation 6.17, the same method as above is employed, except that the Fourier coefficients are $|F|^2$'s instead of F's. The procedure is best described in tabular form.

Sequence of operation in summing Equation 6.23.

TABLE 6.1

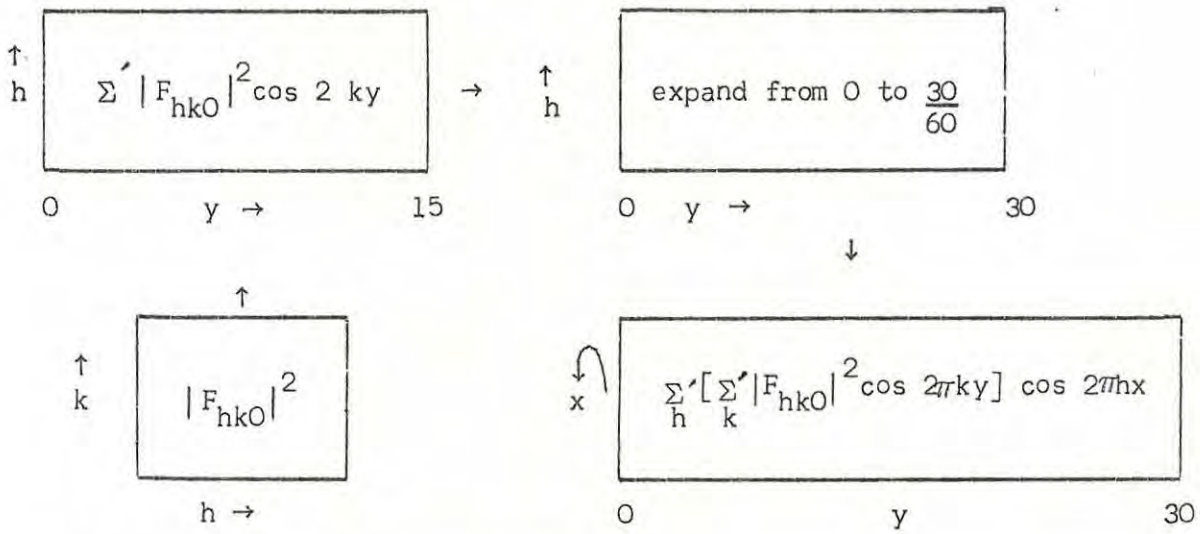

The operation may be summarised as follows:

$$|F_{hk0}|^2$$
$$\downarrow$$
$$\Sigma'_k |F_{hk0}|^2 \cos 2\pi ky$$
$$\downarrow$$
expand over y = 0 to $\frac{1}{2}$
$$\downarrow$$
$$\Sigma'_h [\Sigma'_k |F_{hk0}|^2 \cos 2\pi ky] \cos 2\pi hx$$
$$\downarrow$$

- expand over -

expand over $x = 0$ to $\frac{1}{2}$

$$\sum_h{}' \sum_k{}' |F_{hk0}|^2 \cos 2\pi hx \cos 2\pi ky$$

The last expansion of x from $\frac{15}{60}$ to $\frac{30}{60}$ is best done on a scaled projection of the crystal cell, conveniently drawn on graph paper. Contours can then be drawn on the paper at the desired intervals.

The summation of the Patterson function.

The intensities of the X-ray reflections with the crystal oscillating about the b axis were corrected as described in Section 6.5. They were then arranged in tabular form as shown in Table 6.2. The summation was carried out first over h, then over l. The odd and even values of h were tabulated separately to facilitate summation. To facilitate expansion ΣCe terms were placed above ΣCo terms in Table 6.3. $|F_{h0l}|^2$ values for axial reflections were halved. The origin was taken as zero because the intensities were not measured on an absolute basis. On Table 6.4 x was expanded from $\frac{15}{60}$ to $\frac{30}{60}$. Table 6.5 shows the final summation. The final expansion of z from $\frac{15}{60}$ to $\frac{30}{60}$ was carried out directly on a large sheet of graph paper. Contours were drawn round the sample points at arbitrary intervals of 1000 arbitrary units. The resulting Patterson map is shown in Fig. 6.8

TABLE 6.2

h ↑											
11	0	21	6	75	0	15					
9	0	0	78	0	14	0	35	21			
7	0	27	286	19	129	0	0	45	40		
5	0	184	11	271	0	0	42	100	34	38	
3	0	235	248	711	0	57	133	125	79	20	
1	0	0	797	87	361	48	97	173	156	30	0
12	0	64									
10	17	0	0	0	52	15	27				
8	200	0	97	0	58	0	86	74			
6	35	7	0	53	32	87	12	0	0	65	
4	0	1236	0	0	0	332	0	110	0	3	
2	55	104	76	123	272	455	143	62	19	68	101
0	0	0	885	0	377	0	511	0	0	0	18
	0	1	2	3	4	5	6	7	8	9	10
					1 →						

TABLE 6.3

l ↑																
10	119 0	117 0	110 0	100 0	86 0	68 0	49 0	28 0	8 0	$\overline{13}$ 0	$\overline{32}$ 0	$\overline{50}$ 0	$\overline{64}$ 0	$\overline{74}$ 0	$\overline{81}$	$\overline{83}$
9	136 88	123 82	84 64	36 41	$\overline{8}$ 14	$\overline{32}$ 7	$\overline{34}$ 20	$\overline{16}$ 23	10 15	$\overline{30}$ 1	30 14	8 26	$\overline{34}$ 31	$\overline{80}$ 27	$\overline{117}$ 16	$\overline{130}$ 0
8	19 309	19 289	17 238	15 170	13 110	9 71	6 56	2 57	$\overline{2}$ 60	$\overline{6}$ 55	$\overline{9}$ 36	$\overline{13}$ 10	$\overline{15}$ 14	$\overline{17}$ 24	$\overline{19}$ 18	$\overline{19}$ 0
7	246 464	207 423	106 319	$\overline{7}$ 192	$\overline{82}$ 86	$\overline{98}$ 24	$\overline{66}$ 4	$\overline{23}$ 5	2 12	$\overline{4}$ 14	$\overline{23}$ 12	$\overline{27}$ 18	$\overline{7}$ 23	29 24	48 16	22 0
6	779 307	732 279	623 213	526 137	500 81	540 48	599 23	613 9	567 53	477 90	396 99	354 72	356 25	381 11	406 18	415 0
5	889 120	825 108	657 83	429 66	194 60	$\overline{19}$ 55	$\overline{183}$ 33	$\overline{296}$ 1	$\overline{352}$ 29	$\overline{355}$ 35	$\overline{313}$ 26	$\overline{262}$ 19	$\overline{223}$ 26	$\overline{213}$ 35	$\overline{219}$ 27	$\overline{225}$ 0
4	791 504	734 463	604 362	488 254	450 193	478 201	505 263	475 334	385 363	285 327	218 230	190 112	172 12	138 40	98 38	79 0
3	176 1163	163 1042	128 747	84 418	39 136	8 110	5 365	4 594	4 708	5 651	8 487	39 336	84 269	128 240	163 157	176 0
2	1058 1426	1024 1299	944 988	868 655	841 456	875 438	938 535	982 625	966 607	892 454	799 223	739 2	746 150	806 185	876 123	906 0
1	1411 467	1257 412	872 271	412 103	45 47	509 165	954 248	1252 292	1268 278	1006 209	599 120	173 48	248 22	678 22	1041 18	1189 0
0	307 0	224 0	32 0	146 0	195 0	100 0	68 0	186 0	179 0	56 0	100 0	197 0	178 0	74 0	44 0	93 0
	0	1	2	3	4	5	6	7	8	9	10	11	12	13	14	15
	30	29	28	27	26	25	24	23	22	21	20	19	18	17	16	15

x →

TABLE 6.4

y ↑	x = 0	1	2	3	4	5	6	7	8	9	10	11	12	13	14	15	16	17	18	19	20	21	22	23	24	25	26	27	28	29	30
10	119	117	110	100	86	68	49	28	8	$\overline{13}$	$\overline{32}$	$\overline{50}$	$\overline{64}$	$\overline{74}$	$\overline{81}$	$\overline{83}$	$\overline{81}$	$\overline{74}$	$\overline{64}$	$\overline{50}$	$\overline{32}$	$\overline{13}$	8	28	49	68	86	100	110	117	119
9	224	205	148	77	6	$\overline{39}$	$\overline{54}$	$\overline{39}$	$\overline{5}$	29	44	34	$\overline{3}$	$\overline{53}$	$\overline{101}$	$\overline{130}$	$\overline{133}$	$\overline{127}$	$\overline{65}$	$\overline{18}$	16	31	25	7	$\overline{14}$	$\overline{25}$	$\overline{22}$	$\overline{5}$	20	41	48
8	328	308	255	185	123	80	62	59	58	49	27	$\overline{3}$	$\overline{29}$	$\overline{41}$	$\overline{37}$	$\overline{19}$	$\overline{1}$	7	$\overline{1}$	$\overline{23}$	$\overline{45}$	$\overline{61}$	$\overline{62}$	$\overline{55}$	$\overline{50}$	$\overline{62}$	$\overline{97}$	$\overline{155}$	$\overline{221}$	$\overline{270}$	$\overline{290}$
7	710	630	425	185	4	$\overline{74}$	$\overline{62}$	$\overline{18}$	14	10	$\overline{11}$	$\overline{9}$	16	53	64	22	32	5	$\overline{30}$	$\overline{45}$	$\overline{35}$	$\overline{18}$	$\overline{10}$	$\overline{28}$	$\overline{70}$	$\overline{122}$	$\overline{168}$	$\overline{197}$	$\overline{213}$	$\overline{216}$	$\overline{218}$
6	1086	1011	836	663	581	588	622	604	514	387	297	282	331	392	424	415	388	370	381	426	495	567	620	622	576	492	419	389	410	453	472
5	1009	933	740	495	254	36	$\overline{150}$	$\overline{197}$	$\overline{381}$	$\overline{390}$	$\overline{339}$	$\overline{281}$	$\overline{249}$	$\overline{248}$	$\overline{246}$	$\overline{225}$	$\overline{192}$	$\overline{178}$	$\overline{197}$	$\overline{243}$	$\overline{287}$	$\overline{320}$	$\overline{323}$	$\overline{295}$	$\overline{216}$	$\overline{74}$	134	363	574	717	769
4	1295	1197	966	742	643	679	768	809	748	612	448	302	184	98	60	79	136	178	160	78	$\overline{12}$	$\overline{42}$	22	141	242	277	257	234	242	271	287
3	1339	1205	875	502	175	$\overline{102}$	$\overline{370}$	$\overline{598}$	$\overline{704}$	$\overline{646}$	$\overline{495}$	$\overline{375}$	$\overline{353}$	$\overline{368}$	$\overline{320}$	$\overline{176}$	$\overline{6}$	112	185	297	479	656	712	590	360	118	$\overline{97}$	$\overline{334}$	$\overline{619}$	$\overline{879}$	$\overline{987}$
2	2484	2323	1932	1523	1297	1313	1473	1607	1573	1346	1022	737	596	621	753	906	999	991	896	741	576	438	359	357	403	437	385	213	$\overline{44}$	$\overline{275}$	$\overline{368}$
1	1878	1669	1143	515	$\overline{92}$	$\overline{674}$	$\overline{1202}$	$\overline{1544}$	$\overline{1546}$	$\overline{1215}$	$\overline{719}$	$\overline{221}$	226	656	1023	1189	1059	700	270	$\overline{125}$	$\overline{479}$	$\overline{797}$	$\overline{990}$	$\overline{960}$	$\overline{706}$	$\overline{344}$	2	309	601	845	944
0	307	224	32	$\overline{146}$	$\overline{195}$	$\overline{100}$	68	186	179	56	$\overline{100}$	$\overline{197}$	$\overline{178}$	$\overline{74}$	44	93	44	$\overline{74}$	$\overline{178}$	$\overline{197}$	$\overline{100}$	56	179	186	68	$\overline{100}$	$\overline{195}$	$\overline{146}$	32	224	307

x ⟶

z ↑

TABLE 6.5

z																															
15	15	1759	1722	1625	1505	1393	1310	1246	1185	1110	1003	912	867	886	956	1029	1085	1289	1176	1232	1259	1196	1039	848	735	768	882	925	769	423	70	81
		0	0	0	0	0	0	0	0	0	0	0	0	0	0	0	0	0	0	0	0	0	0	0	0	0	0	0	0	0	0	0
16	14	1658	1624	1536	1420	1308	1220	1157	1110	1057	975	897	847	848	899	966	1029	1164	1139	1182	1186	1089	904	698	589	628	747	783	610	239	135	294
		8	12	59	83	65	3	88	95	76	107	48	13	4	19	43	54	113	157	160	211	305	408	457	405	258	48	191	445	700	896	973
17	13	1406	1383	1317	1214	1099	1001	939	918	919	898	844	780	732	729	770	849	857	1013	1040	976	798	548	315	218	287	425	452	239	185	604	787
		16	15	83	129	100	12	151	159	210	192	100	28	20	35	28	11	101	201	255	383	578	782	870	766	488	108	319	765	1217	1566	1705
18	12	1113	1105	1071	995	880	769	696	698	742	777	750	660	542	466	466	555	520	786	798	702	413	100	144	205	84	98	133	100	559	1007	1194
		0	28	87	122	85	41	189	167	292	243	137	27	93	193	246	227	73	96	259	492	766	1069	1189	945	673	186	342	887	1438	1877	2051
19	11	871	879	880	836	736	718	532	530	588	650	633	515	332	179	126	207	283	499	515	358	56	280	503	504	312	71	3	203	640	1069	1248
		85	89	98	75	12	108	222	203	319	236	141	5	211	422	554	527	341	98	194	523	873	1239	1373	1205	793	275	257	802	1363	1821	2007
20	10	719	736	763	757	687	591	485	460	500	554	535	408	191	16	120	66	175	254	293	144	151	461	636	573	423	33	91	147	398	756	906
		285	205	130	17	98	215	283	242	309	180	82	87	353	651	841	799	588	278	98	484	894	1254	1398	1238	842	363	103	576	1080	1510	1686
21	9	646	665	701	723	693	622	536	486	486	514	499	392	189	34	176	162	142	148	212	101	151	407	524	419	149	148	299	235	4	256	362
		375	314	157	44	220	346	381	333	301	106	12	197	485	817	1027	964	678	385	8	388	778	1127	1284	1157	816	415	54	314	729	1103	1259
22	8	642	655	679	708	710	680	605	548	510	513	511	460	311	114	43	74	114	194	330	214	20	177	250	139	103	356	489	467	330	177	114
		385	314	125	116	325	466	503	478	336	78	93	299	575	892	1093	1030	797	432	82	250	593	909	1078	997	724	408	148	115	426	733	861
23	7	676	677	681	698	714	702	641	556	490	483	515	530	457	300	141	76	66	290	392	374	149	95	50	143	327	500	583	565	484	399	364
		237	175	9	191	383	539	622	669	453	153	89	326	594	891	1091	1068	845	490	189	93	388	679	854	810	589	336	148	26	247	474	574
24	6	632	633	639	655	661	626	532	414	330	334	411	494	483	356	208	116	10	284	404	433	359	295	240	309	435	538	567	533	468	414	392
		58	16	97	229	378	558	733	893	670	374	50	249	534	833	1071	1129	933	604	315	49	225	495	675	656	456	224	68	48	185	337	407
25	5	289	320	393	461	467	377	209	34	52	6	145	286	321	222	56	60	127	78	223	306	295	247	238	287	379	447	459	419	356	343	288
		138	91	20	143	303	551	857	1150	991	723	318	60	397	737	1044	1205	1056	757	431	140	136	397	568	552	363	128	32	116	208	298	340
26	4	575	475	242	28	28	120	386	616	676	538	287	65	6	91	274	415	423	301	129	8	54	40	27	50	128	207	215	241	192	149	126
		699	649	405	137	166	562	1033	1447	1387	1147	665	197	208	600	977	1227	1138	861	484	158	125	373	533	526	345	100	88	194	264	322	348
27	3	1995	1795	1319	861	868	857	1206	1474	1468	1187	784	458	346	444	652	819	694	736	544	363	277	284	328	343	282	170	59	4	13	47	68
		1943	1730	1210	603	7	621	1273	1773	1809	1569	1011	457	2	427	843	1138	1110	850	446	99	168	390	542	557	407	161	65	219	315	376	401
28	2	3686	3367	2619	1866	1545	1693	2089	2360	2265	1815	1238	790	628	721	946	1145	1127	1101	898	690	592	616	715	790	757	609	426	293	249	264	280
		3430	3075	2195	1153	177	720	1539	2082	2196	1913	1289	673	186	242	656	951	979	727	333	2	232	422	562	613	510	281	19	194	347	438	403
29	1	5082	4672	3706	2730	2256	2368	2777	3124	2859	2271	1551	1001	790	877	1114	1333	1498	1325	1121	904	807	858	1014	1243	1140	971	733	538	449	447	456
		4674	4203	3013	1600	302	815	1755	2312	2483	2137	1461	806	315	96	488	760	826	576	214	96	287	440	580	665	607	399	112	156	359	489	532
30	0	5619	5180	4131	3067	2535	3628	3042	3293	3080	2437	1662	1071	840	922	1163	1391	1647	1398	1194	975	882	945	1126	1279	1288	1112	855	635	529	520	527
		5160	4642	3331	1774	347	853	1836	2396	2622	2212	1520	852	363	40	420	680	760	512	263	134	306	448	586	686	646	447	151	136	363	508	556
		0	1	2	3	4	5	6	7	8	9	10	11	12	13	14	15	16	17	18	19	20	21	22	23	24	25	26	27	28	29	30

x →

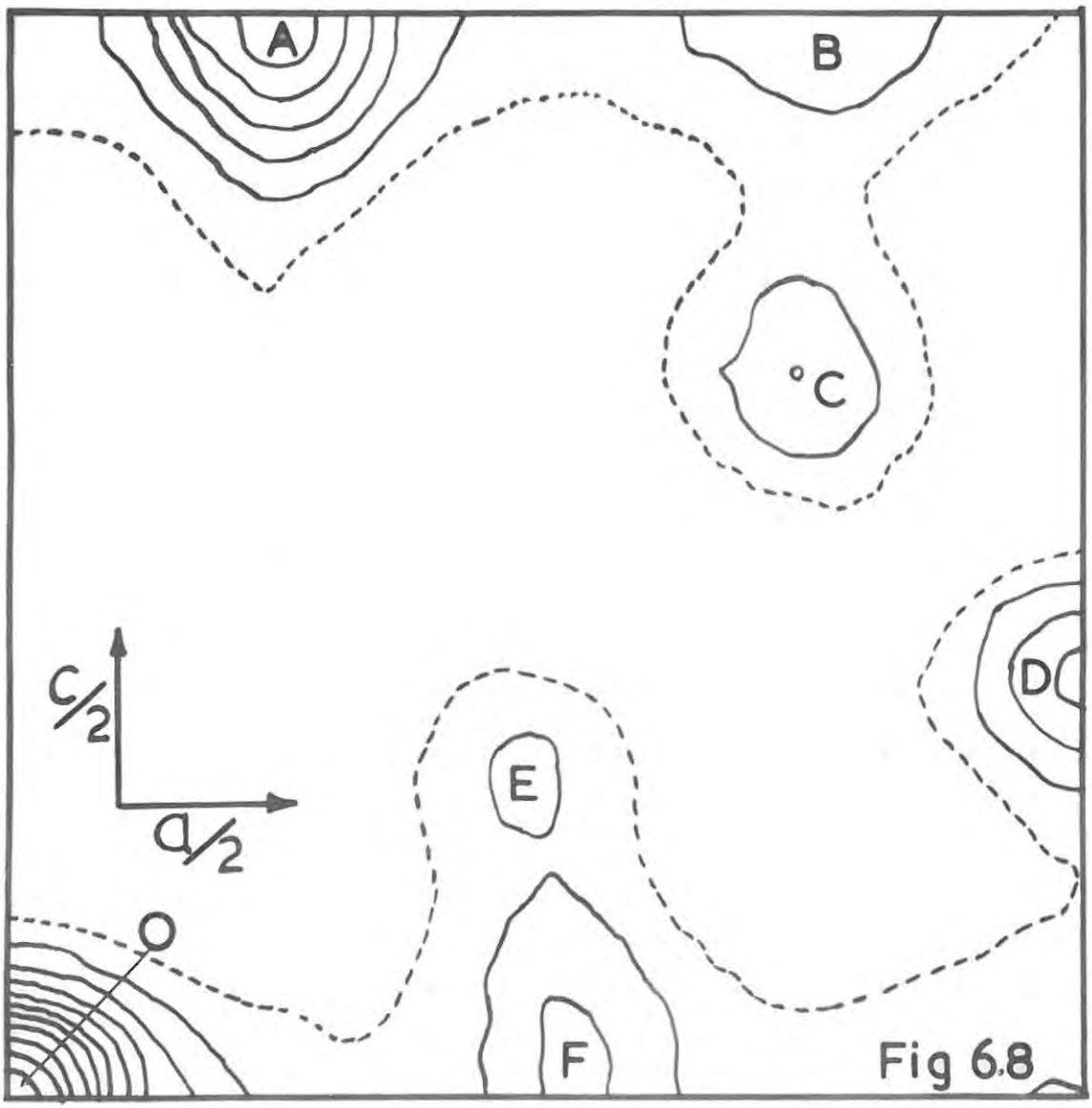

Fig 6.8

6.7 THE INTERPRETATION OF THE PATTERSON MAP.

The Patterson function, when summed, gives P(u,w), the value of the electron density product at the points (u,w) on the Patterson map. The crystal was rotated about the b axis thus the symmetry of the plane projection of the crystal is pgg. The plane group pgg is shown in Fig. 6.9 and its Patterson representation is shown[52] in Fig. 6.10 In this figure a rotation peak is indicated by a black circle and a reflection satellite by an open circle. It can be shown[53] that a point r, having coordinates x,y on the projection pgg has rotation peaks on the Patterson which are of single weight and have coordinates $\pm$ 2x, $\pm$ 2y referred to an origin at 00. There are two kinds of reflection satellites of double weight. If we place a satellite origin at $\frac{1}{2}$, $\frac{1}{2}$, the satellites have coordinates $\pm$ 2x, 0 and 0, $\pm$ 2y. This is illustrated in Figs. 6.11A and 6.11B.

Since peak C on the Patterson map (Fig. 6.8) was strong and showed reflection satellites (peaks A and D) at approximately expected positions, this was taken as the Cs - Cs rotation peak. This had a height of 2034 (arbitrary units). The coordinates of this peak on the Patterson map, expressed as fractions of the unit cell edges were $x = \frac{22.2}{60}$, $z = \frac{19.8}{60}$, while the coordinates of the two reflection satellites (taking the origin at $\frac{1}{2}$, $\frac{1}{2}$ as in Fig. 6.11B) were:

peak A $x = \frac{22.5}{60}$, $z = 0$ (height 5700)

peak D $x = 0$, $z = \frac{18.5}{60}$ (height 3300)

If these peaks were only due to the Cs atoms, they should be approximately two times the height of the rotation peak C. Two Cs atoms were thus placed in the positions indicated by Cs_2 and Cs_3 in Fig. 6.12, which shows a projection of the unit cell. The other two caesium

- atoms were -

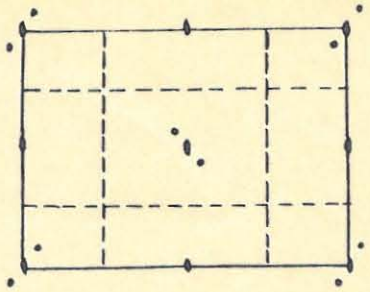

Plane group

p g g

Fig 6.9

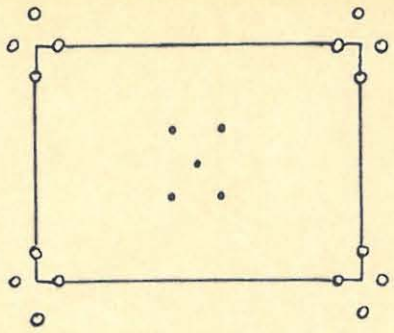

Patterson

Representation

Fig 6.10

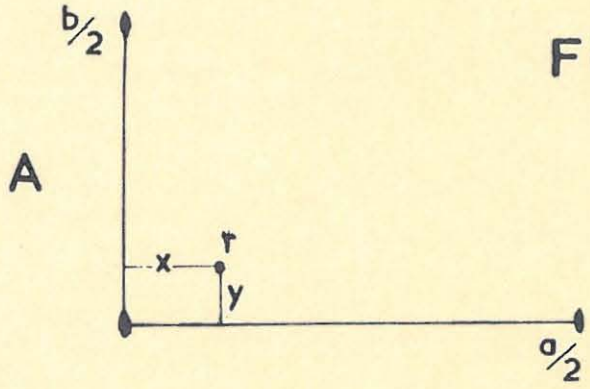

Fig 6.11

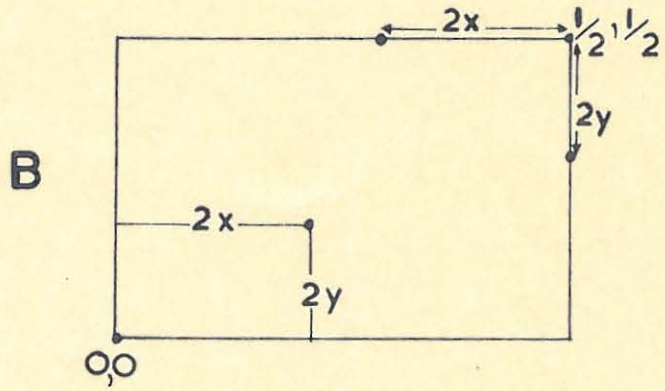

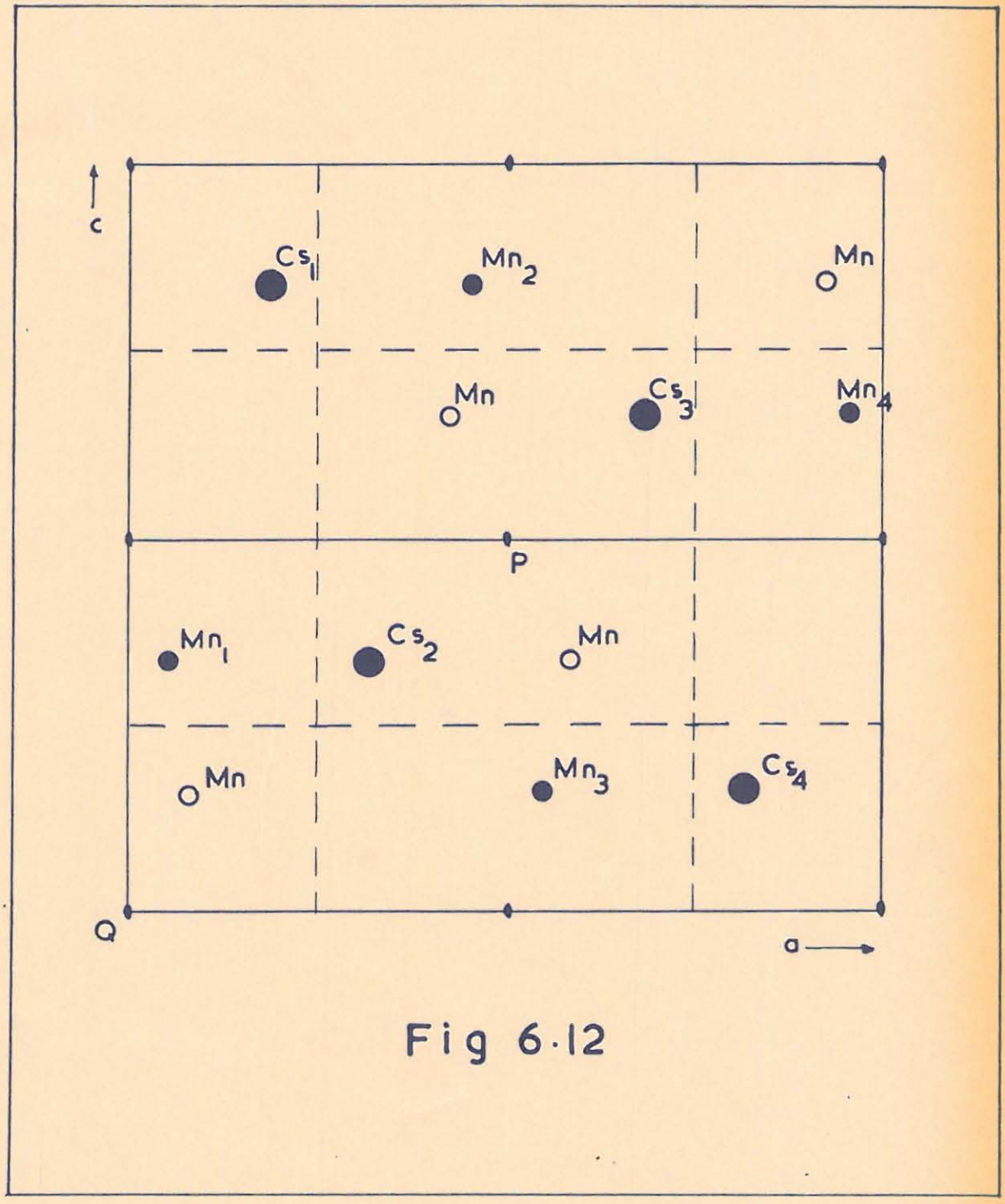

Fig 6.12

atoms were placed in positions Cs_1 and Cs_4 by glide reflection across the glide planes. The atoms Cs_2 and Cs_3 have coordinates which are half in value to the coordinates of their rotation peak C, namely $x = \pm \frac{11.1}{60}$, $z = \pm \frac{9.9}{60}$, the origin being taken at the point P. The second highest peak in the map was the peak F (height 2407). This was taken as a Cs - Mn peak and had coordinates $x = \frac{16}{60}$, $z = \frac{0}{60}$ on the Patterson map. The Mn atoms could thus be placed in relation to the Cs atoms. There arise two possibilities however: for any one Cs atom, a Mn atom can be placed either to the left or right of it, as can be clearly seen with Cs_2 and Cs_3 in Fig. 6.12. The Mn atoms can thus be placed in two general positions, shown as closed and open circles respectively in Fig. 6.12.

The Patterson Box.

The positions of the atoms which were calculated from the Patterson map were checked by the Patterson diagrams obtained from a Patterson box, the theory of which was discussed in Section 1.5. The two screens AA′ and BB′ (Fig. 1.25) were prepared by punching circular holes in sheets of cardboard. The distances AA′ to BB′ and BB′ to CC′ were made equal (12.7 cm), so that the pattern on AA′ was drawn twice as large as that drawn on BB′. The punched card AA′ is shown in Fig. 6.13, which is drawn to scale. Following Buerger[54] the holes of the Cs atoms were punched in the positions shown and the area of the holes was proportional to the number of electrons of the element. Thus number of electrons proportional to area proportional to r^2

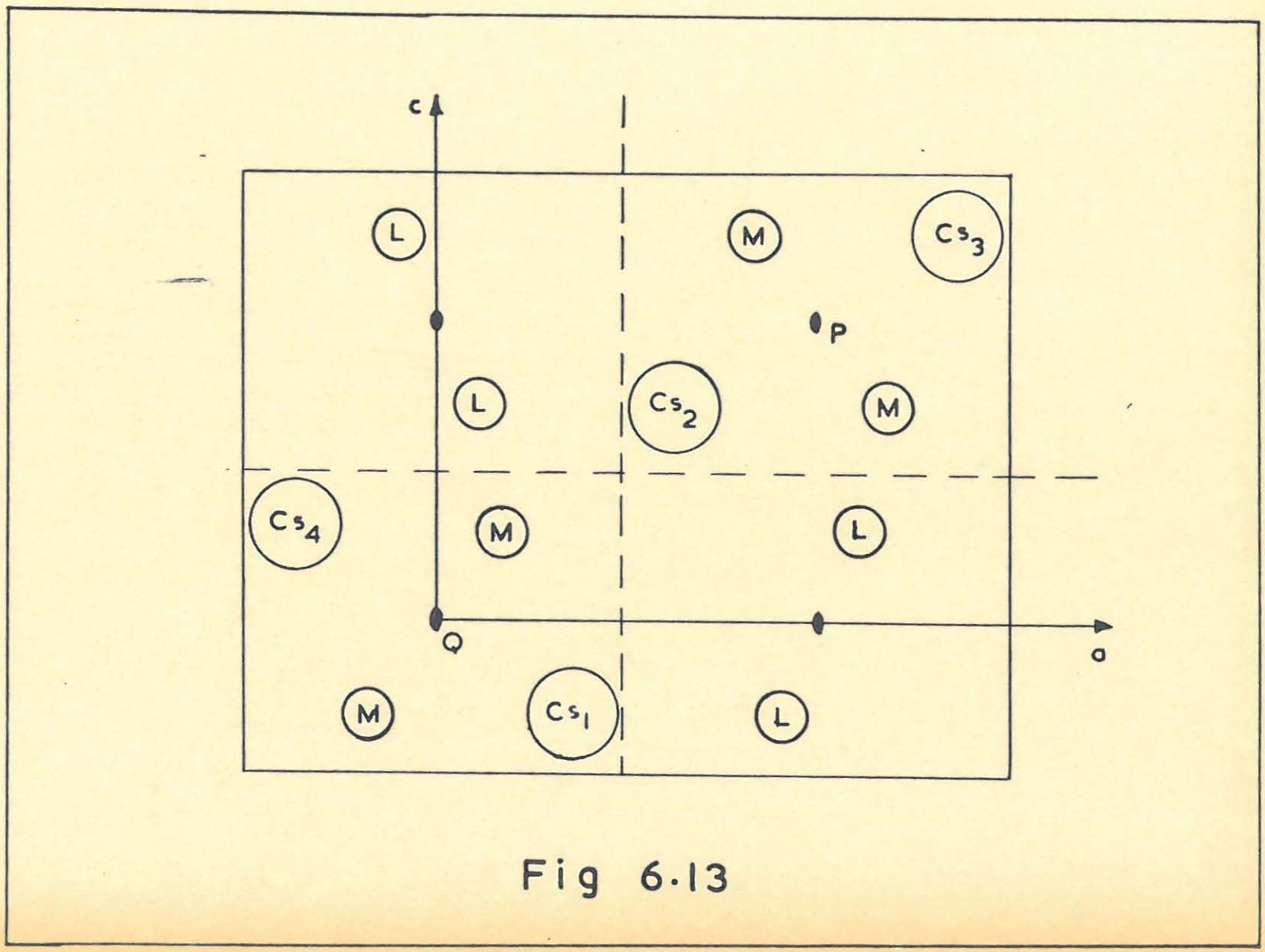

Fig 6.13

			card AA′	card BB′
For	Cs^+	r^2 proportional to 54	r = 7.35 mm	r = 3.6 mm
	Mn	r^2 " " 23	r = 4.80 mm	r = 2.40 mm

Two sets of holes corresponding to Mn atoms were punched. The set marked L corresponds to the Mn atoms marked by closed circles in Fig. 6.12, while the set marked M corresponds to the Mn atoms marked by open circles. The object of experimenting with the Patterson box was not only to confirm the positions of the Cs atoms, but to find the correct relative positions L or M of the Mn atoms.

The screen AA′ was illuminated from the left (Fig. 1.25) by a strong diffused light and the peaks in the Patterson diagram appeared on the surface CC′. The projection surface CC′ was a milk-glass plate which was viewed from the right. The distances of the screens were large in comparison with atomic parameters and the contours of the Patterson peaks obtained were circular, the diameter of a circle being the sum of the diameters of the two corresponding atom holes in AA′. The Patterson box thus gives diagrams which have these important features of the real Patterson function. The Patterson diagrams which were thus obtained were photographed by placing a sheet of X-ray film at CC′. These are shown in Fig. 6.14, only 1/4 of each Patterson diagram is shown for convenience. Fig. 6.14 A shows the Patterson map (Fig. 6.8) drawn to scale. Fig. 6.14 B shows the diagram obtained by placing only the Cs atoms on the punched cards. The peaks obtained on the photographic film were of high intensity and well defined. They correspond to the Cs - Cs rotation peak C, and the two reflection

satellites A and D of the Patterson map. This confirmed that the positions of the Cs atoms were correct.

Fig. 6.14 shows the diagram obtained by placing only the Mn atoms in position L on the punched cards. Two peaks were obtained at the borders of the diagram corresponding to the peaks B and D of the Patterson map and a small peak of low intensity which probably corresponds to the tip of peak A in the Patterson map. The diagram shown in Fig. 6.14D, was obtained by placing both the Cs and the Mn atoms (position A) on the cards. Two additional peaks corresponding to the peaks E and F were obtained, which must be due to Cs - Mn vectors. The peak corresponding to F was of higher intensity than that corresponding to C. The diagram shown in Fig. 6.14E, was obtained by placing only the Mn atoms in positions M. Two small peaks obtained at the borders corresponded to the peaks B and D of the Patterson map, but the third peak did not match with any peaks at all. Finally the diagram shown in Fig. 6.14F, was obtained by placing the Cs atoms and the Mn atoms (positions M). This diagram is similar to that shown in Fig. 6.14D, except that there was a large peak, due to a Cs - Mn vector which did not correspond to any peak on the Patterson map. This shows that the Mn atoms cannot be placed in positions M, and the positions L are thus correct. In each diagram there was a large origin peak, as can be expected. The diagram shown in Fig. 6.14D resembles the Patterson map (Fig. 6.14A) very closely.

The Minimum Function.

Accepting peak C of the Patterson function as the correct location of the Cs - Cs rotation peak, one can then set up the

Fig 6.14

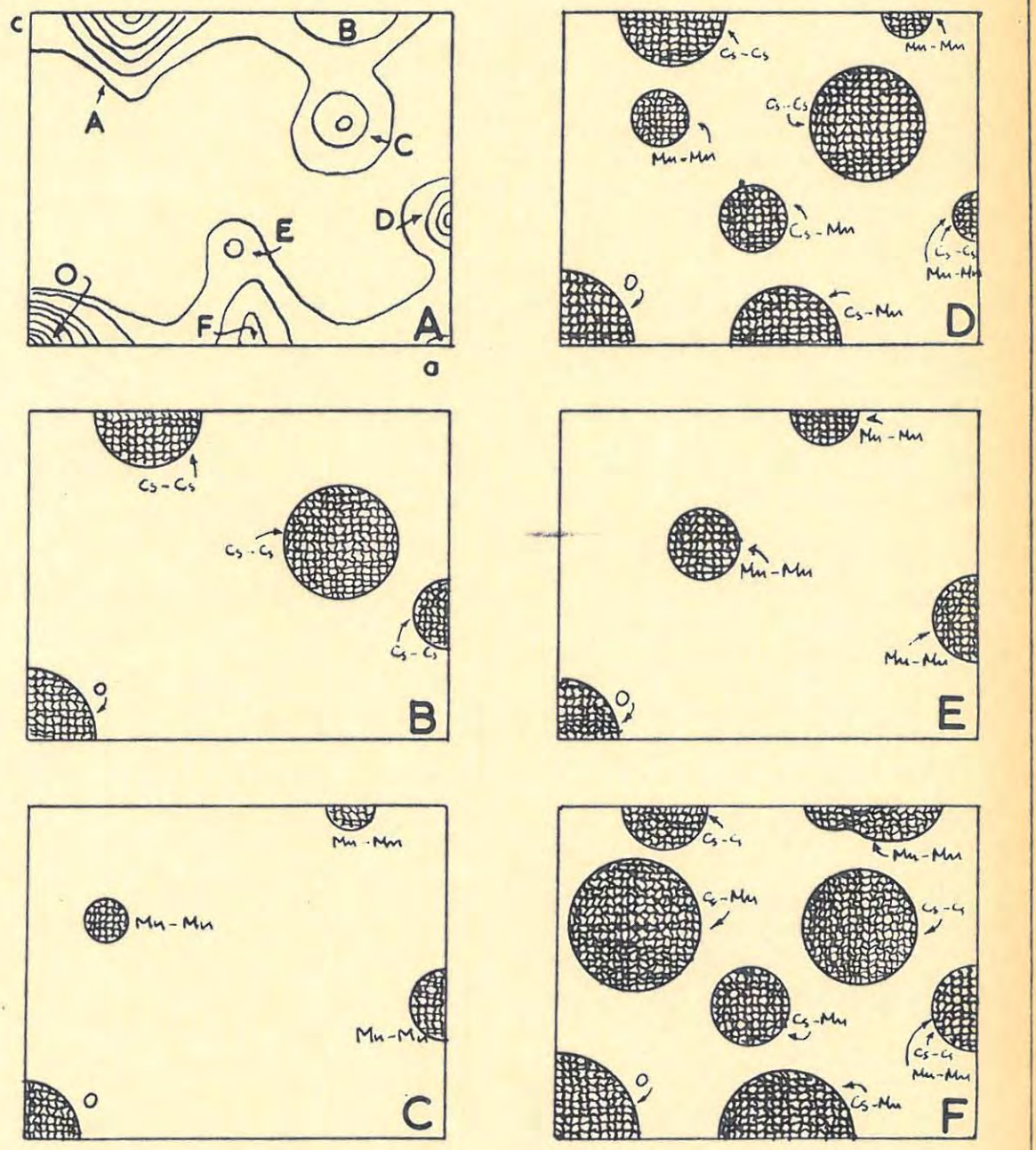

function based upon the coordinates of this point, plus those of the origin. The minimum function is then found by placing one Patterson map over another, the origin of one being placed at the peak C of the other. The M_2 map was obtained by contouring the minimum as previously described in Section 1.5 (c). Following Buerger[55], who discusses a similar example on a projection having the same plane group pgg, a map of the M_4 function and finally a map of the M_8 function was traced. The resulting $M_8(x,y)$ map is shown in Fig. 6.15, which clearly shows the positions of the Cs and Mn atoms corresponding to Cs_2 and the Mn atom in position L in the bottom left quarter of the unit cell of Fig. 6.12.

The result of the Minimum function thus confirms the positions of the Cs and Mn atoms obtained by direct analysis of the Patterson map, and the Patterson diagrams obtained from the Patterson box.

For convenience the point Q (Fig. 6.12) was taken as the origin of the unit cell, and the final positions of the atoms obtained were:

	Cs	Mn
Result of Minimum function	x = 0.318	x = 0.053
	z = 0.332	z = 0.315
Direct analysis of Patterson map	x = 0.315	x = 0.048
	z = 0.335	z = 0.335

These values agree closely. It was decided that the coordinates of the atoms obtained from the M_8 map of the Minimum function were more accurate than those obtained by direct analysis of the Patterson map, because no account was taken of the Cs - O and Mn - O vectors. The

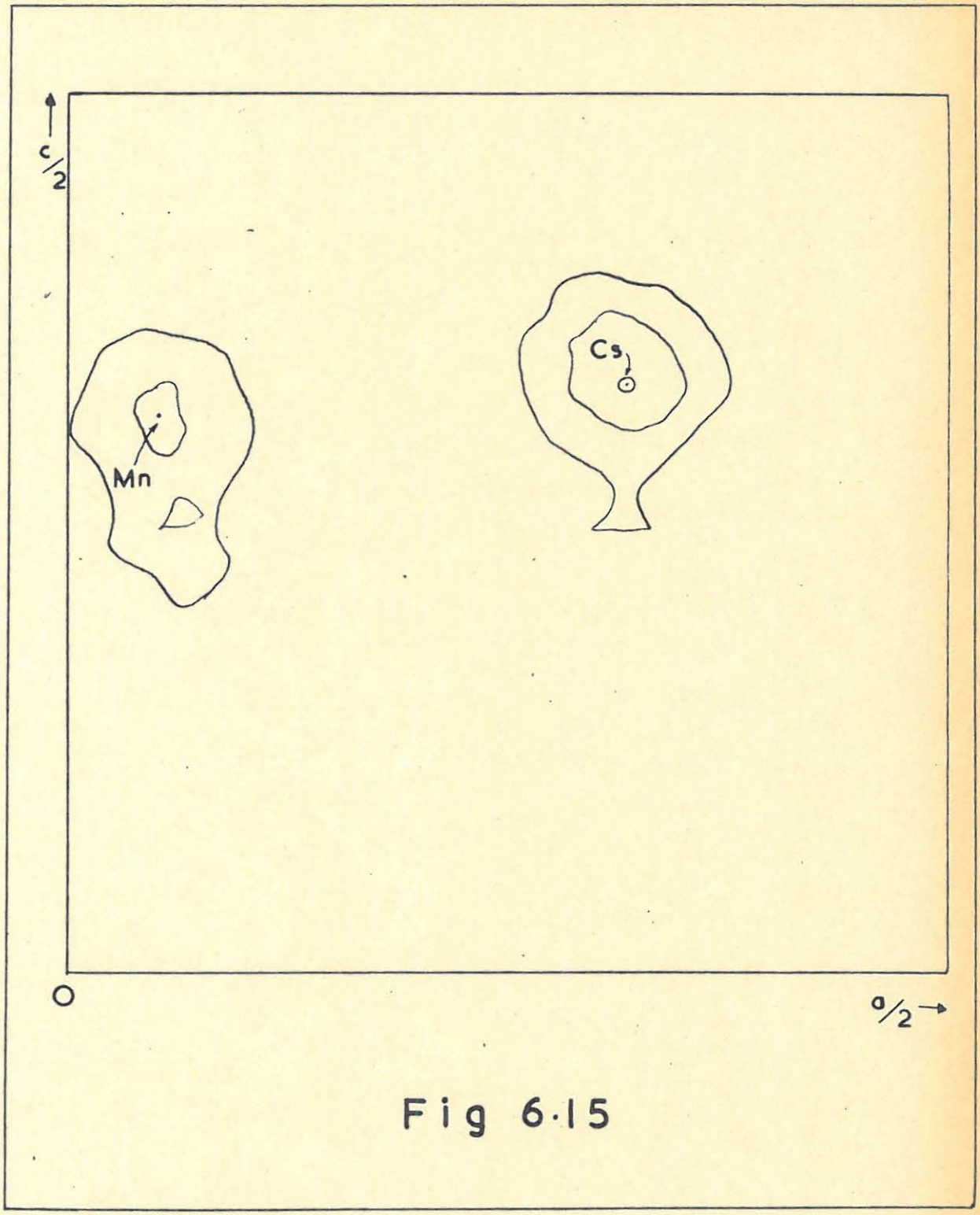

Fig 6.15

contribution due to the latter vectors, although small, would obviously influence the Patterson map to some extent, so that the peaks in the map cannot be regarded as being solely due to Cs - Cs, Cs - Mn and Mn - Mn interactions.

6.8 THE SUMMATION OF THE FOURIER SERIES: (010) PROJECTION.

Having found the positions of the Cs and Mn atoms, the signs of the structure factors were calculated for all the reflections. In Section 1.4 it was shown that the structure factor F_{hkl} could be expressed as

$$F_{hkl} = (\sum_j f_j A_j) + i(\sum_j f_j B_j) \quad \ldots\ldots\ldots \quad 1.23$$

where $A = \cos 2\pi(hx + ky + lx)$

$$B = \sin 2\pi(hx + ky + lz) \quad \ldots\ldots\ldots \quad 1.24$$

For the plane group pgg[56]

$$A = 4 \cos 2\pi(hx + \tfrac{h+l}{4}) \cos 2\pi(lz - \tfrac{h+l}{4}) \quad \ldots\ldots\ldots \quad 6.25$$

$B = 0$ $\therefore$ the structure factors are either positive or negative (Section 1.4 (a)).

Equation 6.25 may be written in product form to facilitate computation

$$\text{for } h + l = 2n \quad A = 4 \cos 2\pi hx \cos 2\pi lz \quad \ldots\ldots\ldots \quad 6.26$$

$$\text{for } h + l = 2n+1 \quad A = -4 \sin 2\pi hx \sin 2\pi lz \quad \ldots\ldots\ldots \quad 6.27$$

If there are n different atoms in the unit cell the structure factor for any reflection hkl may be written as

$$F_{hkl} = f_1 A_1 + f_2 A_2 + f_3 A_3 + \ldots\ldots + f_n A_n$$

where f_1, f_2, f_3 ..... f_n are the scattering factors of the atoms and A_1, A_2, A_3 ..... An are given by Equations 6.26 and 6.27.

- In our case -

In our case only the positions of the Cs and Mn Atoms were known, so the structure factor calculations took no account of the oxygen atoms at this stage. The latter have much lower atomic scattering factors however and it was thus assumed that the heavier Cs and Mn atoms pay a much higher contribution than the O atoms, and thus control the signs of the structure factors. This proved to be correct.

The signs of the structure factors were calculated, the computations being set out as recommended by Lipson and Cochran[57]. The atomic scattering factors were obtained from ables[58, 59]. The square roots of the $|F_{hOl}|^2$ values used in the Patterson summation were calculated and the appropiate positive or negative sign was given to each structure factor. These were then scaled to suit the Beevers-Lipson strips summation, and a Fourier synthesis was computed. For the plane group pgg the general relation for the electron density given in Equation 1.31 can be modified to[60]

$$\rho(x,z) = \frac{4}{S} \sum_{h+l=2n}{}' \sum{}' F_{hOl} \cos 2\pi hx \cos 2\pi lz - \sum_{h+l=2n+1}{}' F_{hOl} \sin 2\pi hx \sin 2\pi lx \quad \ldots\ldots\ldots \quad 6.28$$

The prime marks after the $\sum'$s indicate that the structure factors of the axial reflections enter the series at half value because they occur on a line of symmetry. S is the area of the projection; since the F_{hOl}'s are not on an absolute scale, 4/S which is a constant, was left out of the summation.

- The sequence -

The sequence in which the series was summed is as follows:

$$\sum_{h+l=2n}\sum' \cos 2\pi lz - \sum_{h+l=2n+1}\sum' \sin 2\pi hx \sin 2\pi lz \quad \ldots\ldots \quad 6.29$$

F_{hOl}

F_{hOl}, $h+l=2n$	F_{hOl}, $h+l=2n+1$
$\sum_{l}' F_{hOl} \cos 2\pi lz$	$\sum_{l}' F_{hOl} \sin 2\pi lz$
expand over $z = 0$ to $\frac{1}{2}$	expand over $z = 0$ to $\frac{1}{2}$
$\sum_{h}' [F_{hOl} \cos 2\pi lz] \cos\pi 2\, hx$	$\sum_{h}' [F_{hOl} \sin 2\pi lz] \sin 2\pi hx$
expand over $x = 0$ to $\frac{1}{2}$	expand over $x = 0$ to $\frac{1}{2}$

\+ -

$$\sum_{h+l=2n}\sum' F_{hOl} \cos 2\pi hx \cos 2\pi lz - \sum_{h+l=2n+1}\sum' F_{hOl} \sin 2\pi hx \sin 2\pi lz$$

The method of summation, using Beevers-Lipson strips, was similar to that used for the summation of the Patterson function, which is described in detail in Section 6.6 (b). The cell edges were divided into intervals of $\frac{1}{120}$, in the hope that the detailed Fourier map would show the positions of the oxygen atoms. The resulting electron density projection is shown in Fig. 6.16. The figure shows two large peaks, the larger one showing the position of the Cs atom and the other the Mn atom. The positions of these atoms, as obtained

- from the -

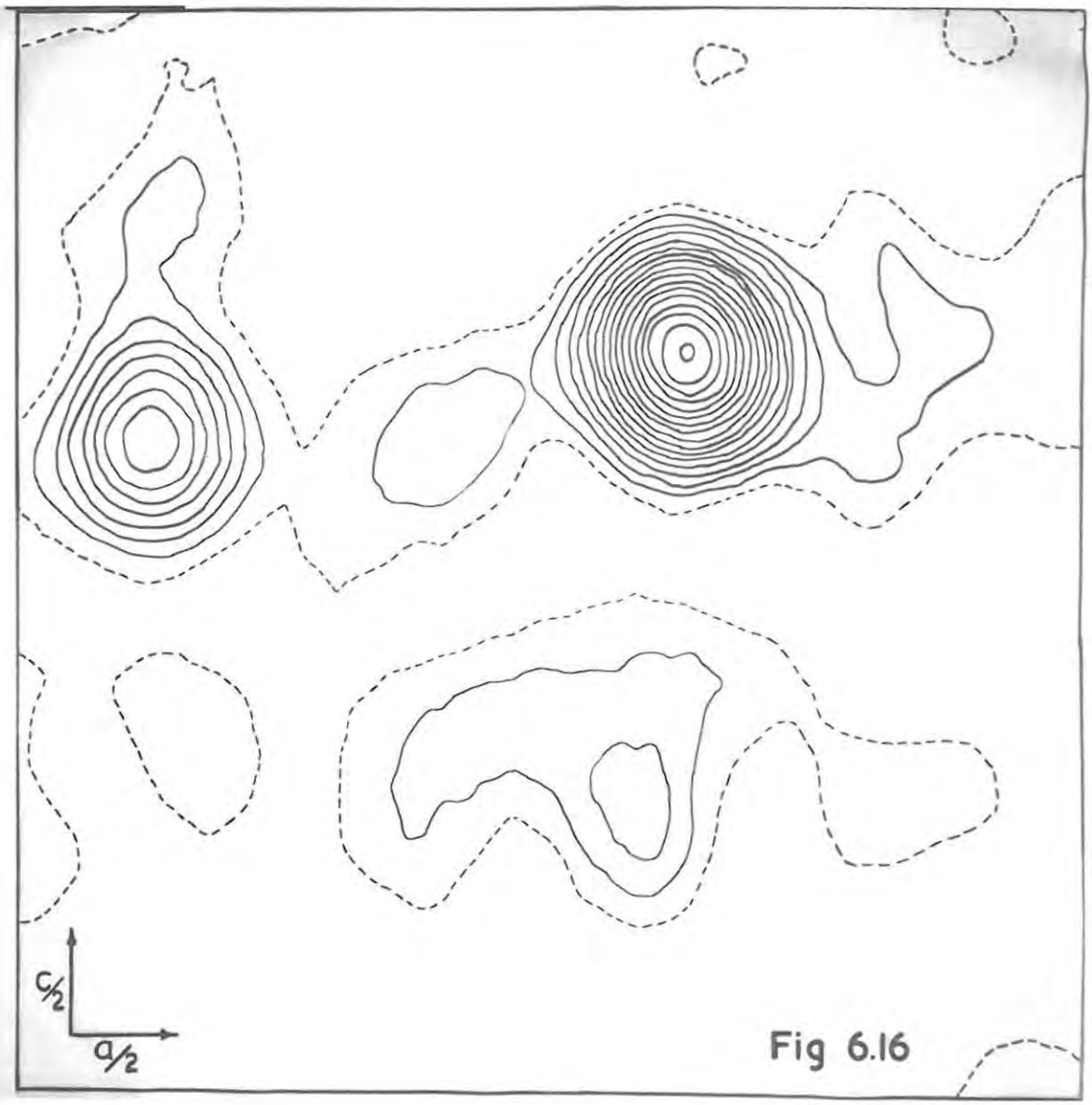

Fig 6.16

from the Fourier map by drawing sections through the electron density peaks, were:

Cs	Mn
x = 0.316	x = 0.062
z = 0.342	z = 0.302

These values compare favourably with those obtained from the minimum function and the direct analysis of the Patterson map (Section 6.7). The broken line drawn on the Fourier map shows the zero contour, while the other contours were drawn at arbitrary intervals of 50 units. The other peaks in the Fourier map are of small magnitude and diffuse shape. They did not give any clue as to the oxygen positions.

The structure factors were calculated by placing the Cs and Mn atoms in the positions obtained from the Fourier synthesis. The F_o and F_c values being on different scales, they were normalised on reflection (108). This particular reflection was chosen because it was of high angle, and thus little affected by the oxygen contribution, and of fairly high intensity so that it could be accurately measured. The residual R was found to be R = 36.22%. This value is high, indicating that the heavy atoms are not in their correct positions or that the oxygens pay a large contribution to the calculated structure factors.

It was now decided to place the oxygens tetrahedrally round the Mn atom as in $KMnO_4$[36]. This was only a tentative arrangement, the Mn-O bond length was taken as 1.59 Å, which was the mean value obtained by Mooney in the crystal structure of $KMnO_4$. It was further assumed that the tetrahedron was regular. The positions of the oxygen atoms, calculated on the above basis, were:

$O_1 + O_2$ (superimposed in projection) x = 0.053 z = 0.188

O_3 x = 0.208 z = 0.404

O_4 x = 0.446 z = 0.071

The contribution of the oxygen atoms thus placed was taken into account in the calculated structure factors, and the value of the residual was found to be R = 38.11%. This showed that the oxygen contribution was small and that they were probably not in the correct position, because on addition of the oxygens, the residual should have decreased.

At this stage it was felt that the structure should be refined in order to bring the value of the residual to below 25%. Better absorption corrections, correction due to thermal vibration of the atoms and small changes in the coordinates of the heavy atoms would have to be taken into account. Before starting to refine the structure on the AC projection, however, it was decided that, the space group should be unambiguously determined.

6.9 THE UNAMBIGUOUS DETERMINATION OF THE SPACE GROUP.

In the determination of the space group (Section 6.4) it was found that from analysis of the systematic absences of the reflections there were two possible space groups namely, Pnma and $Pna2_1$, depending on the choice of axes. Both these space groups, however, give rise to the plane group pgg when projected down the b and c axes respectively, so that up to now the ambiguity of the space group has been of no consequence. The space group Pnma was chosen by analogy with the structure of $KMnO_4$[36], but this now had to be proved.

The space group Pnma has the special positions 1/4 and 3/4 along the b axis. It was thus decided to compute a Fourier synthesis on the (001) projection and show that the y coordinate of the Cs and Mn atoms was 1/4 or 3/4. This would in turn check the x coordinate of the two heavy atoms, as obtained by the Fourier synthesis computed on the (010) projection.

The space group Pnma, when projected along the c axis, gives rise to the plane group pgm[61]. In Section 1.4 it was shown that the structure factor could be expressed as

$$F_{hkl} = \left(\sum_j f_j A_j\right) + i\left(\sum_j f_j B_j\right) \quad \ldots\ldots \quad 1.23$$

For the plane group pgm it can be shown that[62]

$$A = 4 \cos 2\pi(hx + \tfrac{h}{4}) \cos 2\pi(ky - \tfrac{h}{4}) \quad \ldots\ldots \quad 6.30$$

$B = 0$ $\therefore$ the structure factors are either positive or negative (Section 1.4 (a)).

- Equation 6.30 -

Equation 6.30, written in product form, yields the expressions:

for $K = 2n$ $\quad A = 4 \cos 2\pi hx \cos 2\pi ky$ 6.31

$K = 2n+1$ $\quad A = -4 \sin 2\pi hx \sin 2\pi ky$ 6.32

The Cs and Mn atoms we placed at the positions corresponding to Cs_2 and Mn_2 of Fig. 6.12, these atoms being related, by analogy with the structure of $KMnO_4$ [36] by both having their y coordinate equal to 0.250.

Cs	Mn
x = 0.316	x = 0.438
y = 0.250	y = 0.250

and the signs of the structure factors calculated as discussed in Section 6.8.

Weissenberg photographs were taken with the crystal oscillating about the c axis, the reflections were indexed and the Bragg angle Θ for each reflection was calculated from Equation 6.9 and the Bragg equation. A set of integrated reflections was obtained by using an integrating Weissenberg goniometer. The spots on the photograph all showed a plateau of constant area, and the density of this plateau was measured with the photometer as described in Section 5.7. The intensities were then corrected for the Lorentz, polarisation and absorption factors. The crystal used was block-shaped, and was approximated to a sphere having mean radius R = 0.0119 cm giving a value of $\mu R = 848.7 \times 0.0119 = 10$ (Section 6.5). The square roots of the relative corrected intensities were calculated and used to compute a Fourier summation. For the plane group pgm the general relation for the electron density given in Equation 1.31 can be

- modified to -

modified to[62]:

$$\rho(x,y) = \frac{4}{S} \sum_{k=2n}{}' \sum{}' F_{hk0} \cos 2\pi hx \cos 2\pi ky - \sum_{k=2n+1}{}' \sum{}' F_{hk0} \sin 2\pi hx \sin 2\pi ky \quad \ldots\ldots\ldots \quad 6.33$$

The prime marks after the $\sum'$s indicate that the structure factors of the axial reflections enter the series at half value because they occur on a line of symmetry. The sequence in which the series was summed is the same as that adopted for the Fourier synthesis in the (010) projection. The cell edges were divided in intervals of $\frac{1}{60}$ and the resulting electron density projection is shown in Fig. 6.17. In this map the cell edges were divided into intervals of $\frac{1}{60}$ and the contours were drawn at arbitrary intervals of 100 units. The figure shows the Cs and Mn peaks clearly, showing that the y coordinate is exactly 0.250 as expected. The x coordinates of the two atoms compare closely with the ones obtained from the Fourier synthesis on the (010) projection:

	Cs	Mn
(010)	x = 0.316	x = 0.438
(001)	x = 0.310	x = 0.448

The x coordinates obtained from the (001) projection were not regarded as accurate, however, because only 27 reflections were available for the Fourier summation and series-termination errors are thus liable to be serious[63]. These coordinates are thus only offered as a check. Due to the lack of a sufficient number of reflections it was also

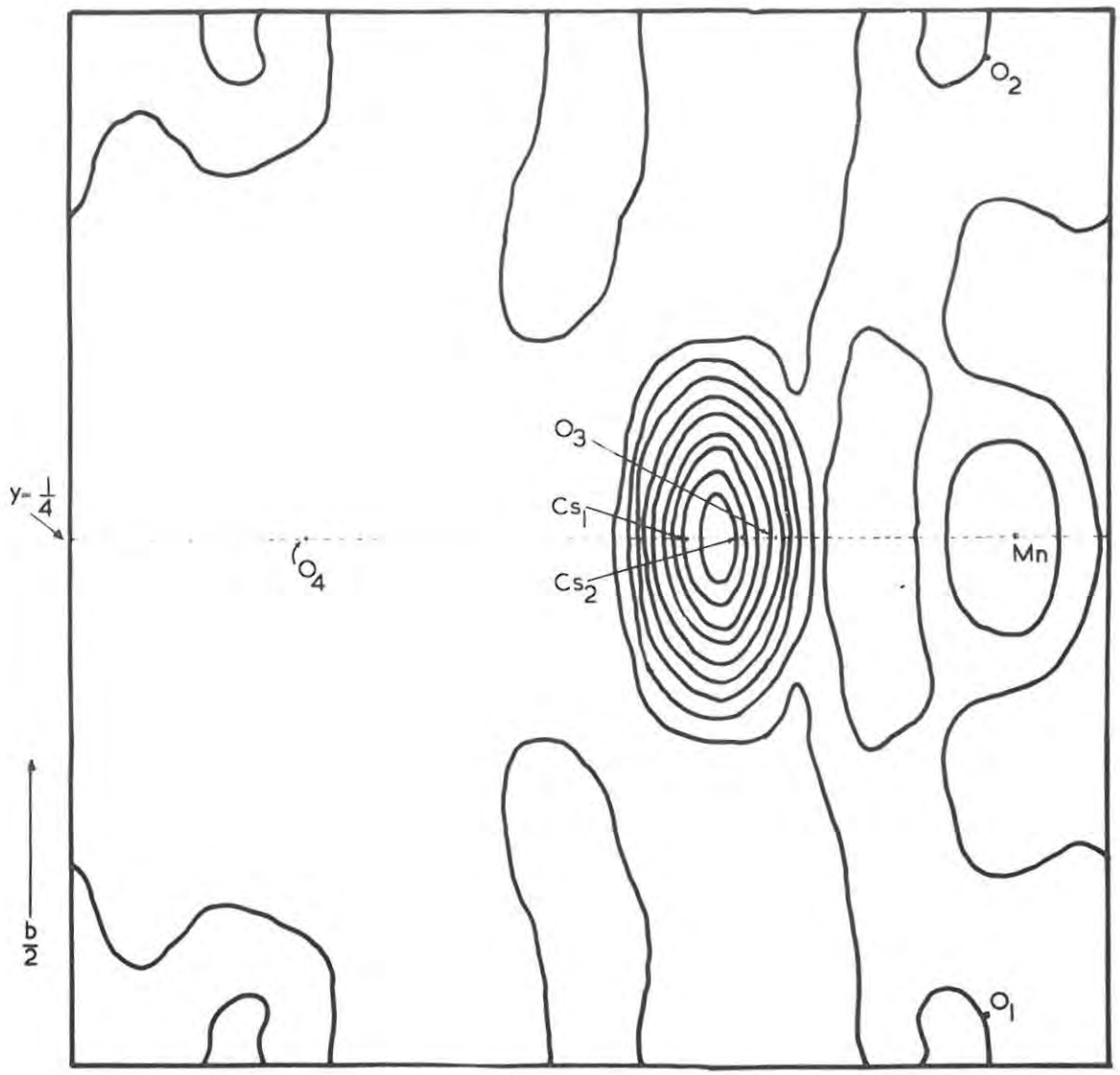

Electron Density Projection Fig 6.17

decided not to attempt refinement of the coordinates of the heavy atoms or to attempt to locate the oxygen atoms on the (001) projection. The positions of the oxygen atoms, as found later from difference syntheses on the (010) projection, are also shown on Fig. 6.17.

REFINEMENT.

.1 THE DIFFERENCE SYNTHESIS.

Let us suppose that two Fourier syntheses are computed, one with F_o and the other with F_c. The former will give rise to peaks at the the true atomic positions, while the latter has peaks where the postulated structure has atoms. If the F_c synthesis is subtracted from the F_o synthesis we obtain the "Difference" synthesis which has interesting properties. If an atom has been placed correctly, then its F_o and F_c peaks will coincide, and in the difference Fourier, where we effectively subtract the two peaks, the atom will lie in an area of low relief. But if an atom has not been correctly placed, then its true position will be given by the F_o peak and its postulated position by the F_c peak. On the difference map the postulated location is in a hole and the correct location on a peak, so that the postulated position may be corrected by shifting from the hole to the peak. If the error is small, the postulated location is on a steep gradient and can be improved by shifting up the slope. This is illustrated in Fig. 7.1. The direction of the shift is always normal to the contours on the difference map. The magnitude of the shift (ϵ) can be determined geometrically. This is done by drawing duplicate profiles of the atom from the electron density map and displacing the two until the observed gradient in the difference map is obtained[64]. The above method was used when the positions of the atoms were moved and proved fairly successful.

Fig 7.1

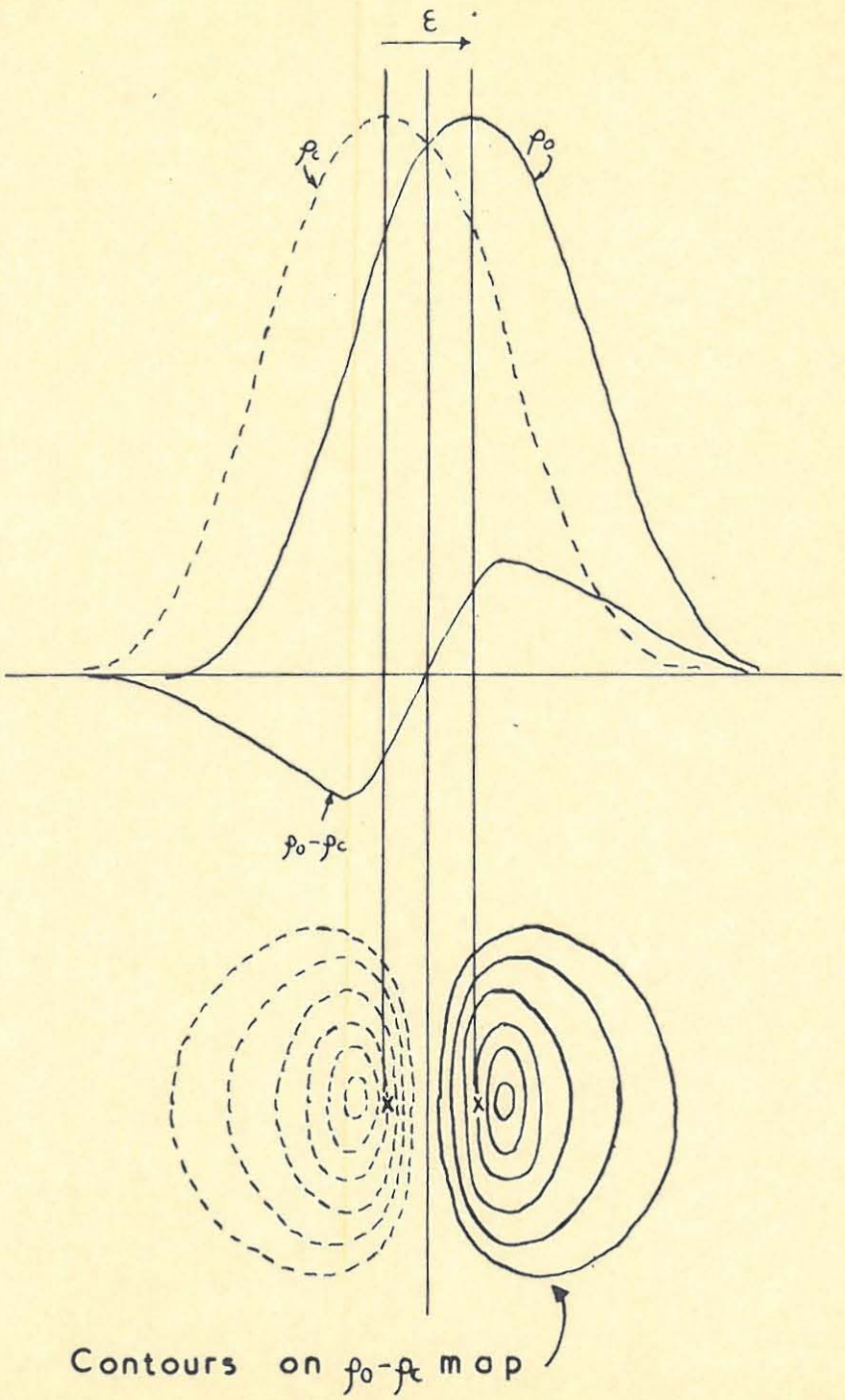

Difference syntheses can be calculated by subtracting, point by point, the results of the syntheses using F_o and F_c as coefficients in the Fourier series. This, however, is equivalent to a single synthesis using $(F_o - F_c)$ as coefficients. This can be shown by considering the two dimensional syntheses

$$\rho_o = \frac{1}{S} \sum_h \sum_k F_o e^{-i2\pi(hx + ky)} \quad \ldots\ldots \quad 7.1$$

$$\rho_c = \frac{1}{S} \sum_h \sum_k F_c e^{-i2\pi(hx + ky)} \quad \ldots\ldots \quad 7.2$$

$$\rho_o - \rho_c = \frac{1}{S} \sum_h \sum_k (F_o - F_c) e^{-i2\pi(hx + ky)} \quad \ldots\ldots \quad 7.3$$

In the earlier stages of structure analysis the phases of the F_o's are not known, so only those terms $(F_o - F_c)$ can be used in the error synthesis for which F_o is zero or very small. A Fourier series made up of such terms only is called a "Bunn error synthesis"[65]. In the later stages of refinement, however, most or all the phases of the F_o's become known and a full difference synthesis may thus be computed. The full difference synthesis was suggested as a means of refinement by Booth[66], while its properties were exploited by Cochran[67, 68]. Difference syntheses have the advantage that when the proposed and actual structures are nearly the same, their series termination errors are similar and thus fall away on subtraction. Moreover, since the Fourier coefficients are all differences, they are small, and the series is easy to compute.

The most fundamental property of the difference Fourier is that

- when the -

when the proposed model matches the crystal structure exactly, the difference map should be flat. If the proposed structure is slightly incorrect, the discrepancies reveal themselves in the difference map and the structure is modified in such a way as to produce a nearly featureless difference map.

The $(F_o - F_c)$ values which were employed in the calculation of the residual (Section 6.8), were used to calculate the first difference Fourier. The oxygen contribution, with the oxygen atoms tentatively placed as in $KMnO_4$ [36], was taken into account in the calculation of the F_c's. The resulting difference Fourier is shown in Fig. 7.2. The $\rho_o - \rho_c$ values were calculated at intervals of $\frac{1}{120}$ of the cell edges and contours were drawn at arbitrary intervals of 50 units. The map clearly shows that the Mn atom lies in a hollow and is moved towards a peak, at right angles to the contours, as indicated by the arrow. The Cs atom lies in a hollow between two peaks of unequal height. The meaning of these two peaks was not understood at this stage and the Cs atom was moved towards the higher of the two peaks as shown on the map. The topography of the difference Fourier in the regions of the oxygen atoms did not show any significant peaks, so the oxygen positions were left unaltered. The new Cs and Mn parameters were as follows:-

Cs	Mn
x = 0.303	x = 0.050
z = 0.345	z = 0.292

The value of the residual, calculated by placing only the Cs and Mn atoms in the psoitions indicated above, was 32.50% - an improvement of 3.72% on the previous value.

- Since the first -

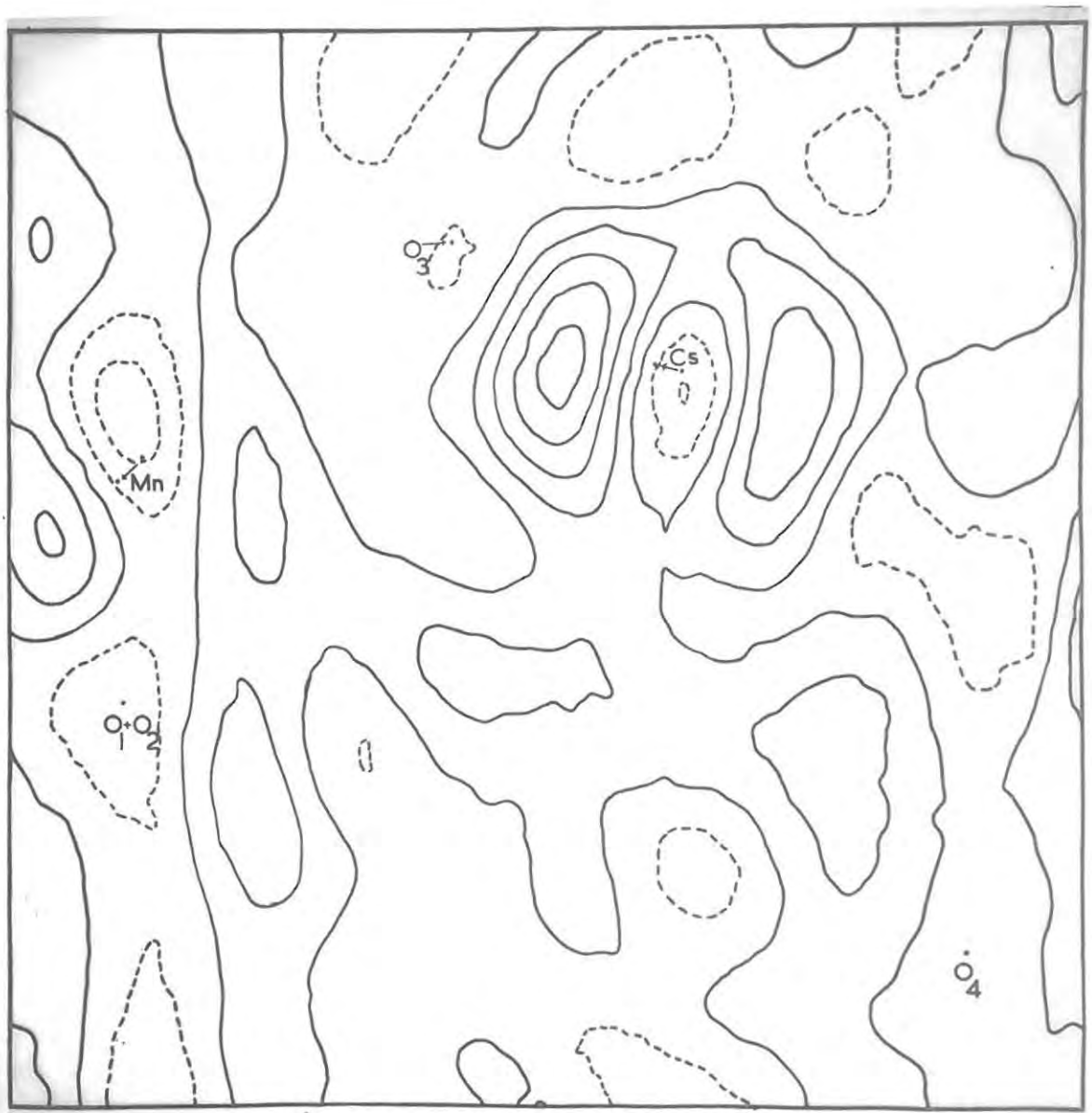

1st Difference Synthesis Fig 7.2

Since the first difference Fourier gave no indication as to the positions of the oxygen atoms, it was decided to move the positions of the oxygen atoms in order to obtain better agreement between the observed and calculated structure factors. This was done by a graphical method. Bragg and Lipson[69] have suggested that the representation of the structure factor should take the form of contours of constant value, they called these diagrams structure factor graphs. Graphs showing the values of such functions as $\cos 2\pi(hx + ky)$ or $\cos 2\pi hx \cos 2\pi ky$ can be constructed, and from these the contribution of a group of atoms may be read at a glance. For the plane group pgg the structure amplitude is given by,

$4 \cos 2\pi hx \cos 2\pi lz$ when $h + l$ is even, and

$-4 \sin 2\pi hx \sin 2\pi lz$ when $h + l$ is odd.

Charts showing the above functions are given in Bunn[70] who also discusses how the charts may be used to show what adjustments of atomic parameters will increase or decrease the structure amplitude. The above method did not prove successful in finding the parameters of the oxygen atoms, however, and was subsequently discarded.

To find the positions of the oxygen atoms it was decided to compute a second difference Fourier without taking any account of the oxygen contribution to the F_c's. If the coordinates of the heavy atoms were correct, this difference Fourier would show a flat topography in the neighbourhood of the Cs and Mn atoms, while the oxygens should show up as peaks. This is the technique used to find hydrogen atoms in organic substances[71]. The F_c's were calculated by placing the Cs and Mn atoms in the refined positions obtained from the first difference Fourier,

- and the second -

and the second difference Fourier was subsequently computed. The resulting map is shown in Fig. 7.3. The $\rho_o - \rho_c$ values were calculated at intervals of $\frac{1}{120}$ of the cell edges, and contours were drawn at arbitrary intervals of 50 units. The second difference map showed that although the Mn was now lying half-way up the slope of a low peak, it was still in an area of relatively high topography. The Cs atom was still in a hollow between two high peaks, which were still unexplained, although they were now of approximately equal height. The oxygen peaks did show up however, the oxygens having coordinates,

$O_1 + O_2$	O_3	O_4
x = 0.040	x = 0.158	x = 0.392
z = 0.179	z = 0.425	z = 0.167

At this stage it was realised that in order to lower the residual appreciably a better absorption correction and a correction due to the thermal motion of the atoms would have to be applied.

7.2 IMPROVEMENT OF THE ABSORPTION CORRECTION.

The second difference Fourier shown in Fig. 7.3 showed that although the Mn atom did not lie in the vicinity of any high peaks, it was situated in an area of somewhat high topography. If the F_o and F_c values were correct the difference Fourier would show the Mn not only in a flat area, but an area where the topography was low, theoretically on a zero contour. Since the F_c's were evidently approximately correct, it was decided that the discrepancy lay in the observed structure factors and the absorption correction applied to the crystal would have to be adjusted so that the Mn would lie in an area of low topography

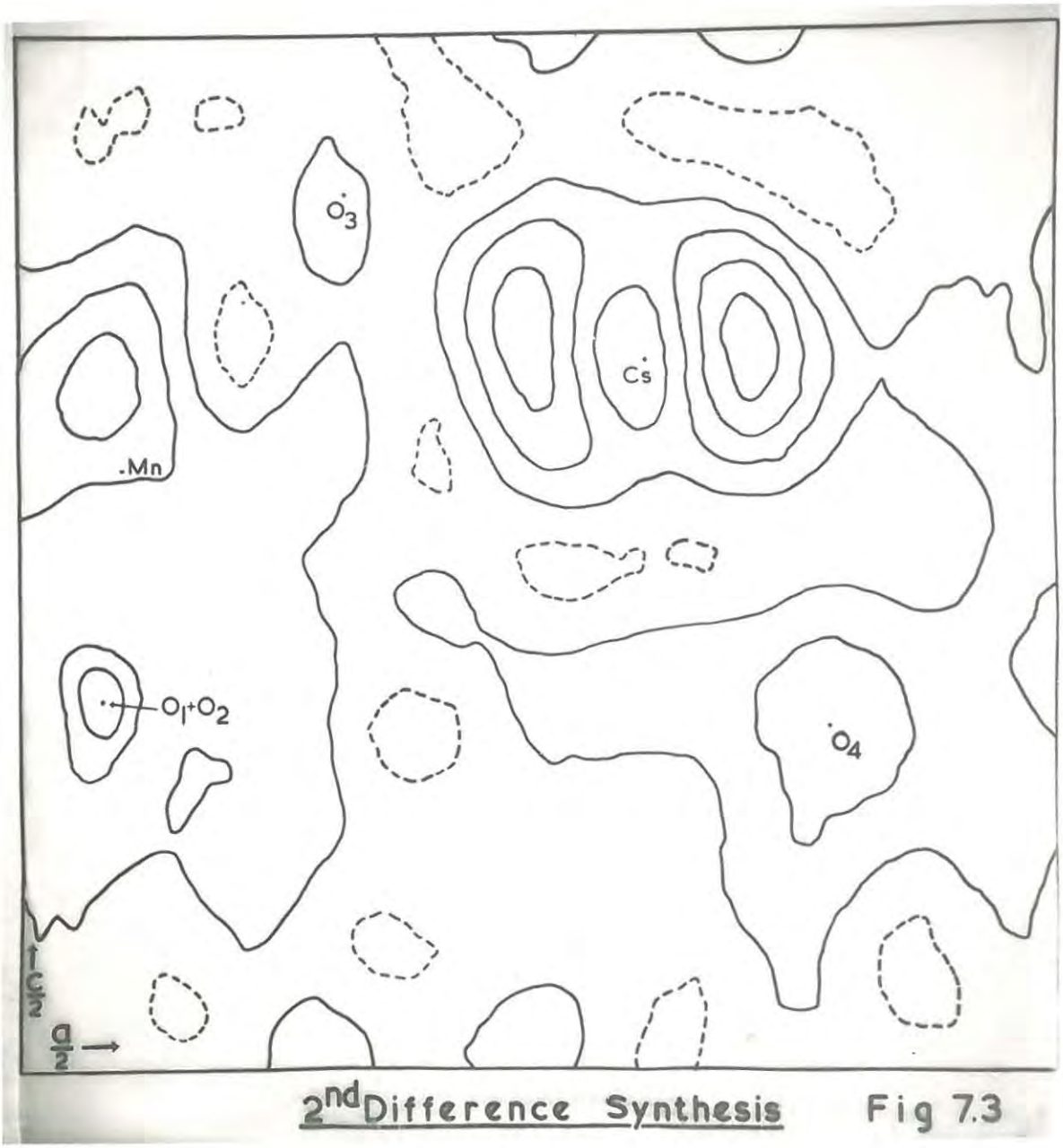

2nd Difference Synthesis Fig 7.3

on a difference map. At first it was thought that the absorption correction $\mu R = 7.4$ was too low and a new set of observed structure factors was computed applying an absorption correction of $\mu R = 10$. The $(F_o - F_c)$ values were then calculated and a one dimensional difference Fourier was computed. It was decided to calculate the Fourier section at a fixed value of x, namely at $x = \frac{6}{120}$ and not to include the oxygen contribution to the F_c's. The difference Fourier section would thus pass through the Mn position and show whether the $\rho_o - \rho_c$ value at this point decreased. The section would also pass close to the superimposed oxygens $(O_1 + O_2)$ position and show if the change in the absorption correction had any effect on the double oxygen peak. The resulting $\rho_o - \rho_c$ section is shown in Fig. 7.4A. The figure shows that, on increasing the absorption correction to $\mu R = 10$, the topography at the Mn position increases as compared with the height of the Mn in Fig. 7.4B which shows the $\rho_o - \rho_c$ section having an absorption correction of $\mu R = 7.4$. It was thus decided to lower the absorption correction to the minimum possible value allowed by the shape of the crystal, namely $\mu R = 3$, and the resulting $\rho_o - \rho_c$ section is shown in Fig. 7.4C. This shows that the height of the Mn has lowered considerably and the absorption correction of $\mu R = 3$ was taken as correct. In all three sections in Fig. 7.4 the $\rho_o - \rho_c$ values were computed at intervals of $\frac{1}{120}$ of the c axis, and the heights of the peaks are in arbitrary units. Fig. 7.4 also shows that the oxygen peak does not alter its position on applying different absorption corrections.

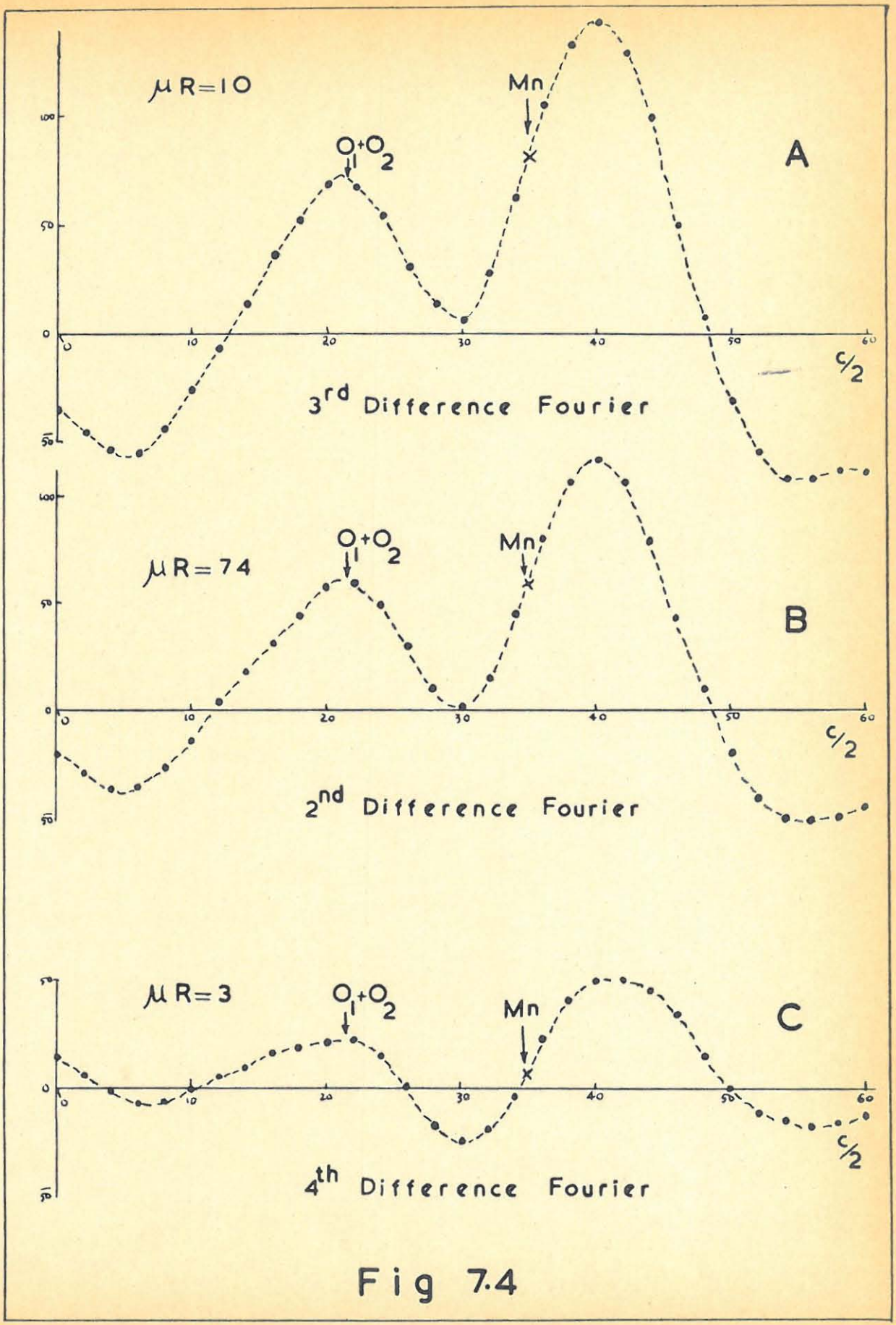
μR=10
Mn
O+O2
A
0
10
20
30
40
50
60
c/2
3rd Difference Fourier
μR=74
Mn
O+O2
B
2nd Difference Fourier
μR=3
Mn
O+O2
C
4th Difference Fourier

Fig 7.4

7.3 THE TEMPERATURE FACTOR.

So far the crystal structure has been assumed to be a static one with atoms in fixed positions. Temperature modifies this situation, however, because it requires that the atoms should undergo thermal motion. This motion has the effect of causing the f curves of the atoms to fall off more rapidly with $\frac{\sin\theta}{\lambda}$ than for the same atoms at rest.

Waller[72] showed that an approximation to the effect of thermal motion on the intensities of the X-ray reflections can be made for isometric structures containing only one kind of atom. For this case,

$$f = f_o\, e^{-(B \sin^2\theta)/\lambda^2} \qquad \ldots\ldots\ldots \qquad 7.4$$

where B is the temperature coefficient.

This simple form of temperature correction is often used as an approximation and it assumes that, in thermal motion, each atom of the crystal undergoes the same isometric motion. When this assumption is made the correction $e^{-(B \sin^2\theta)\lambda^2}$ can be used for each f in the summation for F, so that

$$T_F = {}^{o}F\, e^{-(B \sin^2\theta)/\lambda^2} \qquad \ldots\ldots\ldots \qquad 7.5$$

and $$|T_F|^2 = |{}^{o}F|^2\, e^{-(2B \sin^2\theta)/\lambda^2} \qquad \ldots\ldots\ldots \qquad 7.6$$

where ${}^{o}F$ = the structure factor at $0^{o}K$

T_F = the structure factor at the temperature of the experiment.

The value of B can be found by a method first presented by Wilson[73], and later by Harker[74]. It can be shown[75] that

/102

$$\frac{\overline{|F_{obs}|^2}}{\sum_j {}^{o}f_j} = Ke^{-(2B \sin^2\Theta)/\lambda^2} \qquad \ldots\ldots\ldots \qquad 7.7$$

where $\overline{|F_o|^2}$ is the average of the squares of the observed structure factors,

$\overline{\sum_j {}^{o}F_j^2}$ is the average of the sum of the squares of the scattering factors of the atoms at 0^oA.

K is a constant which places the $|F_{obs}|^2$ on an absolute scale.

B is the temperature coefficient.

Θ and λ are the Bragg angle and the wavelength of the X-ray radiation respectively.

If the logarithms are taken of both sides of Equation 7.7 we obtain the expression

$$\ln\left(\frac{\overline{|F_{obs}|^2}}{\overline{\sum {}^{o}f_j^2}}\right) = -\frac{2B \sin^2\Theta}{\lambda 2} + \ln K \qquad \ldots\ldots\ldots \qquad 7.8$$

This has the form $y = mx + c$ $\ldots\ldots\ldots$ 7.9

The value of B was found graphically by following a procedure suggested by Buerger[75]. The reciprocal lattice was divided into five equal $\sin^2\Theta$ zones and all the $|F_{obs}|^2$ were plotted on the reciprocal lattice. The average for each zone was found, counting zero intensities and extinguished reflections as points having zero intensity. Since only one quarter of the reciprocal lattice was plotted in this case, border points were taken at half value. $\overline{\sum {}^{o}f_j^2}$ was calculated for each zone and a table of $\overline{|F|^2}/\overline{\sum {}^{o}f_j^2}$ for the five zones was prepared. The results of the

- above -

above calculation are shown in Table 7.1.

TABLE 7.1

Zone No.	Sin Θ range	$\overline{\sin^2\Theta}$	$\overline{\lvert F_{obs}\rvert^2}$	$\overline{\Sigma_j {}^o f_j{}^2}$	$\overline{\lvert F_{obs}\rvert^2}/\overline{\Sigma_j {}^o f_j{}^2}$	$\ln \overline{\lvert F_{obs}\rvert^2}/\overline{\Sigma_j {}^o f_j{}^2}$
1	0-0.447	0.0932	108.1	2625	0.04118	$\bar{4}$.8101
2	0.447-0.632	0.3010	74.3	1551	0.04790	$\bar{4}$.9613
3	0.632-0.775	0.4993	33.7	1156	0.02915	$\bar{4}$.4647
4	0.775-0.894	0.6913	24.4	940	0.02593	$\bar{4}$.3477
5	0.894-1.000	0.9068	16.4	800	0.02050	$\bar{4}$.1126

Equation 7.5 has the form of a straight line (Equation 7.6), and hence $\ln \overline{\lvert F_{obs}\rvert^2}/\overline{\Sigma_j {}^o f_j{}^2}$ was plotted against the mean $\sin^2\Theta$ value for each range.

The plot obtained is shown in Fig. 7.5. The point for range 1, representing the reflections of lowest angle, was omitted for theoretical reasons[76]. The slope of the graph, measured from the plot shown in Fig. 7.5 was found to be - 1.296. From Equation 7.8 the slope of the graph $= -\frac{2B}{\lambda^2}$

hence $-1.296 = -\frac{2B}{(1.542)^2}$

$$B = 1.54$$

The calculated structure factors were thus corrected according to Equation 7.6, the values of $\exp(-B \sin^2\Theta/\lambda^2)$ being obtained from tables[77].

With improved absorption and temperature corrections applied to the F_o's and F_c's respectively the value of the residual was

- calculated with -

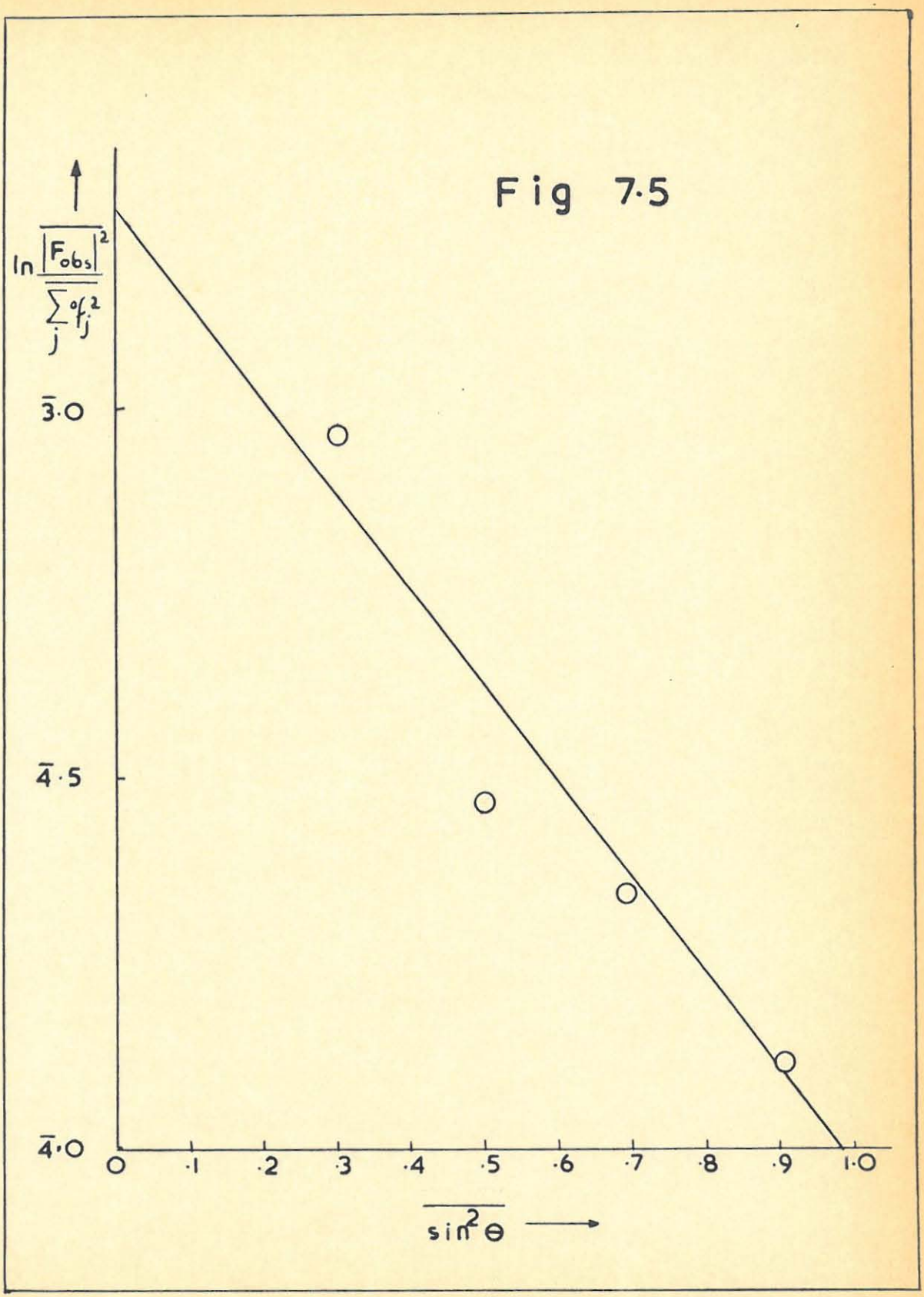
Fig 7·5
$\ln \frac{\overline{|F_{obs}|^2}}{\sum_j \overline{f_j^2}}$
$\bar{3}\cdot0$
$\bar{4}\cdot5$
$\bar{4}\cdot0$
0
·1
·2
·3
·4
·5
·6
·7
·8
·9
1·0
$\overline{\sin^2\theta}$

calculated with the Cs and Mn atoms only and found to be 29.08%. On placing the oxygens in the positions found by the second difference Fourier, the residual value was 27.39%. This value of the residual, although considerably improved, was still too high. The oxygen peaks obtained from the 2nd difference Fourier were ill defined and small as compared with the double peak near the Cs atom, and thus the oxygen positions could not be accurately determined. At this stage it was realised that the double peak on either side of the Cs atom on the difference maps was due to anisotropic thermal motion of this atom[78]. Since the Cs atom has a high diffracting power and thus pays a high contribution to the structure factors, it was important that a correction be applied for anisotropic thermal motion.

7.4 THE CORRECTION FOR ANISOTROPIC THERMAL MOTION.

The characteristic pattern obtained in the difference maps shows that the Cs is undergoing anisotropic thermal motion. The position of the two positive peaks in the difference maps shows that the direction of greatest motion is parallel to the x axis. Since the temperature anomaly is anisotropic, the temperature coefficient B varies with the angle between the direction of greatest thermal motion and the direction of the reciprocal lattice point.

Cochran[79] and Hughes[80] both discuss methods of correcting for anisotropic thermal motion. These methods of correction are difficult and tedious, however, so it was decided to use the fractional atom method[81, 82] which does not require the introduction of new constants for a fictitious distorted lattice. In this method an atom having anisotropic thermal motion may be represented in the structure factor calculation by two or four isotropic fractional atoms placed symmetrically about the atom centre and at small distances from it This has the advantage of being able to treat the fractional atoms as vibrating isotropically. The agreement between this method and the correct representation of anisotropically moving atoms is very high.

Up to this point all the Fourier summations were computed by hand with the aid of Beevers-Lipson strips. Since this method was both tedious and slow, the subsequent refinement was carried out on an IBM 1401 computer.

In order to correct for the anisotropic thermal vibration the

Cs atom was split into two half atoms placed 0.1912 Å apart along the x direction. The two half atoms were not placed symmetrically about the mean position of the Cs atom (x = 0.303, z = 0.345) as found after the first difference Fourier. This is because in the second difference Fourier map the positive peak on the left of the Cs was somewhat higher than the one on the right, showing that the Cs had evidently been moved a little too far to the left. In order to compensate for this the two half atoms were placed at

Cs	Cs_2
x = 0.296	x = 0.315
z = 0.345	z = 0.345

The mean x coordinate of the Cs atom was x = 0.3055, so that the atom as a whole underwent a small move back towards the right.

The Mn coordinates were left at x = 0.050 z = 0.292. A set of F_c's, with only the two half Cs atoms and the Mn atom in the above positions, was calculated. The F_o's and F_c's were normalised by multiplying the F_o's by the ratio $\Sigma F_c / \Sigma F_o$ and the value of the residual was found to be 24.07%. The fifth difference Fourier was then calculated, the resulting map is shown in Fig. 7.6. The $\rho_o - \rho_c$ values were computed at intervals of $\frac{1}{100}$ of the cell edges and contours were drawn at arbitrary intervals of 50 units. The map clearly shows the positions of the oxygen atoms which occur on high, well defined peaks. The half Cs atom Cs_2, the manganese and the osygen atoms were all shifted as indicated by the arrows on the map and the new atomic parameters were:

/107

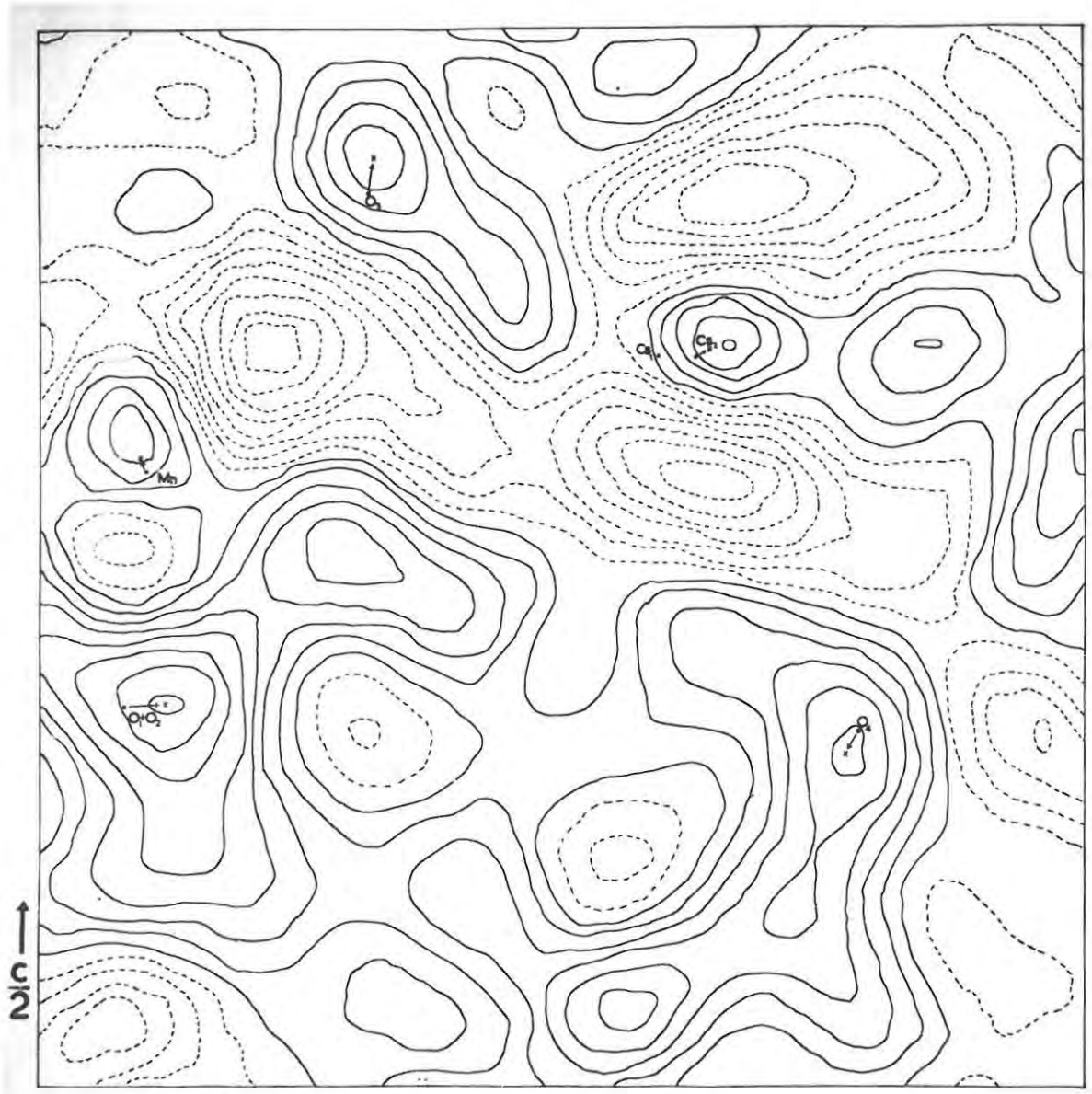

5th Difference Synthesis Fig 7.6

	x	z
Cs_1	0.296	0.345
Cs_2	0.322	0.348
Mn	0.049	0.298
O_1+O_2	0.060	0.180
O_3	0.160	0.440
O_4	0.387	0.157

With the atoms at the above positions a new set of structure factors was calculated, the oxygens' contribution was included, and the F_o's and F_c's were again normalised by multiplying the F_o's by the ratio $\Sigma F_c / \Sigma F_o$. The residual was found to be 15.83%. The sixth difference Fourier was computed, the map is shown in Fig. 7.7. The $\rho_o - \rho_c$ values were computed at intervals of $\frac{1}{50}$ of the cell edges and contours were drawn at arbitrary intervals of 100 units. The map shows that the atoms are not close to any peaks and so their coordinates cannot be further improved.

The uneven peaks on either side of the half caesium atoms can be attributed to anisotropic absorption errors. Jellinek[83] pointed out that if the crystal specimen is elliptical but its absorption is approximated by assuming that it is cylindrical, as was done in our case, the heavy atoms show an absorption anomaly which resembles a temperature anomaly, but has greater extension. This can be seen from Fig. 7.7 which shows that the peaks are not close to the half-caesium positions.

A final Fourier synthesis was computed and the final electron density map is shown in Fig. 7.8. The map clearly shows the Cs and Mn peaks. The final coordinates of the atoms are marked on the map. The electron density was computed at intervals of $\frac{1}{50}$ of the cell edges and

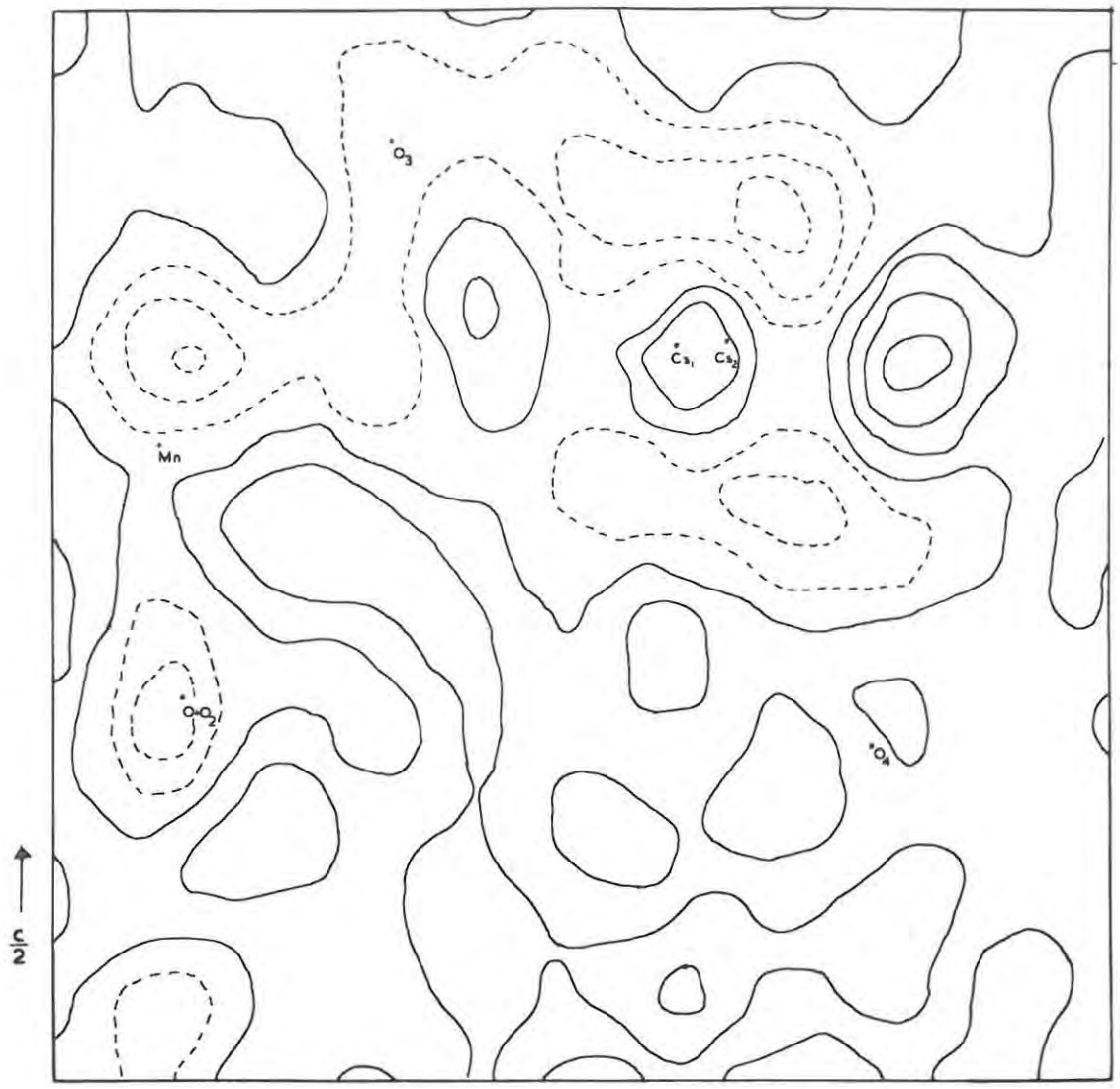

6th Difference Synthesis

Fig 7.7

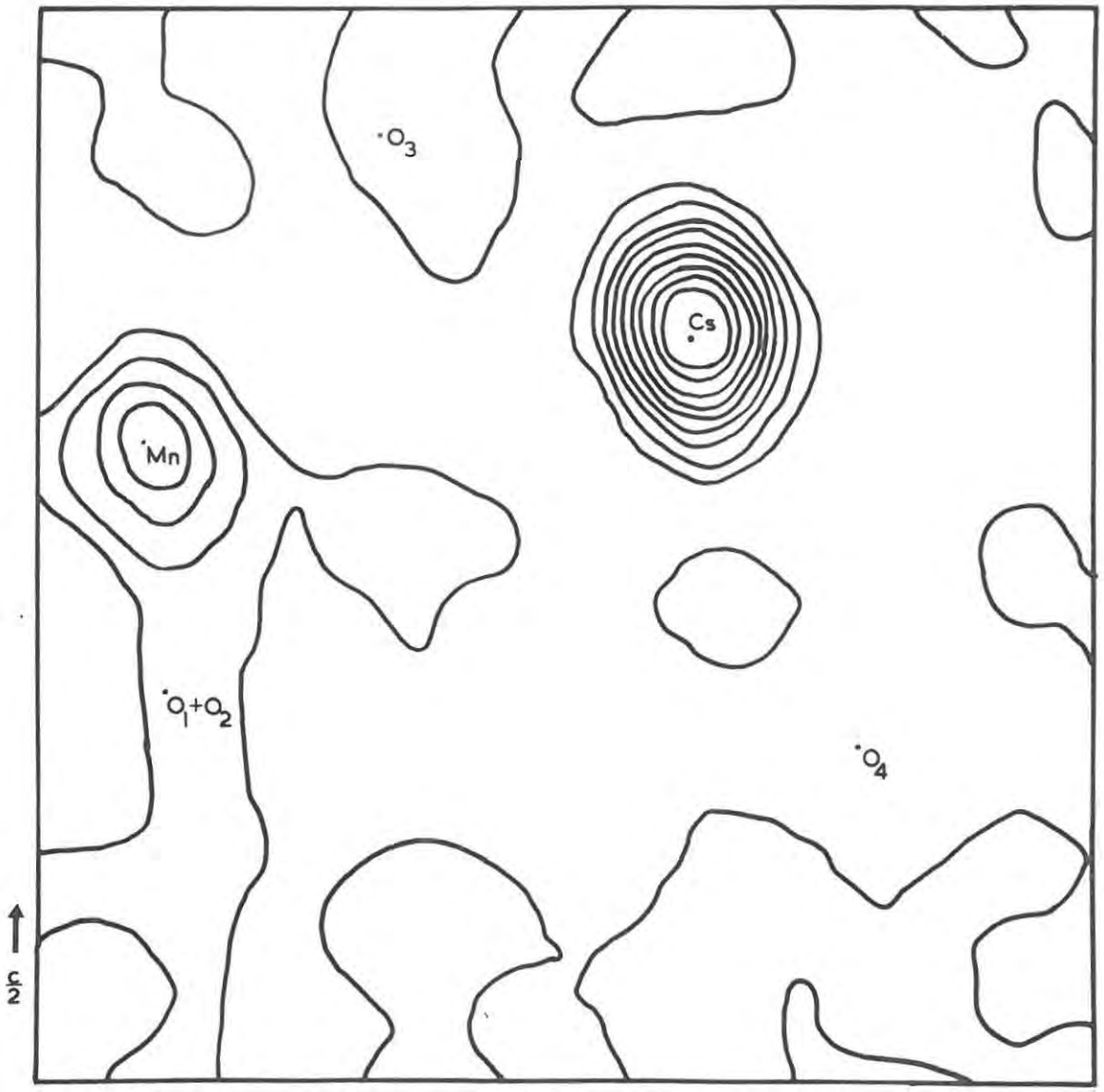

Final Electron Density Projection Fig 7.8

contours on the map were drawn at arbitrary intervals of 50 units.

The final values of the observed and calculated structure factors, as obtained by placing the atoms in the positions obtained from the fifth difference Fourier, are shown in Table 7.2. The value of the residual for the (010) projection was 15.83%. The (102) reflection was then omitted from the calculation because of extinction effects, and the final value of the residual for this projection was 15.14%. It should be noted that in order to suit the computer programme the structure factors were calculated by placing the atoms in half of the unit cell. The F_c values shown in Table 7.2 thus correspond to

$$A = 2 \cos 2\pi hx \cos 2\pi lz \quad \text{for } h + l = 2n$$

$$A = 2 \sin 2\pi hx \sin 2\pi lz \quad \text{for } h + l = 2n + 1$$

The F_c for the (001) projection were calculated on the same basis.

TABLE 7.2

hOl	F_o	F_c	hOl	F_o	F_c	hkO	F_o	F_c
002	41.8	40.6	503	55.1	58.1	040*	60.6	107.0
004	35.8	26.9	506	20.1	18.0	060*	25.6	55.8
006	46.4	32.1	507	31.2	35.0	210	86.0	87.4
0010	10.3	9.4	508	18.6	18.3	220	42.6	49.0
102*	58.1	81.2	509	20.5	19.1	230	46.2	58.6
103	22.0	16.1	600	22.8	23.8	250	33.4	44.6
104	49.8	38.0	601	7.6	0	260	9.0	18.8
106	25.1	15.5	603	20.5	26.2	270	18.2	23.6
107	39.9	29.4	604	16.7	22.0	410	53.4	53.6
108	39.1	31.7	605	28.1	27.4	430	67.0	47.8
109	17.9	14.1	606	10.6	11.9	450	25.6	25.8
200	19.0	21.2	609	27.0	22.3	610	61.6	80.2
201	19.8	19.4	701	20.1	18.9	620	59.8	39.6
202	19.4	18.8	702	51.3	52.5	630	73.4	59.8
203	27.7	23.0	703	22.4	21.0	640	25.6	20.8
204	42.9	44.8	704	33.8	34.3	650	40.8	46.2
205	59.7	48.4	707	21.7	17.8	660	15.4	18.4

7.5 THE FINAL POSITIONS OF THE ATOMS.

The refinement carried out on the (010) projection allowed us to find the x and z coordinates of all the atoms. In Section 6.9 it was proved that the y coordinates of the Cs and Mn atoms were 1/4, but the Fourier summation computed in the (001) projection (Fig. 6.17) did not give any direct clue as to the oxygen positions. It thus remained to find the y coordinates of the oxygen atoms.

Fig. 7.9 shows the positions of all the atoms on the (010) projection. By analogy with the crystal structure of $KMnO_4$ [36], the oxygen atoms labelled O_3 and O_4 were taken as lying in the same plane as their respective Mn atoms, i.e. at y = 1/4 or 3/4. This was confirmed by the values of the Mn - O distances for these oxygen atoms which were

$$Mn - O_3 = 1.588 \text{ Å} \qquad Mn - O_4 = 1.670 \text{ Å}$$

The above distances were in good agreement with values obtained by Mooney[36] for the structure of $KMnO_4$, who gave 1.59 Å as the mean Mn - O distance. The positions of these two oxygen atoms cannot be seen directly from the Fourier map shown in Fig. 6.17, but a section drawn through y = 1/4 showed a small peak corresponding closely with the expected position of O_4, while O_3 was swamped by the Cs peak. The section is shown in Fig. 7.10.

The y coordinate of the oxygen atoms O_1 and O_2 could not be obtained with any certainty from the Fourier map shown in Fig. 6.17. It was thus decided to calculate their position on the assumption that the Mn - O bond length was 1.629 Å, which is the mean of the Mn - O_3, - Mn - O_4 distances -

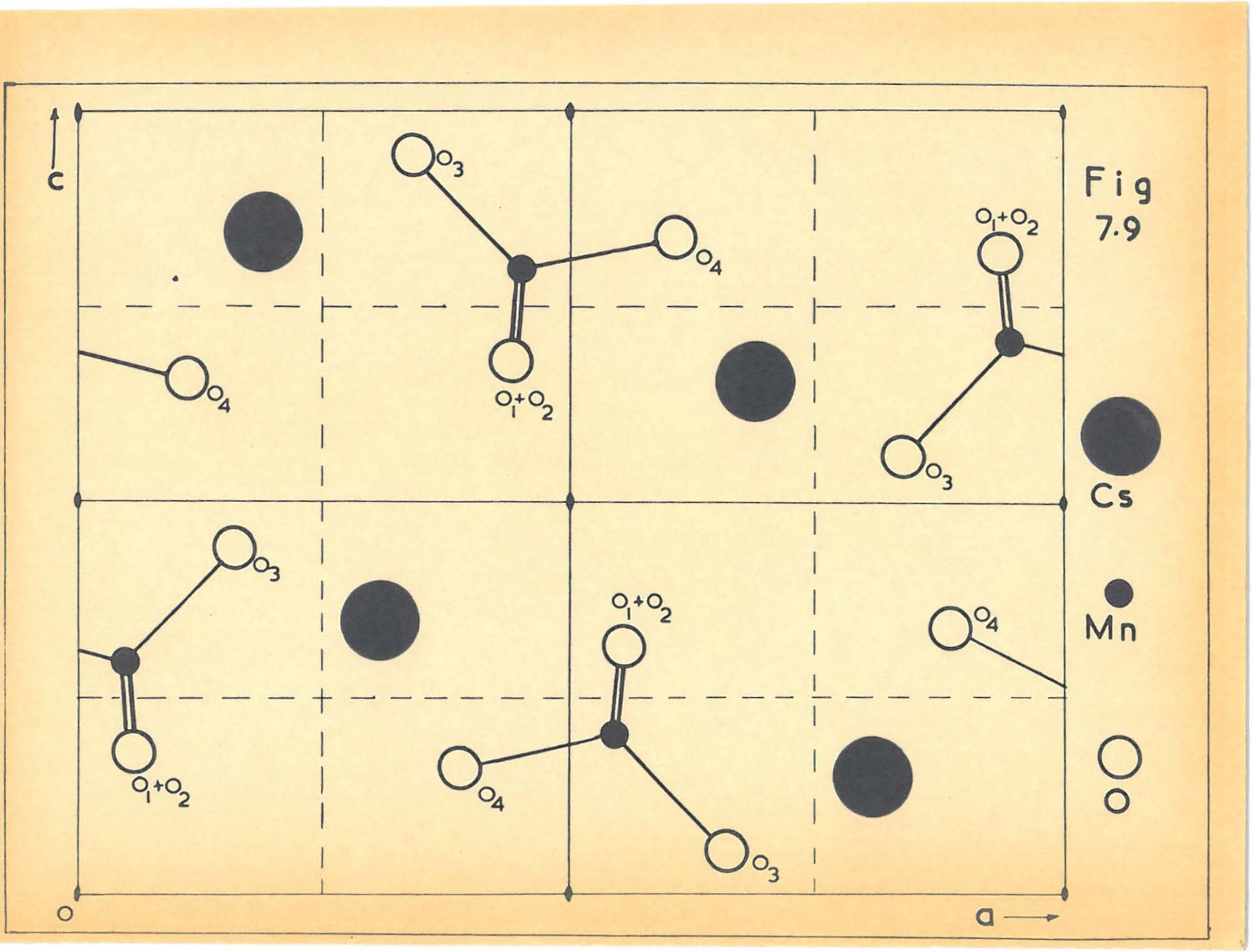

Fig 7.9

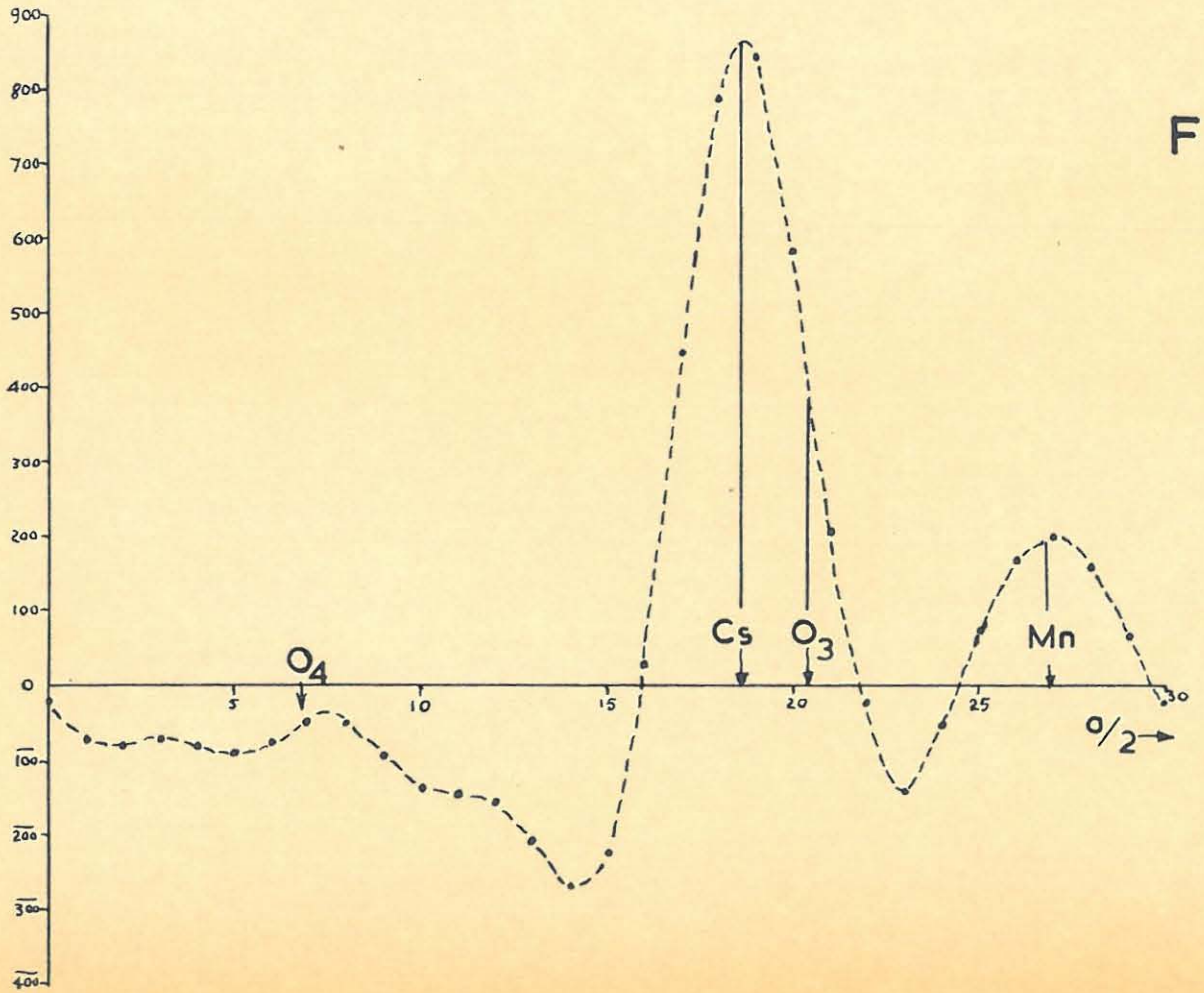
900
800
700
600
500
400
300
200
100
0
100
200
300
400
5
10
15
20
25
30
O4
Cs
O3
Mn
a/2

Fig 7.10

Mn - O_4 distances calculated above. The fifth difference Fourier showed the position of the superimposed oxygens, O_1 and O_2. The projected distance Mn - (O_1 + O_2) was found to be 0.9441 Å, and by Pythagoras' theorem the Mn - O_1 and Mn - O_2 distance along the y direction was found to be 1.3275 Å. The y coordinates of these two oxygen atoms were thus

$$O_1 : y = 0.479 \quad O_2 : y = 0.021$$

These atoms are shown in Fig. 6.17, they are situated near two small peaks. The (001) projection of the unit cell was then drawn. This is shown in Fig. 7.11.

The coordinates of the atoms, as shown in the lower left quarter of the (010) projection (Fig. 7.9), are given below. The two half Cs atoms are recorded separately, and the mean Cs position is also given. For convenience the origin was taken at point O.

	x	y	z
Cs_1	0.296	0.750	0.345
Cs_2	0.322	0.750	0.348
Cs (mean)	0.309	0.750	0.3465
Mn	0.049	0.250	0.298
O_1	0.060	0.479	0.180
O_2	0.060	0.021	0.180
O_3	0.160	0.250	0.440
O_4	0.387	0.250	0.157

The final values of the observed and calculated structure factors on the (001) projection are also given in Table 7.2. The value of the residual, omitting reflections (040) and (060) due to extinction effect was 24.74%.

The overall value of the residual, taking reflections from both the (010) and (001) projections into account was 18.11%.

Fig 7.11

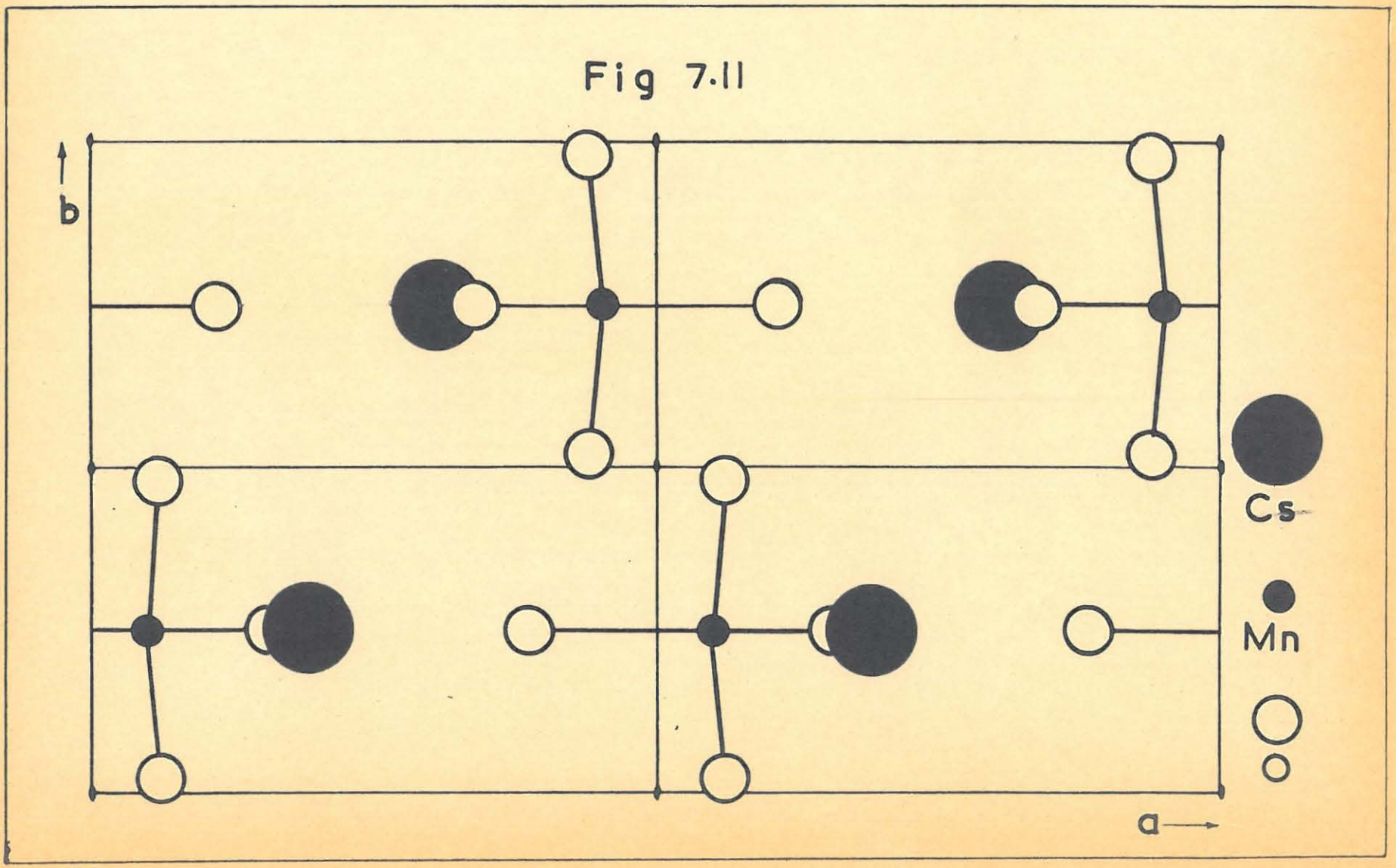

7.6 THE CALCULATION OF INTERATOMIC DISTANCES AND INTERATOMIC ANGLES.

For c ystals belonging to the orthorhomic system it can be shown[84] that the distance between two atoms is given by

$$\text{interatomic distance} = [(\Delta x)^2 a^2 + (\Delta y)^2 b^2 + (\Delta z)^2 c^2]^{\frac{1}{2}} \quad \ldots\ldots \quad 7.10$$

where Δx, Δy, Δz are the differences in coordinates of the atoms,

a, b, c are the parameters of the unit cell.

Suppose an atom, 1, has two neighbours, 2 and 3. If ψ is the interatomic angle $2\hat{1}3$, then for an orthorhombic crystal,

$$\cos\psi = \Delta_2 x \, \Delta_3 x a^2 + \Delta_2 y \, \Delta_3 y b^2 + \Delta_2 z \Delta_3 z c^2 / d_2 \times d_3 \quad \ldots \quad 7.11$$

where $\Delta_2 x$, $\Delta_3 x$ are the differences in coordinates of atoms 1, 2 and 1, 3 respectively etc.,

and d_2, d_3 are the interatomic distances between atoms 1 - 2 and 1 - 3 respectively.

Using the above equations, the following values were obtained for the interatomic distances:

Mn - O_1	= 1.629 Å	O_1 - O_2	= 2.655 Å
Mn - O_2	= 1.629 Å	O_1 - O_3	= 2.656 Å
Mn - O_3	= 1.588 Å	O_1 - O_4	= 3.598 Å
Mn - O_4	= 1.670 Å	O_2 - O_3	= 2.656 Å
Cs - Mn	= 3.929 Å	O_2 - O_4	= 3.598 Å
Average Mn - O	= 1.629 Å	O_3 - O_4	= 3.207 Å

The O - Mn - O interatomic angles were as follows:

$O_1\hat{Mn}O_2$	= 109° 10'	$O_2\hat{Mn}O_3$	111° 10'
$O_1\hat{Mn}O_3$	= 111° 10'	$O_2\hat{Mn}O_4$	100° 56'
$O_1\hat{Mn}O_4$	= 100° 56'	$O_3\hat{Mn}O_4$	122° 02'

The Cs atom is surrounded by 8 Mn atoms at a mean distance of 4.381 Å. Four Mn atoms have the same y coordinate as the Cs atom, i.e. they lie in the same plane. Their distances from the Cs atom are 3.862 Å, 4.581 Å, 4.587 Å and 6.263 Å. The other four Mn atoms lie in planes whose y coordinates differ from the Cs y-coordinate by $\pm$ 1/4. Their distances from the Cs atom are, two at 3.929 Å and two at 3.948 Å.

For comparison it may be remarked that the silicon to oxygen distance in the SiO_4 group is given as 1.54 - 1.64 Å [85], the sulphur to oxygen distance in the SO_4 group is 1.5 Å [86], the phosphorus to oxygen distance in the PO_4 group is 1.56 Å [87] and the chlorine to oxygen distance in ClO_4 is 1.56 Å [88].

8. SUMMARY.

The crystal structure of caesium permanganate has been determined. $CsMnO_4$ crystallises in the orthorhombic space group Pnma. There are four molecules per unit cell with

$$a = 10.0692\ \text{Å},\quad b = 5.8080\ \text{Å},\quad c = 7.9470\ \text{Å}.$$

The structure was determined by Fourier syntheses on the (010) and (001) projections and refined by two-dimensional difference syntheses. The structure is similar to that of $KMnO_4$. The manganese is surrounded by four oxygen atoms at an average distance of 1.629 Å arranged in a slightly distorted tetrahedron. The caesium is surrounded by eight manganese atoms at an average distance of 4.381 Å.

B I B L I O G R A P H Y

1. Bunn: Chemical Crystallography, p. 154 (Oxford 1961).
2. Buerger: X-Ray Crystallography, p.107 (John Wiley and Sons, 1958).
3. Bernal: Proc. Roy. Soc. A 113, 117 (1926).
4. Bragg and Bragg: The Crystalline State, Vol. 1 p. 214. (G. Bell and Sons, Ltd., 1955).
5. Bretano: Z. Physik. 70, 74-83 (1931).
6. Dawton: Proc. Phys. Soc. (London) 50, 919-925 (1938).
7. Robertson and Dawton: J. Sci. Instr. 18, 126-128 (1941).
8. Darwin: Phil. Mag. 43, 808 (1922).
9. W.H. Bragg: Trans. Roy. Soc. A 215, 253 (1915).
10. Lipson and Cochran: Determination of Crystal Structures, Vol. III: Crystalline State, Chapter 1 (G. Bell and Sons, Ltd., 1957).
11. Buerger: Vector Space, Chapter 2 (John Wiley and Sons, 1959).
12. Buerger: Acta Cryst. 4, 531-544 (1951).
13. Robertson: Nature 152, 411-412 (1943).
14. Hägg: Nature 153, 81 (1944).
15. Bragg: Nature 154, 69-78 (1944).
16. Vand: Nature 154, 545-546 (1944).
17. W. Muthmann: Ber. 26, 1018 (1893). Zeit. Kryst. 22, 540 (1894).
18. Meyer and Best: Zeit. Anorg. Chem. 22, 187 (1899).
19. Moles and Crespi: Zeit. Phys. Chem. 100, 337 (1922). Anal. Fis. Quim. 20, 556, 693 (1922). 21, 305 (1923). 23, 198 (1925). Estudios acerca de los permanganatos, Madrid (1925).

20. Saslawsky: Zeit. Anorg. Chem. 146, 315 (1925).

21. Woods: M.Sc. Thesis, Rhodes University, 1962 .

22. Buerger: X-Ray Crystallography, p. 178-180 (John Wiley and Sons, 1958).

23. Bunn: Chemical Crystallography, p.186 (Oxford 1961).

24. Bairsto: J. Sci. Instr. 25, 215 (1948).

25. Weist and Cole: J. Sci. Instr. 25, 213 (1948).

26. Hendershot: Rev. Sci. Instr. 8, 436 (1937).

27. Buerger: Crystal Structure Analysis, p.95 (John Wiley and Sons, 1960).

28. ibid p.98.

29. ibid p.99.

30. Nassimbeni, Prout and Woods: J. Sci. Instr. 40, 333 (1963).

31. Henry, Lipson and Wooster: The Interpretation of X-Ray Diffraction Photographs, Chapter 13, (Macmillan and Co., Ltd., London 1961).

32. ibid p.194.

33. Buerger: X-Ray Crystallography, p.426 (John Wiley and Sons, 1958).

34. Int. Tables for X-Ray Crystallography, 3, 60 (1962).

35. ibid Vol. 1.

36. Mooney: Phys. Rev. 37, 1306 (1931).

37. Int. Tables for X-Ray Crystallography, 2, 108 (1959).

38. ibid 2, 266 (1959).

39. ibid 2, 268-269 (1959).

40. ibid 3, 175-192 (1962).

41. Buerger: Crystal Structure Analysis, p.74-75 (John Wiley and Sons, 1960).

42. Int. Tables for X-Ray Crystallograpy, 2, 295-298 (1959).

43. ibid 2, 302-305, (1959).

44. Buerger: Vector Space, p.22-25 (John Wiley and Sons, 1959).

45. Lipson and Cochran: Determination of Crystal Structures, Vol. III, Crystalline State, p.15 (G. Bell and Sons, Ltd., 1957).

46. Int. Tables for X-Ray Crystallography, 1, 526 (1952).

47. Lipson and Cochran: Determination of Crystal Structures, Vol. III, Crystalline State, p.88-89 (G. Bell and Sons, Ltd., 1957).

48. Beevers and Lipson: Phil. Mag. 17, 855-859 (1934).

49. Beevers and Lipson: Nature, 137, 825-826 (1936).

50. Lipson and Beevers: Proc. Phys. Soc. (London) 48, 772-780 (1936).

51. Patterson and Tunell: Am. Mineralogist, 27, 655-679 (1942).

52. Buerger: Vector Space, p.106 (John Wiley and Sons, 1959).

53. ibid p.95-96.

54. ibid p.94.

55. ibid p.281-285.

56. Int. Tables for X-Ray Crystallography, 1, 370 (1952).

57. Lipson and Cochran: Determination of Crystal Structures, Vol. III, Crystalline State, p.59 (G. Bell and Sons, 1957).

58. Int. Tables for X-Ray Crystallography, 3, 220-221 (1962).

59. Bragg and Bragg: The Crystalline State, Vol. 1, p.329 (G. Bell and Sons 1959).

60. Buerger: Crystal structure Analysis, p. 495 (John Wiley and Sons 1960).

61. Int. Tables for X-Ray Crystallography, 1, 151 (1952).

62. ibid 1, 370 (1952).

63. Buerger: Crystal Structure Analysis, p.296-600 (John Wiley and Sons 1960).

64. ibid p.604-605 ibid

65. Crowfoot, Bunn, Rogers-Low and Turner-Jones: The Chemistry of Penicillin, p.310-367 (Princeton University Press 1949).

66. Booth: Nature, 161, 765-766 (1948).

67. Cochran: Acta Cryst. 4, 81-92 (1951).

68. Cochran: Acta Cryst. 4, 408-411 (1951).

69. Bragg and Lipson: Z. Krist. 95, 323 (1936).

70. Bunn: Chemical Crystallography, p.286-291 (Oxford University Press).

71. Nyburg: X-Ray Analysis of Organic Structures, p.159-161 (Academic Press, New York and London 1961).

72. Waller: Ann. Physik. 83, 153-183 (1927).

73. Wilson: Nature, 150, 152 (1942).

74. Harker: Am. Mineralogist, 33, 764-765 (1948).

75. Buerger: Crystal Structure Analysis, p.233-237 (John Wiley and Sons 1960).

76. Lipson and Cochran: The Determination of Crystal Structures, Vol. III, Crystalline State p.237 (G. Bell and Sons, 1957).

77. Int. Tables for X-ray Crystallography, 2, 241-264 (1959).

78. Buerger: Crystal Structure Analysis, p.606 (John Wiley and Sons 1960).

79. Cochran: Acta Cryst. 4, 81-92 (1951).

80. Hughes: J. Am. Chem. Soc. 63, 1737-1752 (1941).

81. Kartha and Ahmed: Acta Cryst. 13, 532-534 (1960).

82. Vos and Smits: Acta Cryst. 14, 1299-1300 (1961).

83. Jellniek: Acta Cryst. 11, 677-679 (1958).

84. Buerger: Crystal Structure Analysis, p.629-634 (John Wiley and Sons 1960).

85. W.L. Bragg: Zeits. f. Krist. 74, 237 (1930).

86. Bradley: Phil. Mag. 49, 1225 (1925).

87. West: Zeits. f. Krist. 74, 306 (1930).

88. Zachariasen: Zeits. f. Krist. 73, 2, 141 (1930).